Investigating the Performance of High Resolution Soil Moisture Data Derived from Remotely Sensed Precipitation Estimates

Dissertation zur Erlangung des Doktorgrades
an der Fakultät für Geowissenschaften
der Ludwig-Maximilians-Universität München

Vorgelegt von

Thomas Ramsauer

München, 17.07.2025

Erstgutachter: Prof. Dr. Ralf Ludwig
Zweitgutachter: Prof. Dr. Philip Marzahn

Tag der Mündlichen Prüfung: 09.12.2025

Investigating the Performance of High Resolution Soil Moisture Data Derived from Remotely Sensed Precipitation Estimates

Thomas Ramsauer

Acknowledgements

What a long time; many pledged deadlines passed. Yet, finally! This thesis has reached a finished state.

Possible cause, one might say, yet moreover the help and harbor in tough times are my two fairies - maybe only one, and one butterfly bibo - and their "fairy queen".
In infinite love I want to thank my family to have endured and supported me on the not-so-wild but challengingly long ride.

This naturally extends to my loving parents and very dear brother, whose support I highly appreciate. I love you.

The thesis was quickly becoming a side effort over the last years, me being the biggest critic of the contents. Many other interesting projects - professional and private - came up and attracted my attention and occupied my time. I am all the more proud to have pulled through and finished the rough final state of this work in solitude with lake view.

Along the way many kind humans helped guide my way and poke me in the right moments reminding me to continue. The journey started with Alex giving me the initial trust to start working on the topic in his working group. After a still incomprehensible tragedy, Ralf and Philip became my new, yet already well known, supervisors. With Ralf, I could not have wished for an advisor showing more humaneness and, above all, patience. Philip was a close companion already in former theses and of course especially in the last years leading up to this PhD thesis and is sorely missed in Munich. A "Mach's fertig!" was gladly received on the occasion and traveling together to many conferences and project meetings, with the to be expected side-events, really was a joy!

It was always enjoyable, but also soothingly relieving to share the office with such nice colleagues as I have, many sitting in the same boat, facing the same struggles. Thomas is to be named as friend and close collaborator; together mastering field campaigns and traveling Europe to almost countless project meetings and conferences was great! Finally, Vera must not be forgotten, for her persistent reminding and teasing about status updates on the writing progress, but more so for the nice conversations over coffee and for always lending the greatly appreciated helping hand with organizational matters.

Summary

Soil moisture is a highly critical variable in the global energy and water cycle. Accurate knowledge of the current state is of paramount importance for different applications, from hydrological modeling to agricultural yield forecasting. The significance of soil moisture lies in its control over key fluxes at the land-atmosphere interface, such as evapotranspiration, infiltration, and runoff, which govern not only local water availability but also larger climatic and ecological dynamics. As such, soil moisture is recognized as an Essential Climate Variable (ECV) by the Global Climate Observing System (GCOS), and its consistent monitoring is vital for hydrological or agricultural studies.

Several modeling and monitoring concepts and data sets exist. However, these often present trade-offs between spatial coverage, temporal resolution, and accuracy. In situ sensors provide highly accurate point-scale data but lack spatial representativeness. Satellite-based data sets, while expansive in scope, frequently suffer from coarse spatial or temporal resolution, rendering them insufficient for rapidly changing hydrological conditions or local assessments. For exploitation of current and future satellite missions in data fusion schemes, and for use cases where spatially distributed information on soil moisture at very high temporal resolution is needed, data sets are lacking. This deficiency particularly shows when attempting to monitor sub-daily fluctuations in soil water content, information that is critical for modeling hydrological extremes such as flash floods. Addressing this need for temporally dense, spatially resolved soil moisture products is the central motivation of this thesis.

Therefore, the gridded precipitation products RADOLAN - a gauge-adjusted weather radar data set - and GPM - a set of quantitative precipitation estimates from a satellite constellation - are consulted to provide moisture input at inherently high temporal sampling for an empirical soil moisture modeling algorithm. These precipitation products were chosen for their complementarity: RADOLAN offers high spatial resolution and regional accuracy over Germany, while GPM provides global coverage with similar sub-hourly sampling, making it highly suitable for scaling the approach beyond regional boundaries. The foundation therefore is the Antecedent Precipitation Index (API), which is significantly expanded to deliver actual soil moisture values over a full range of ecosystems and soil types. Tradi-

tionally used as a relative index for moisture availability, the API is re-engineered in this work to approximate volumetric soil moisture by incorporating auxiliary information such as air temperature and soil texture. The extended model includes spatially adaptive loss functions for the global use case, allowing for better alignment with observed evapotranspiration and drainage behavior across different climatic conditions. The resulting data sets RADOLAN_API and GPM_API - provide high temporal resolution soil moisture information on regional and global scales, and are characterized by a very timely representation of the soil moisture course. The RADOLAN_API data set demonstrates strong agreement with ground-based soil moisture measurements from the International Soil Moisture Network (ISMN) and with ESA's Climate Change Initiative (CCI) soil moisture product. The model effectively captures both rapid moisture upsurges following precipitation and gradual declines e.g. due to evapotranspiration, validating its utility for dynamic hydrological monitoring in Central Europe. On a global scale, the GPM_API product leverages GPM IMERG satellite precipitation data in combination with globally available soil maps and temperature reanalysis to simulate hourly surface soil moisture. Spatially diverse parameterizations are embedded to represent regional soil and vegetation characteristics. Evaluation against in situ data and the ESA CCI product confirms its capability to reflect soil moisture patterns across continents, climates, and land uses.

In summary, the approach delivers very capable representations of different soil moisture regimes. By emphasizing temporal responsiveness and physical consistency, the developed models fill a critical gap in the remote sensing and modeling soil moisture landscape. Both RADOLAN_API and GPM_API are poised to serve as valuable inputs to e.g. data assimilation systems, forecasting models, and drought monitoring platforms. Furthermore, for application in a data fusion scheme, the exact indication of soil moisture state change is highly beneficial and will be of great service to monitor soil moisture at very high temporal and spatial scales when combined with upcoming satellite-based sensors. This includes integration with synthetic aperture radar (SAR) data for spatial and temporal downscaling or with thermal infrared observations for improved surface energy balance modeling. The lightweight computational design of the API-based approach also enables near real-time deployment, making it attractive for operational environmental monitoring services.

The thesis is structured around three peer-reviewed scientific publications. The first article focuses on evaluating the RADOLAN and GPM IMERG precipitation data sets over Germany, highlighting strengths and limitations in spatial coherence and seasonal rainfall pattern agreement. The second article presents the RADOLAN_API soil moisture product, detailing its validation and the adjustments made to the empirical loss factors to enhance the match with soil moisture records. The third article introduces the global-scale GPM_API soil moisture data, emphasizing the scalability of the approach and its ability to capture global soil moisture variability. Collectively, these articles form a coherent narrative demonstrating the feasibility and value of high-temporal-resolution soil moisture mapping based on remotely sensed precipitation. The contributions lie not only in the methodological innovation but also in delivering practical, scalable tools for environmental monitoring and research.

Zusammenfassung

Die Bodenfeuchte ist eine äußerst wichtige Variable im globalen Energie- und Wasserkreislauf. Genaue Kenntnis über ihren aktuellen Zustand sind für verschiedene Anwendungen, von der hydrologischen Modellierung bis zur Vorhersage landwirtschaftlicher Erntererträge von größter Bedeutung. Die Bedeutung der Bodenfeuchte liegt in ihrer kontrollierenden Rolle gegenüber Energie- und Stoffkreisläufen zwischen Landoberfläche und Atmosphäre, wie Evapotranspiration, Infiltration und Abfluss, die nicht nur die lokale Wasserverfügbarkeit, sondern auch größere klimatische und ökologische Dynamiken bestimmen. Daher wird die Bodenfeuchte vom Global Climate Observing System (GCOS) als wesentliche Klimavariable (ECV) anerkannt, und ihre konsequente Überwachung ist für hydrologische und landwirtschaftliche Studien von entscheidender Bedeutung.

Es gibt bereits zahlreiche verschiedene Modellierungs- und Überwachungskonzepte und Datensätze, welche jedoch meist mit Kompromissen zwischen räumlicher Abdeckung, zeitlicher Auflösung und Genauigkeit verbunden sind. Messstationen liefern hochgenaue Punktdaten, denen es jedoch an räumlicher Repräsentativität mangelt. Satellitengestützte Datensätze haben zwar einen großen Erfassungsbereich, weisen aber häufig eine grobe räumliche oder zeitliche Auflösung auf, so dass sie für stark volatile hydrologische Bedingungen oder die lokale Betrachtung derer unzureichend sind. Für die Nutzung zusammen mit aktuellen und zukünftigen Satellitenmissionen, beispielsweise in Datenassimilierungsverfahren, oder - grundsätzlich - für Anwendungsfälle, in denen räumlich verteilte Informationen über die Bodenfeuchte mit sehr hoher zeitlicher Auflösung benötigt werden, fehlen jedoch passende Datensätze. Die Schwäche bestehender Datensätze, sehr kurzfristige Schwankungen des Bodenwassergehalts nur bedingt abbilden zu können, erweist sich beispielsweise in der Modellierung hydrologischer Extremereignisse wie Sturzfluten als problematisch. Die zentrale Motivation dieser Arbeit ist es, diesen Bedarf an zeitlich hoch aufgelösten, räumlich verteilten Bodenfeuchteprodukten zu decken.

Die Informationen verschiedener Datensätze werden in dieser Arbeit als Eingangsdatensatz für ein empirisches Bodenfeuchtemodellierungsverfahren verwendet: *i*) der RADOLAN Wetterradardatensatz des Deutschen Wetterdienstes und *ii*) ein der "Global Precipitation Measu-

rement Mission" angehöriger Niederschlags-Datensatz, welcher von einer Satellitenkonstellation unter Leitung der NASA erstellt wird. Diese Niederschlagsprodukte wurden aufgrund ihrer Komplementarität ausgewählt: RADOLAN bietet eine hohe räumliche Auflösung und regionale Genauigkeit über Deutschland, während GPM eine globale Abdeckung mit ähnlicher (sub-)stündlicher Abtastung bietet, wodurch sich diese Daten hervorragend für die Skalierung des Ansatzes über regionale Grenzen hinaus eignen. Die Grundlage für die Modellierung bildet ein neu entwickelter, erheblich erweiterter Vorregenindex, welcher tatsächliche Bodenfeuchtewerte für eine ganze Reihe von Ökosystemen und Bodentypen zu liefern im Stande ist. Der Vorregenindex, welcher traditionell als relativer Index für die Feuchtigkeitsverfügbarkeit herangezogen wird, wird in dieser Arbeit überarbeitet und erweitert, um den korrekten Wertebereich volumetrischer Bodenfeuchtigkeit durch die Einbeziehung von Zusatzinformationen wie Lufttemperatur und Bodentextur zu approximieren. Das erweiterte Modell enthält räumlich anpassbare Verlustfunktionen für den globalen Anwendungsfall, welche eine bessere Abbildung von Evapotranspiration und Entwässerungsverhalten unter verschiedenen klimatischen Bedingungen ermöglichen. Die resultierenden Datensätze RADOLAN_API und GPM_API liefern zeitlich hoch aufgelöste Bodenfeuchtedaten auf regionaler und globaler Ebene und zeichnen sich durch eine sehr genaue Darstellung von Änderungen im Bodenfeuchteverlauf aus.

Der RADOLAN_API-Datensatz zeigt eine starke Übereinstimmung mit bodengestützten Bodenfeuchtemessungen des International Soil Moisture Network (ISMN) und mit dem Bodenfeuchteprodukt der Climate Change Initiative (CCI) der ESA. Das Modell erfasst sowohl schnelle Feuchtigkeitsanstiege nach Niederschlägen als auch allmähliche Abnahmen aufgrund von beispielsweise Evapotranspiration und bestätigt damit den Nutzen für das hydrologische Monitoring in Deutschland und Mitteleuropa. Auf globaler Ebene nutzt das GPM_API-Produkt die GPM IMERG Satellitenniederschlagsdaten in Kombination mit global verfügbaren Bodenkarten und Temperaturreanalysedaten zur Simulation der stündlichen Bodenfeuchte. Räumlich angepasste Parametrisierungen werden verwendet, um regionale Boden- und Vegetationseigenschaften darzustellen. Der Vergleich mit Messdaten und dem CCI-Produkt der ESA bestätigt, dass der Bodenfeuchteverlauf über Kontinente, Klimazonen und Landnutzungen hinweg wiedergegeben werden kann.

Zusammenfassend lässt sich sagen, dass der Ansatz verschiedene Bodenfeuchtigkeitsregime sehr gut abbildet. Durch den Fokus auf die sehr hohe zeitlichen Auflösung unter Einhaltung physikalischen Grenzen, füllen die entwickelten Modelle eine kritische Lücke in der Bodenfeuchtemodellierung. Sowohl RADOLAN_API als auch GPM_API können als wertvolle Eingangsdaten für z.B. Datenassimilationssysteme, Vorhersagemodelle und Dürreüberwachungsplattformen dienen. Darüber hinaus ist für die Anwendung in der Datenfusionierung die genaue Angabe von Änderungen des Bodenfeuchtezustands von großem Nutzen und wird in Kombination mit künftigen satellitengestützten Sensoren bei der Überwachung der Bodenfeuchte auf sehr hohen zeitlichen und räumlichen Skalen von großem Nutzen sein. Dazu gehört beispielsweise auch die Integration mit SAR-Daten (Radar mit synthetischer Apertur) für die räumliche und zeitliche Herunterskalierung oder von thermischen Infrarotbeobachtungen für eine verbesserte Modellierung der Oberflächenenergiebilanz. Das leichtgewichtige Design des API-basierten Ansatzes ermöglicht auch einen Einsatz nahezu in Echtzeit, was ihn für operative Umweltüberwachungsdienste attraktiv macht.

Der Arbeit liegen drei wissenschaftliche Veröffentlichungen zu Grunde. Der erste Artikel konzentriert sich auf den Vergleich der RADOLAN- und GPM-IMERG-Niederschlagsdatensätze über Deutschland und zeigt die Unterschiede sowohl der räumlichen, wie auch der saisonalen Niederschlagsmuster auf. Der zweite Artikel stellt das RADOLAN_API-Bodenfeuchteprodukt vor und beschreibt dessen Validierung sowie die Anpassungen, die an den empirischen Verlustfaktoren vorgenommen wurden, um die Übereinstimmung mit Messdaten zu verbessern. Im dritten Artikel werden die globalen Bodenfeuchtedaten des GPM_API vorgestellt, wobei die Skalierbarkeit des Ansatzes und seine Fähigkeit zur Erfassung der globalen Bodenfeuchteschwankungen hervorgehoben werden. Zusammengenommen bilden diese Artikel eine kohärente Darstellung, die die Machbarkeit und den Wert von Bodenfeuchtemodellierung mit hoher zeitlicher Auflösung auf der Grundlage von fernerkundungsbasierten Niederschlagsdaten aufzeigt. Die Beiträge liegen nicht nur in der methodischen Innovation, sondern auch in der Bereitstellung praktischer, skalierbarer Algorithmen für die Umweltüberwachung und Forschung.

Contents

List of Figures

List of Acronyms

AirMOSS Airborne Microwave Observatory of Subcanopy and Subsurface

API Antecedent Precipitation Index

CCI Climate Change Initiative

CDHE Compound Dry And Hot Extreme

CDR Climate Data Record

ECMWF European Centre for Medium-Range Weather Forecasts

ECV Essential Climate Variable

ESA European Space Agency

GCOS Global Climate Observing System

GPCC Global Precipitation Climatology Center

GPCP Global Precipitation Climatology Project

GPM Global Precipitation Measurement

ISMN International Soil Moisture Network

LSM Land Surface Model

LST Land Surface Temperature

MSWEP Multi-Source Weighted-Ensemble Precipitation

OPTRAM Optical Trapezoid Model

PERSIANN Precipitation Estimation from Remotely Sensed Information using Artificial Neural Networks

QPE Quantitative Precipitation Estimates

RMSD Root Mean Square Difference

RZSM Root Zone Soil Moisture

SAR Synthetic Aperture Radar

SM Soil Moisture

SSM Surface Soil Moisture

TOTRAM Thermal-Optical Triangle Method

WMO World Meteorological Organization

1 Introduction

1.1 Context and Significance

"Water is the driving force of all nature." — Leonardo da Vinci

The relationships of soil moisture

Water availability determines the fullness of life. But water not only finds itself in streams, lakes and the ocean; as rain in the atmosphere and as puddle on land. Soil moisture, the water content in the root zone of the soil, although inconspicuous, is yet so very crucial to life on earth (Legates et al. 2010). Only 0.001 % of total water on the globe is - in an exemplary and simplified form - not only responsible for plant growth (Shiklomanov 1993); rather, on a bigger picture yet more precisely, the part of the fresh water controls the major energy exchange processes that take place at the land surface (Vereecken et al. 2015; Katul et al. 2012; Western et al. 2002). In this very thin layer on the Earth's surface, the soil moisture state and related hydrological processes define the path that water takes in the terrestrial system (Vereecken et al. 2015). Legates et al. (2010) even state, that beyond its fundamental role in hydrology, soil moisture is a key variable that relates to all aspects of physical geography.

Factors that affect hydrology and hence soil moisture include topography, vegetation, soil characteristics and meteorology (Entin et al. 2000). Naturally, inherent to the contributing features, the amplitude, variability and temporal course of soil moisture content depends on the specific location and time of year (Vereecken et al. 2014; Zucco et al. 2014). Yet, the general spatial distribution of soil moisture follows the expectations with wet soils in humid regions, for example the northern latitudes and dry soils in arid regions (Reichle et al. 2004) as precipitation is the main contributor to the subsurface water storage (Seneviratne et al. 2010; Manning et al. 2018; Legates et al. 2010).

But also, substantial differences in soil moisture development occur in seemingly similar regions. Entin et al. (2000) present that such behavior can be attributed to spatial coherence of soil moisture related to different scales: small scales (10m, one day) accordingly relate to the hydrological scale with land surface types (thus e.g. soil properties) causing similarities and differences in soil moisture schemes. The consistency of soil moisture on a larger scale

(100km, months) contrasts the just mentioned context, and is rather based on general atmospheric forcing and atmospheric modes, like the North-Atlantic Oscillation (Entin et al. 2000; Nicolai-Shaw et al. 2016). The general soil water availability is initially fundamentally interrelated with the existing soil water capacity. Properties like particle size distribution - the soil textural type - define the hydraulic characteristics of a soil (Cosby et al. 1984). These vary greatly from place to place (Lehmann et al. 2018; Liu et al. 2018; Fredlund et al. 1994; Cambardella et al. 1994) and the resulting, spatially divers relative soil moisture status in turn is the most influential factor for the regional partitioning or compartmentalization of incoming precipitation into infiltration and surface runoff generation (Robinson et al. 2008), letting it take a highly critical role in the hydrological cycle (McColl et al. 2017a; Robock et al. 2000; Vereecken et al. 2022).

Further variables in the earth system, concerning energy exchange, are tied to the state of Surface Soil Moisture (SSM). The availability of water in the upper soil layers for instance limits the actual evapotranspiration and hence is closely connected to the division of radiation between latent and sensible heat flux (Or and Lehmann 2019; Small et al. 2018; Miralles et al. 2012). Feedback mechanisms between soil moisture content and the state of the atmosphere even can exacerbate climate extremes (Seneviratne et al. 2010; Hirschi et al. 2010, 2014). In the future, ubiquitous increase in evaporative demand in the atmosphere due to globally risen temperatures is to be expected, which in turn intensifies soil moisture loss through evapotranspiration (Dai et al. 2018).

The earth's carbon and nitrogen cycles are also closely related to soil moisture. Low soil moisture content results in ecosystem water stress that reduces photosynthetic activity and hence gross primary production (Humphrey et al. 2021; Zhao and Running 2010). Consequently, carbon uptake by the terrestrial ecosystems is reduced (Green et al. 2019). Currently observed trends in declining soil moisture result in permanently damaged ecosystems (Schwalm et al. 2017) which in turn are associated with accelerated atmospheric CO_2 increase (Green et al. 2019).

Summarizing, the status of soil moisture is highly relevant for a multitude of processes in the land-atmosphere interface and, again, Legates et al. (2010) appropriately calls soil moisture the 'central and unifying theme in physical geography'.

The importance of soil moisture

The classification as an Essential Climate Variable (ECV) by the World Meteorological Organization (WMO)'s Global Climate Observing System (GCOS) further expresses the prominence, interconnectedness and thus relevance of soil moisture in the climate and earth system (GCOS 2016). Justification therefor can further be obtained by recognizing the significant role of soil moisture in the land atmosphere interface, especially in the context of climate change, influencing both natural ecosystems and human activities (Berg and Sheffield 2018). A meteorological drought with the absence of precipitation depletes the soil water storage and commonly leads to an agricultural drought with severe implications on farming production. Generally, a reduction of soil moisture especially in dry-seasons can lead to significant detrimental effects besides the mentioned decreased agricultural productivity, e.g., increased flood risk, (aeolian) erosion rates of valuable top soil and overall reduced ecosystem health (IPCC 2023; Fécan et al. 1999; Chifflard et al. 2017; Rigden et al. 2020; Vergopolan et al. 2021). Global patterns of decreasing dry-season water availability in the last decades are attributable to anthropogenic forcing, and predominantly in extra-tropical latitudes exacerbate the hydrological imbalance mainly due to increased evapotranspiration (Padrón et al. 2020; Samaniego et al. 2018). Hot and dry summers are expected to become more frequent in the coming decades resulting in more probable occurrence of events like the 2018-2019 Central European Drought (Hari et al. 2020) with even tenfold increase of Compound Dry And Hot Extreme (CDHE) summers under global warming conditions in some European regions (Böhnisch et al. 2025). A stronger negative correlation of soil moisture with the intensity of such CDHE events exists than with solely precipitation or temperature (Böhnisch et al. 2025). Naturally, exceptional soil moisture deficit conditions heavily affect overall vegetation health of grassland, cropland or forests (Reinermann et al. 2019; Reich et al. 2018). Related annual economic drought losses might - in the absence of climate action - rise in the European Union and United Kingdom combined to more than €65 billion per year (Naumann et al. 2021). Crop models that project yield estimates are crucial to ensure agricultural, economic and food security in a (not only) drought related increasingly uncertain future. Information on current state of spatially distributed soil moisture is a strict requirement therefor (Bolten et al. 2010; Rigden et al. 2020). Also, future demand for irrigation water is going to rise in numerous agricultural regions (Busschaert et al. 2022; Zhao et al. 2015) where readily available spatial distributed

soil moisture information can support effective agricultural water management (Singh and Das 2022).

In contrast, a state of high soil moisture content poses great risks likewise. Flooding events result from anomalous high rainfall-runoff transformation due to a combination of soils with reduced infiltrability, resulting from high soil saturation or sealing effects at the soil surface, and a concurrent high intensity precipitation event (Chifflard et al. 2017; Javelle et al. 2010). Devastating flash floods arise in very short time spans, based on the interplay of rapidly increased soil moisture and precipitation excess (Bronstert et al. 2018). A temporally dense information on soil moisture state assists in near real-time numerical weather forecasting and consequently is beneficial in issuing flood warnings (Peng et al. 2021).

In summary, as soil moisture influences many processes that affect both livelihoods and the integrity of natural systems, monitoring this ECV is essential.

The need for high temporal resolution soil moisture data

The knowledge of especially the spatial distributed, accurate, momentary status of soil moisture is crucial for monitoring efforts that need near real-time data as discussed above. Additionally, also in the analyses of past events, a close temporal match of soil moisture state and the to be investigated variable is desirable.

Soil moisture data in the form of spatially distributed grid values is utilized in a plentitude of hydrological modeling applications like streamflow prediction (Alvarez-Garreton et al. 2016), forecasting of characteristics of flood events (Chifflard et al. 2017). Furthermore, gridded soil moisture data is used in agricultural applications like crop yield estimation (White et al. 2020; Vergopolan et al. 2021) or agricultural drought assessment (Souza et al. 2021; Zhu et al. 2019; Ajaz et al. 2019; Carrão et al. 2016) and also at the hydro-agricultural interface with estimation of irrigation water use (Abolafia-Rosenzweig et al. 2019).

Combining soil moisture modeling with high temporal resolution remote sensing data allows for a more certain generation of up-to-date soil moisture value maps, for example through the process of data assimilation (Crow and van den Berg 2010; Lievens et al. 2017; Zhao and Yang 2018). However, soil moisture exhibits a highly volatile nature and associated alleged rapid changes in the moisture state e.g. after brief rain showers (Vereecken et al. 2014). This

characteristic demands from an auxiliary soil moisture data set to itself provide a very fine temporal resolution when combined with acquisition data in synergistic soil moisture estimation. So far, mostly point measurements provide this level of temporal sampling. An hourly, continuously available spatial data set at high resolution is lacking. In comparison, spatially distributed quantitative estimates of precipitation - the main driver for soil moisture changes - exist in very high temporal resolution from weather radars and respective satellites alike. This thesis investigates the possibilities of taking advantage of the availability of such temporal high resolution precipitation data to derive soil moisture values at similar temporal rates.

In the following subsections this introduction examines overall context of precipitation and soil moisture in the earth system (Section 1.2) before highlighting the challenges that monitoring of both the variables poses (Section 1.3). The outline of modeling options and current state of science in soil moisture derivation (Section 1.4) finally lead to the associated novel work of this thesis presented in the main part (Section 2).

1.2 Precipitation and Soil Moisture in the Environmental System

The global water cycle describes fundamental water exchange processes on the earth (McColl et al. 2017a). Both, precipitation and soil moisture are an integral part of this scheme that formulates the connections between water reservoirs like ocean, atmosphere or freshwater on land and in the soil (see Figure 1). Soil moisture in its general definition describes the available soil water content in the vadose zone, encompassing the root zone of the soil column down to the ground water table (see Figure 2), that is available for plant utilization (Legates et al. 2010). Depending on the application, it is distinguished between SSM and Root Zone Soil Moisture (RZSM). SSM only corresponds to the moisture state of the top soil layer of some centimeters, that is also directly available for evaporation. Compartmentalization of incident precipitation into infiltration or runoff happens at the SSM level depending on the saturation. The RZSM in deeper layers in return is directly linked to vegetation growth and health (Kerr et al. 2010).

Precipitation and soil moisture are deeply interconnected and condition and control each other. So does precipitation generally provide the greatest share of moisture input to the soil water storage. Therefore, the dynamics of soil moisture at a given location highly depend on the incident precipitation; but processes like total evapotranspiration, drainage or percolation below the root zone and lateral flow, runoff generation or interception of water at the canopy also affect the soil moisture state (Katul et al. 2007) .

The input and output fluxes to and from a distinct soil column are formalized in Equation 1 by Legates et al. (2010):

$$\frac{dS}{dt} = (P_r + M) - (E + T) - (R_o + R_s + R_g) \tag{1}$$

that relates the rate of change of soil moisture (dS/dt) to the incoming precipitation (P_r) and snow melt (M), the moisture loss through evaporation and plant transpiration ($(E+T)$) and surface runoff (R_o), lateral subsurface flow (R_s) and percolation (R_g) to the saturated zone of the groundwater.

Although Soil Moisture (SM) only accounts for a small share of 0.15% of liquid fresh water, the variable has a large impact on fluxes of water at the soil-plant-atmosphere continuum

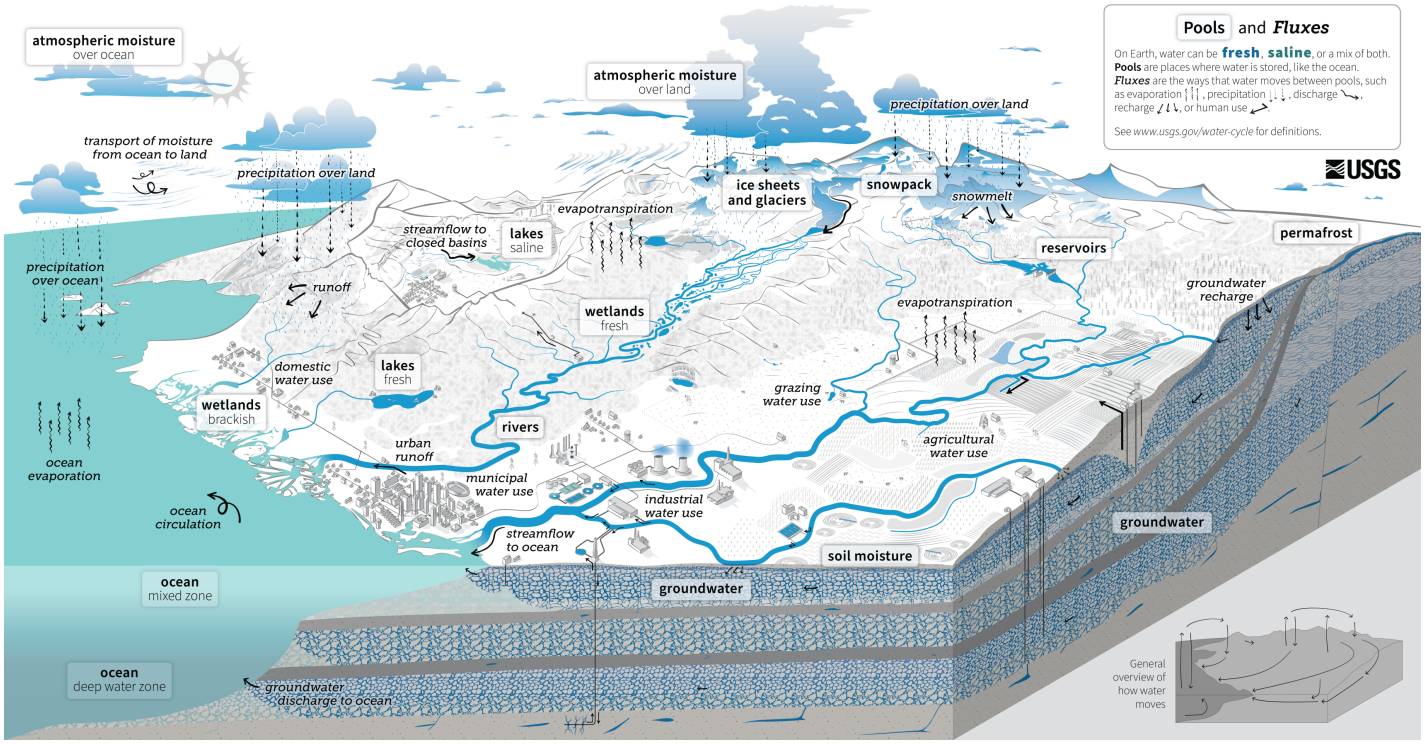

Figure 1: The global water cycle with water pools and fluxes (Corson-Dosch et al. 2022).

(Western et al. 2002; Weil and Brady 2017). That is because soil moisture controls the interface where most of the atmospheric water encounters the earth's surface (McColl et al. 2017a). Hence, the amount of water held in the soil and its vertical distribution regulate the direct evaporation and through plant availability also transpiration rates. With that, water vapor fluxes and consequently partitioning the heat in latent and sensible fluxes released to the atmosphere is directly linked to SM.

Figure 2 displays the main processes that control the soil moisture state at a given location. Some aspects of the relationship in Equation 1 and Figure 2 are unambiguous and indisputable (Sehler et al. 2019). However, other parts of the interaction are complex and even controversial (Krakauer et al. 2010; Sehler et al. 2019). Uncertainties exist regarding feedback mechanisms that alter the mentioned processes and thus the relationship between soil moisture and soil hydrological variables (Koster et al. 2004). The correlation direction and magnitude between SM and precipitation for example vary regionally (Sehler et al. 2019; Guillod et al. 2015). Additionally, related feedback mechanisms contribute to the intricacies of the

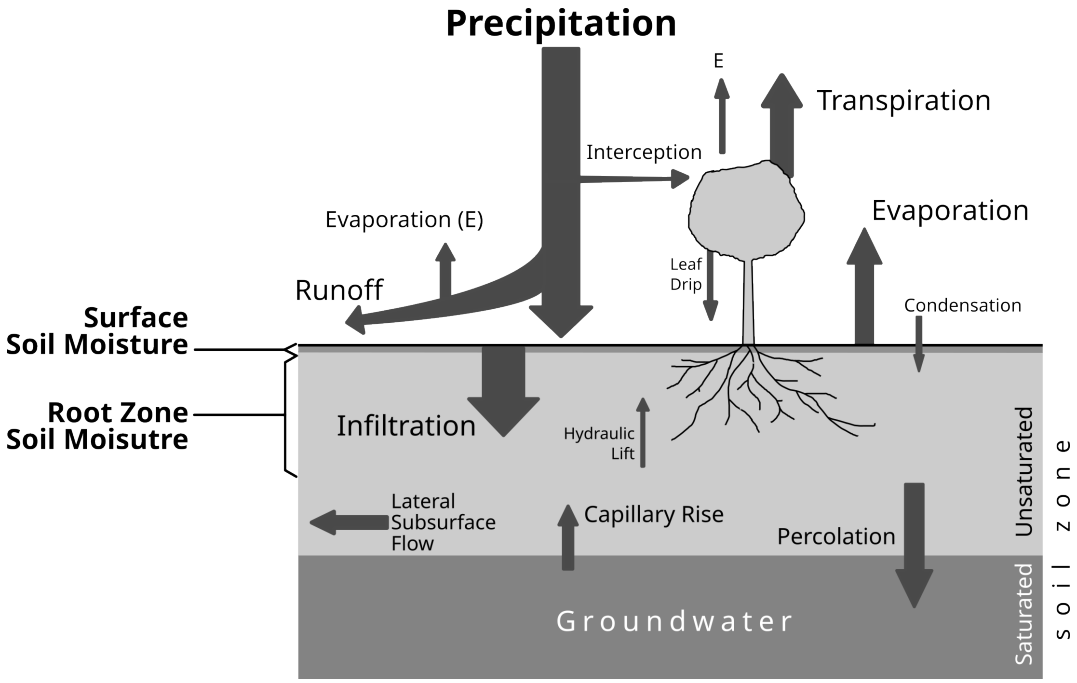

Figure 2: Schematic illustration of main soil hydrological processes and soil moisture related fluxes (adapted from Scholten (2004)).

interplay, for example between evaporation and precipitation, where negative correlation at convective scale and positive at continental scale is found (Balsamo et al. 2018; Guillod et al. 2015; Hohenegger et al. 2009).

Soil moisture is interconnected with so many processes and variables, making it highly representative for the complexity of the ecosystem. The next sections will elaborate on the current possibilities to monitor and model soil moisture.

1.3 Monitoring of Precipitation and Soil Moisture Across Scales

The characteristics of scale in monitoring and in models can, according to Blöschl and Sivapalan (1995), be described as the triplet of "spacing", "support" and "extent". The term "spacing" refers to the temporal or spatial distance between measurement points or modeled cells, "support" describes area or time range over which measurements or model integrations are performed and "extent" denotes the overall coverage (see Figure 3; Babaeian et al. 2019; Western et al. 2002). With changing "support", underlying variations are either averaged out or become visible, and increased "spacing" of measurements lowers the recorded detail, yet does not necessarily change the apparent variation in the signal (Western et al. 2002).

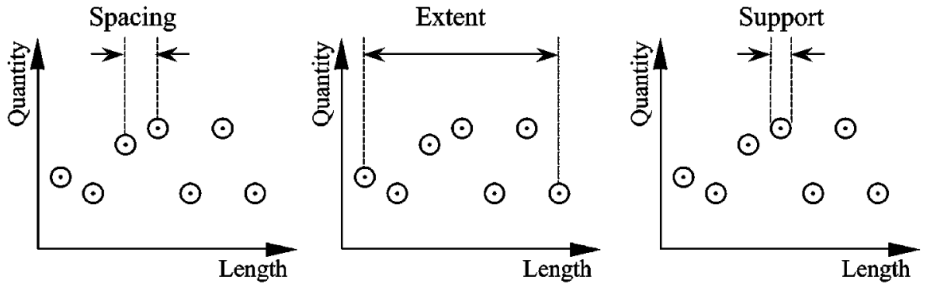

Figure 3: Scale triplet of spacing, extent and support (Western et al. 2002)

Monitoring of both variables, soil moisture and precipitation, starts with point measurements, when regarding the spatial coverage (Miralles et al. 2010). Soil moisture, in the most direct form, is determined from wet bulk samples taken from a study site. The weight difference of the defined volume of soil before and after it is oven-dried, allows for inference of the gravimetric SM θ_m in $[g/g]$: the ratio of the mass of water within the sample and the mass of oven-dried soil material. The volumetric SM θ_v in $[Vol\%]$ then is expressed as

$$\theta_v = \theta_m \left(\frac{\rho_b}{\rho_w} \right) \tag{2}$$

where ρ_b is the dry bulk density of the soil sample (g/cm^3) and ρ_w is the density of water (g/cm^3) (Robinson et al. 2008). Point observations of soil moisture are furthermore obtained with in situ sensing techniques that exploit the response of an electromagnetic field to moisture, either through measurement of travel time through the medium (TDR, time domain reflectometry) or the change in frequency of a reflected electromagnetic wave (FDR, fre-

quency domain reflectometry)(Babaeian et al. 2019). Proximal sensing methods like ground-penetrating radar and cosmic-ray neutron measurements cover larger spatial footprints than above mentioned techniques and can also be employed in mobile sampling setups, thereby facilitating the transition to field-scale measurements (Zhou et al. 2019; Wu et al. 2019; Duygu and Akyürek 2019; Montzka et al. 2017). Operationally, the International Soil Moisture Network aggregates and distributes data from >2800 soil moisture measurement stations (Dorigo et al. 2021).

Monitoring precipitation, meaning the process but also the amount of water that is deposed from the atmosphere in solid or liquid form, appears to be simple at the point scale (Kidd et al. 2017). Rain gauges are the most common and provide the most direct measurement of in situ precipitation (New et al. 2001; Foehn et al. 2018). Retrieved rain rates are very accurate at optimal conditions, however the measurement is also error-prone if adversities arise. The highest uncertainties stem from wind-induced measurement errors (Kochendorfer et al. 2017). Considering rain gauges spatially representative of their surrounding remains - although necessary - a strong claim (Foehn et al. 2018). Furthermore, focusing the large number of globally available precipitation gauges (> 100.000) masks imbalances in regional coverage (New et al. 2001; Kidd et al. 2017): the gauges are placed population centric, meaning that many regions on the globe are deficient in precipitation gauges; when extending the coverage region around every gauge that reports to the Global Precipitation Climatology Center (GPCC) by 5 km (no overlap), still only 1% of the Earth's surface is covered (Kidd et al. 2017).

The challenge with point measurements of both soil moisture and precipitation lies in their inability to adequately capture the inherent high spatial variability of these parameters. The spatial 'support' of the data points is small and the 'spacing' mostly large, which in summary hinders a straightforward inference of a spatial representation, especially for soil moisture where not only the variability of precipitation input but additionally soil structural differences have an effect. Remote sensing approaches deliver spatially explicit soil moisture and precipitation measurements. Instruments onboad of aircrafts and UAVs can produce regional data sets of soil moisture whereas weather radar systems show similar capabilities in spatial coverage for quantitative precipitation estimates (Wu et al. 2019; Babaeian et al. 2019; Winter-

rath et al. 2019). Operationally, only the latter is feasible over a prolonged period of time. In contrast, satellite-based sensors might provide global coverage for both variables at regular time intervals.

Estimation of soil moisture from space exploits the interaction of electromagnetic waves in the optical, thermal and microwave range of the spectrum. Optical remote sensing sensors capture radiation from 350 to 2,500 nm whereby the spectral resolution differs and classifies the instruments in multi- and hyperspectral sensors (Babaeian et al. 2019). Optical imagery based algorithms respectively allow for soil moisture retrieval of the top soil layer (SSM) with strong limitations imposed by cloud and vegetation cover. The combination of optical data with thermal imagery (3,5-14 µm) enables soil moisture estimation via, inter alia, the i) Thermal-Optical Triangle Method (TOTRAM), which interprets the combination of pixel-based Land Surface Temperature (LST) and a vegetation index, the ii) Optical Trapezoid Model (OPTRAM), which exploits the physical relationship between transformed shortwave infrared reflectance and soil moisture or iii) a model that employs the elliptical relationship between LST and net surface shortwave radiation (Sadeghi et al. 2015; Babaeian et al. 2018, 2019; Wang et al. 2018). However, continuous satellite-based monitoring of soil moisture is feasible primarily through active and passive microwave sensors, as these can record imagery of the Earth's surface independent of cloud coverage (Njoku and Entekhabi 1996; Wigneron et al. 1998; Owe et al. 2001; de Jeu et al. 2008; Naeimi et al. 2009; Das and Paul 2015). Furthermore, the active radar variants penetrate canopy and even soil depending on the utilized wavelength. The recorded backscatter is related to the dielectric properties of the surface that greatly differ between solid, air and water phase (Ochsner et al. 2013). Hence, this signal is used to infer soil water content (Babaeian et al. 2019). Among the most prominent sensors are the Soil Moisture and Ocean Salinity (SMOS, Kerr et al. (2001)) mission, the Advanced Scatterometer (ASCAT, Bartalis et al. (2007); Wagner et al. (2013)), the Soil Moisture Active Passive (SMAP, Entekhabi et al. (2010)) mission, and the Advanced Microwave Scanning Radiometer (AMSR-E/AMSR-2, Njoku et al. (2003); Du et al. (2017)) all with spatial resolution of tens of kilometers (Vereecken et al. 2022). Downscaling procedures (Peng et al. 2017; Merlin et al. 2008; Fang et al. 2018; Li et al. 2018) and multi-sensor integration (Santi et al. 2018; Kim et al. 2018) facilitate the production of soil moisture data sets with higher spatio-temporal resolution and coverage (Piles et al. 2016). A prominent example of sensor integration is Eu-

ropean Space Agency (ESA)'s Climate Change Initiative (CCI) soil moisture product, providing a consistent global soil moisture data set from 1978-now at daily resolution (Gruber et al. 2019; Dorigo et al. 2017, 2015). Synthetic Aperture Radar (SAR) systems, e.g, ESA's Sentinel-1 constellation (Torres et al. 2012), natively produce a higher spatial resolution of tens of meters than the before mentioned radiometers and scatterometers. The utilization of radiative transfer models allows for SAR based soil moisture retrieval at field scale (Mattia et al. 2015; Weiß et al. 2024). With that, the temporal resolution of such procedures is limited to a few days, depending on the respective satellite overpass repeat cycle.

Global gridded precipitation data sets might be deduced from gauge measurements for land-surface precipitation (Schamm et al. 2014; Becker et al. 2013). However, for several decades, satellites have provided spatially explicit quantitative precipitation estimates (Sun et al. 2018). Geostationary satellites carrying sensors that cover the visible and infrared part of the spectrum and low earth orbit platforms that utilize active and passive microwave imaging systems are in use (Kidd and Levizzani 2011). The available data sets oftentimes comprise a whole constellation of satellites, e.g., NASA's Global Precipitation Measurement (GPM, Skofronick-Jackson et al. (2017)) Mission, the Precipitation Estimation from Remotely Sensed Information using Artificial Neural Networks (PERSIANN)-Climate Data Record (CDR) program which aggregates (historical) multi-satellite records (Ashouri et al. 2015) and the Global Precipitation Climatology Project (GPCP) that integrates various satellite data sets with gauge data (Adler et al. 2003). Reanalysis datasets, such as the fifth-generation product from the European Centre for Medium-Range Weather Forecasts (ECMWF), known as ERA5 (Hersbach et al. 2018), along with advanced data merging techniques like the Multi-Source Weighted-Ensemble Precipitation (MSWEP) dataset (Beck et al. 2017), are designed to enhance the accuracy and spatio-temporal consistency of gridded precipitation estimates.

1.4 Modeling of Soil Moisture - Development and State of Science

The reason and ideas behind soil moisture modeling are mostly twofold: i) modeling SM in a Land Surface Model (LSM) to close the hydrological cycle or ii) modeling for immediate subsequent investigation or application of the SM data set. For the second case, direct derivation of related parameters or processes (e.g. erosivity, yield) or the further usage of the created data set in a data fusion scheme are conceivable procedures. Therefore, soil moisture models are diverse in their depth and characteristics and range from simple empirical simulations to physics-based algorithms that are fully integrated into LSMs.

For a homogeneous soil volume, a typical representation of the moisture state and development is the "bucket model" (Guswa et al. 2002): a simple 1D soil moisture balance equation or vertically integrated water budget (Rahmati et al. 2024; McColl et al. 2017b) that adds a dependence on saturation $S(t)$ at time t to the loss rate $L(S(t))$ in comparison to the overall description of soil moisture related processes in Equation 1:

$$C_s \frac{dS(t)}{dt} = P(t) - L(S(t)) = P(t) - [D(S(t)) + ET(S(t)) + Q(S(t))] \tag{3}$$

where $P(t)$ is the rainfall rate, C_s is soil water storage capacity, $Q(S(t))$ is surface runoff rate, $D(S(t))$ is the drainage rate and $ET(S(t))$ is evapotranspiration; all as a function of $S(t)$. For such models application of different loss functions for different saturation regimes is common practice. The amount of precipitation that contributes to the soil water reservoir is indirectly dependent on the saturation state, as runoff $Q(S(t))$ immediately diminishes the change in saturation state.

LSMs mostly implement a more physics based reproduction of the infiltration process in porous media, that is formulated in the Richards equation:

$$\frac{\partial \theta}{\partial t} = \frac{\partial}{\partial z}\left[K(h)\left(\frac{\partial h}{\partial z} + 1\right)\right] \tag{4}$$

where θ is the actual water content in the medium, t is time, z is depth, h is the matrix potential, and $K(h)$ is the hydraulic conductivity function, in dependence on the matrix potential (Vereecken et al. 2019). However, analytical solutions can only be derived if specific initial and boundary conditions are set and with knowledge of the soil hydraulic properties, because

of the nonlinear character of the hydraulic conductivity function $K(h)$ (Vereecken et al. 2019). Therefore, LSMs like HYDRUS-1D (Šimůnek and van Genuchten 2008), ORCHIDEE (de Rosnay et al. 2002) or ISBA-SURFEX (Decharme et al. 2011; Sobaga et al. 2023) normally apply numerical solutions using finite difference methods to solve the Richards equation (Vereecken et al. 2019).

Modeling of soil moisture further can be used to add to and enhance an existing data set (Liu and Yang 2022). Operational data fusion products and downscaling efforts are examples thereof and have already been named in the preceding section. Moreover, interest in distributed, possibly satellite data based, estimation of RZSM is reported (Peng et al. 2021), that can be addressed via assimilation of SSM into LSMs (Kolassa et al. 2017; Kim et al. 2021; Seo et al. 2021; Dumedah et al. 2015) but also through direct modeling of a variants of the Richards equation (see Equation 4) like e.g. Sadeghi et al. (2016) presented for NASA's Airborne Microwave Observatory of Subcanopy and Subsurface (AirMOSS) mission (Babaeian et al. 2019).

Furthermore, machine learning practices are applied to obtain RZSM (Zeng et al. 2019; Kasim et al. 2025), improve regionally retrieval of SSM from polarized microwave imagery (Santi et al. 2019), but also to provide global soil moisture data sets (O and Orth 2021; Zhang et al. 2021a, 2023).

1.5 Thesis Rationale and Outline

Peng et al. (2021) claim the need for long-term soil moisture data sets with high spatial and temporal resolution in many domains. On the road to very high spatial and temporal resolution satellite soil moisture mapping, auxilliary and intermediate data is needed, to support the retrieval and fill in temporal gaps. Tackling the highly volatile nature of soil moisture is merely possible with at least hourly data. With lower temporal resolution, satellite retrievals are likely misinformed. A continuously available spatial data with such temporal sampling is however still lacking.

Precipitation provides the main moisture input to the soil column and Quantitative Precipitation Estimates (QPE) are nowadays available regionally and globally at very high temporal resolution with ever improving monitoring constellations in space and increased availability of weather radar networks. Exploiting that fact in an empirical, transferable modeling approach to derive a SM data set that is capable of providing timely information on upsurge in soil water content, yet also delivers physically sound soil moisture values, is a challenge to be solved. This thesis consequently investigates the performance of high resolution soil moisture data derived from remotely sensed precipitation estimates. More precisely, this work examines especially the merits of high temporal sampling of QPEs in the porposed modeling scheme and the resulting quality of the empirical soil moisture product.

Therefore, firstly, the German weather radar system RADOLAN, that provides gauge-adjusted QPE, and the Global Precipitation Measurement (GPM) mission, providing state-of-the-art QPE from a satellite constellation were identified as precipitation input data sets on regional and global scale respectively. These data sets are evaluated against each other with the following research questions to be answered:

- *RQ1.1: Does the GPM IMERG satellite-based precipitation data set show similar performance of detection of precipitation as the RADOLAN weather radar data?*
- *RQ1.2: Do GPM and RADOLAN show the same spatial and seasonal trends in precipitation patterns?*

Secondly, a temporal high resolution SM data set for the state territory of Germany, based on an adjusted Antecedent Precipitation Index (API) algorithm and utilizing RADOLAN weather radar data is developed (RADOLAN_API). In situ measurements of the International Soil Moisture Network (ISMN) and the gridded ESA CCI SM data set are used to validate the effort. The following questions will be answered:

- *RQ2.1: Can the empirical soil moisture index (RADOLAN_API) based off the antecedent precipitation index resemble the course of local soil moisture measurements throughout Germany?*
- *RQ2.2: Are rapid upsurges in soil moisture and seasonal variations captured in the data set?*
- *RQ2.3: Does the RADOLAN_API perform equally well as the renowned ESA CCI SM data set and adhere to GCOS defined error margins?*

Thirdly, the GPM data is utilized as input and further adjustments and considerations regarding spatial variability are included in the creation of a global SM data set (GPM_API). The same foundational requirements concerning temporal resolution are upheld and the data set similarly is validated against in situ measurements and the ESA CCI SM data set.

- *RQ3.1 Is a quality SSM product deducible from GPM data that adheres to the accuracy requirements for soil moisture products provided by the GCOS?*
- *RQ3.2 Can GPM_API represent different soil moisture regimes on a global scale?*
- *RQ3.3 Does the quality of GPM_API vary across regions and top soil compositions?*
- *RQ3.4 How does the GPM_API data set compare with ESA CCI soil moisture data set?*

These questions are investigated throughout three scientific articles which are presented in the next section.

2 Scientific Publications

This thesis is based on three scientific publications, all of which have been fully published in peer-reviewed journals: Remote Sensing (MDPI) and the International Journal of Remote Sensing (Taylor and Francis). The following sections each present an overview of the research subjects and concepts addressed in the particular article followed by the published version of the manuscript itself.

Article I focuses on the weather radar and satellite based precipitation input data sets that are further used in study two and three respectively. The comparison and evaluation comprises the territory of Germany as the weather radar data is limited to this domain. The investigation presents spatial patterns and seasonal differences between the RADOLAN weather radar data and the GPM IMERG satellite based precipitation estimates.

Article II evaluates the empirical soil moisture product RADOLAN_API for Germany. The data set is based on weather radar precipitation data and utilizes air temperature and soil characteristics as relevant variables in steering the water loss in the top soil. Fitting additional empirical factors in the API based algorithm allows for the derivation of sensible soil moisture values from the enhanced antecedent precipitation index calculation.

Article III extends the spatial scope of investigation to the global scale and demonstrates the performance of a GPM IMERG data based soil moisture data set. Again, the derivation of the soil moisture state utilizes an API based algorithm, with a global soil map and reanalysis temperature data as auxiliary input. To accommodate site specific water loss functions, the calculation includes spatial diverse empirical factors that control the soil moisture decline.

2.1 Article I: Comparison of the GPM IMERG Final Precipitation Product to RADOLAN Weather Radar Data over the Topographically and Climatically Diverse Germany

---

Journal: Remote Sensing **Status**: published **IF**: 5.349

Reference: Ramsauer, T., Weiß, T., & Marzahn, P. (2018): Comparison of the GPM IMERG final precipitation product to RADOLAN weather radar data over the topographically and climatically diverse Germany. *Remote Sensing*. 10 (12), 2029. DOI: 10.3390/rs10122029

Scope and Context:

Article I focuses on the comparison of two precipitation data sets that in the other two contributing publications are used as basis for the soil moisture derivation. The differences of the RADOLAN RW weather radar data and the GPM IMERG satellite based precipitation estimates are evaluated towards the capability of capturing the spatio-temporal variability of rainfall events throughout the domain of Germany. For that, besides standard statistical measures like Root Mean Square Difference (RMSD), correlation and bias, also categorical indices like 'probability of detection' that allow a binary evaluation of the detection characteristics of the precipitation data sets are applied. A gridded ground truth data set is not available, so the gauge adjusted RADOLAN data set is used in that fashion for the investigation. A general lack of spatial variability in the GPM data is apparent due to the lower initial spatial resolution. Hence, topographically-induced rainfall are underestimated. The RADOLAN weather radar data set shows higher detection rates, yet the GPM data is positively biased in the quantity of rainfall overall.

The comparative nature of the article's content plays the introductory role of presenting the precipitation data sets utilized in the soil moisture data generation of article II & III.

remote sensing

MDPI

Article

Comparison of the GPM IMERG Final Precipitation Product to RADOLAN Weather Radar Data over the Topographically and Climatically Diverse Germany

Thomas Ramsauer *, Thomas Weiß and Philip Marzahn

Department of Geography, LMU Munich, Luisenstraße 37, 80333 Munich, Germany;
t.weiss@iggf.geo.uni-muenchen.de (T.W.); p.marzahn@iggf.geo.uni-muenchen.de (P.M.)
* Correspondence: t.ramsauer@iggf.geo.uni-muenchen.de; Tel.: +49-(0)89-2180-4183

Received: 15 October 2018; Accepted: 2 December 2018; Published: 13 December 2018

Abstract: Precipitation measurements provide crucial information for hydrometeorological applications. In regions where typical precipitation measurement gauges are sparse, gridded products aim to provide alternative data sources. This study examines the performance of NASA's Integrated Multi-satellitE Retrievals for the Global Precipitation Measurement Mission (IMERG, GPM) satellite precipitation dataset in capturing the spatio-temporal variability of weather events compared to the German weather radar dataset RADOLAN RW. Besides quantity, also timing of rainfall is of very high importance when modeling or monitoring the hydrologic cycle. Therefore, detection metrics are evaluated along with standard statistical measures to test both datasets. Using indices like "probability of detection" allows a binary evaluation showing the basic categorical accordance of the radar and satellite data. Furthermore, a pixel-by-pixel comparison is performed to assess the ability to represent the spatial variability of rainfall and precipitation quantity. All calculations are additionally carried out for seasonal subsets of the data to assess potentially different behavior due to differences in precipitation schemes. The results indicate significant differences between the datasets. Overall, GPM IMERG overestimates the quantity of precipitation compared to RADOLAN, especially in the winter season. Moreover, shortcomings in detection performance arise in this season with significant erroneously-detected, yet also missed precipitation events compared to the weather radar data. Additionally, along secondary mountain ranges and the Alps, topographically-induced precipitation is not represented in GPM data, which generally shows a lack of spatial variability in rainfall and snowfall estimates due to lower resolution.

Keywords: precipitation; weather; radar; GPM; RADOLAN; QPE

1. Introduction

Precipitation is of paramount importance as a driver of the global water and energy cycle and interactions between the bio-, hydro-, and atmosphere and thus has been declared as an Essential Climate Variable (ECV) [1]. Information on the spatial and temporal distribution of this crucial variable helps in understanding its vast impact on numerous environmental aspects of life on Earth. Water resource management, predicting and monitoring agricultural yields, or disaster prevention and ultimately management are exemplary fields that strongly depend on accurate precipitation measurements. Traditional measurement gauges are sparse in many parts of the world [2], which hindered the deduction of meaningful precipitation estimates for these regions until a few decades ago, when gridded (satellite) products came to close these gaps. Currently, a physically-measured precipitation distribution can be acquired via interpolation of gauge measurements, weather radar estimates, or satellite observation. At the global scale, the spatial variability of rain and snowfall can

be best represented with remote sensing imagery, as radar and gauge measurement stations are not available world-wide with sufficient density and coverage. Moreover, time-series of satellite data let global precipitation patterns and distribution become apparent. Still, region-specific differences in climate and topography are determinant factors for uncertainties in the performance of satellite precipitation products. Currently, developments to improve gridded precipitation data utilize creation or correction approaches for satellite-based precipitation products (SPP) from satellite soil moisture retrieval data [3–8] or combine datasets from various sources like gauge measurements, atmospheric models, and satellite observations [9].

NASA's Global Precipitation Measurement (GPM) mission launched the GPM Core Observatory (CO) as the successor of the well-renowned Tropical Rainfall Measuring Mission (TRMM) spacecraft in 2014 [10]. Additional channels on both the Dual-frequency Precipitation Radar (DPR) and on the GPM Microwave Imager (GMI) make it an advanced replacement of the older satellite. The Integrated Multi-Satellite Retrievals for GPM (IMERG) gridded dataset used in this study is a Level 3 NASA product which, unifies and inter-calibrates data of about 10 constellation satellites from several space agencies based on the GPM CO [11–13].

Numerous comparison studies involving GPM data have been carried out over different spatial domains, e.g., global [14], Canada [15], Singapore [16], Malaysia [17], China [18–20], India [21], Iran [22], and Saudi-Arabia [23]; yet, investigations covering European countries are sparse, and no detailed comparison over Germany exists until today. However, the consistent availability at high temporal and spatial resolution and hence lowered uncertainty propagation in the results of hydrological modeling make GPM a viable data source for applications across European catchments of different scales [24]. Nevertheless, systematic bias and random errors are usually contained in satellite precipitation estimates [25,26]. Mei et al. [27] showed that SPPs furthermore are prone to underestimation of extreme events and hence are the main contributor to the total error in their hydrological modeling setup. Although GPM data are currently barely used in hydrology-related modeling scenarios in Europe, numerous future applications have been proposed. The topics cover, e.g., landslide threshold precipitation in the Italian Umbria region [28], debris flow-triggering rainfall [29], or modeling of flood events in alpine terrain [30]. Moreover, GPM data are now incorporated in the Global Flood Detection System (GFDS [31]) [32]. The insufficient performance of this dataset over Germany, which has been demonstrated in a validation study in the TRMM era [33], generates uncertainty for future usage. Hence, a performance test of GPM over Germany is necessary, to allow questioning these kinds of results over this or similar geographic regions.

Furthermore, the existing comparison setups include different datasets. Speirs et al. [34] for example compared GPM DPR to the MeteoSwiss radar network with a focus on mountainous regions. The radar data are adjusted, yet only to a very limited number of gauges (6–10, 33) and not on an operational basis, but to long-term mean precipitation values. Other studies also evaluated GPM (and mostly the DPR product) against weather radar datasets [35–37] where many focused on performance towards snow detection [38–43]. The resulting findings indicate huge improvements compared to the TRMM era. Yet, the need for future improvements of the algorithm to further enhance the IMERG abilities in freezing conditions still persists [22,34,40,44,45].

Studies on the performance of SPPs are strongly location dependent with highly diverse correlation values to gauge measurements especially in challenging topography [17,46]. Therefore, the evaluation of quantitative precipitation estimates (QPE) is vital before operationally applying them in a specific study site. Germany, in additional to its diverse topography, lies in the transition zone from oceanic to continental climate with different apparent precipitation schemes, making it a very interesting and challenging case study.

The novelty in the presented case is the comparison of the final GPM IMERG data to a temporal and spatial high resolution precipitation product. This product is the state-of-the-art weather radar-derived and operationally gauge-adjusted precipitation product RADOLAN RW from the German Weather Service (DWD, Deutscher Wetter Dienst). Due to the high sampling frequency,

short-scale precipitation events can be captured. Furthermore, the hourly online adjustment routine makes it a balanced dataset, adhering to a high degree to the gauge measurements without cutting out extreme events [47,48].

To assess the performance of GPM over complex terrain, throughout seasons and consequently on different precipitation regimes, the study aims to compare final GPM IMERG against RADOLAN RW data from DWD. Therefore, different standard statistical measures, as well as a range of categorical indices are applied and evaluated on a pixel-by-pixel basis. Utilizing this form of spatial comparison accounts for the drastic topographic differences throughout the study area with landscapes including lowlands, secondary mountain ranges to alpine peaks with heights up to 3000 m.a.s.l., as well as for the different seasons and precipitation regimes. Thus, two hypotheses will be addressed throughout the study: (1) GPM shows similar detection performance over different topographic and climate zones compared to RADOLAN data; (2) GPM and RADOLAN show the same spatial and seasonal trends in precipitation.

2. Study Area

The spatial bounds for the dataset comparison are comprised of the state territory of Germany, which extends from 47° to 55°N and from 5° to 16°E, respectively, and covers an area of 357,021 km^2.

The topography is diverse, with lowlands in the north, uplands and secondary mountain ranges in central region and the foothills of the Alps, and adjacent summits with their highest peak being Zugspitze (2962 m.a.s.l.) in the southern part of Germany. An overview of the study area is given in Figure 1. Accordingly, the relief variability increases towards the southern part, where strong gradients in temperature and precipitation are caused by steep slopes in the mountainous region over a very short horizontal distance. For example, Garmisch-Partenkirchen at the foot of Zugspitze is characterized by a mean temperature of 7.2 °C and annual precipitation of 1231 mm, whereas the summit weather station yields −3.7 °C and 1978 mm. Overall, a temperate seasonal climate prevails with mean temperatures ranging from −3.7 °C to 11.0 °C and a mean annual precipitation ranging from 483 mm to 2340 mm.

The distribution of precipitation in Germany is induced by the spatial position of the state lying in between the oceanic Western Europe and the continental Eastern Europe. Amounts of precipitation, mostly brought by humid westerly winds, decrease towards the eastern parts of the study area, yet regions in the extreme south and parts of the uplands in central Germany show higher precipitation amounts due to their mountainous climate. In the winter time, solid precipitation in the form of snow is more common in areas with continental influence.

The time period from 1 December 2014 to 30 November 2017 is analyzed in this study.

3. Data and Methodology

3.1. Datasets

3.1.1. Weather Radar Data

The gauge-adjusted quality-controlled RADOLAN RW (Radar Online Adjustment) dataset from the German Weather Service (DWD, Deutscher Wetter Dienst) is considered ground truth for the upcoming analyses. It is already widely used, e.g., for training and validation purposes in the machine learning domain [49,50], analyzing extreme flash floods [51], as well as enhancing the respective forecasts [52] and estimating the spatio-temporal variability of soil erosion [53].

The radar dataset is currently derived from 18 C-band weather radars operating on scanning intervals of 5 minutes. All but the radar station “Hohenpeißenberg”, which is used for quality control, contribute to the quantitative precipitation analysis. The observational network’s spatial distribution is shown in Figure 1 along with the associated coverage of each device with a radius of 150 km. Significant overlap within the dense radar network ensures accurate retrievals, since problems from

dampening in the signal with increased distance from the sensor and hence missing or misinterpreting precipitation events are minimized [54]. In the last few years, the weather radars have been gradually updated to dual-polarized scanning devices that allow discriminating the sort of hydrometeors [54]. Within the specific calibration procedure, rain intensity-adapted Z-R relationships (empirical formula to estimate rainfall rates from reflectivity signal strength) and statistical clutter filtering are applied, and orographic shadowing effects are considered [48,55,56].

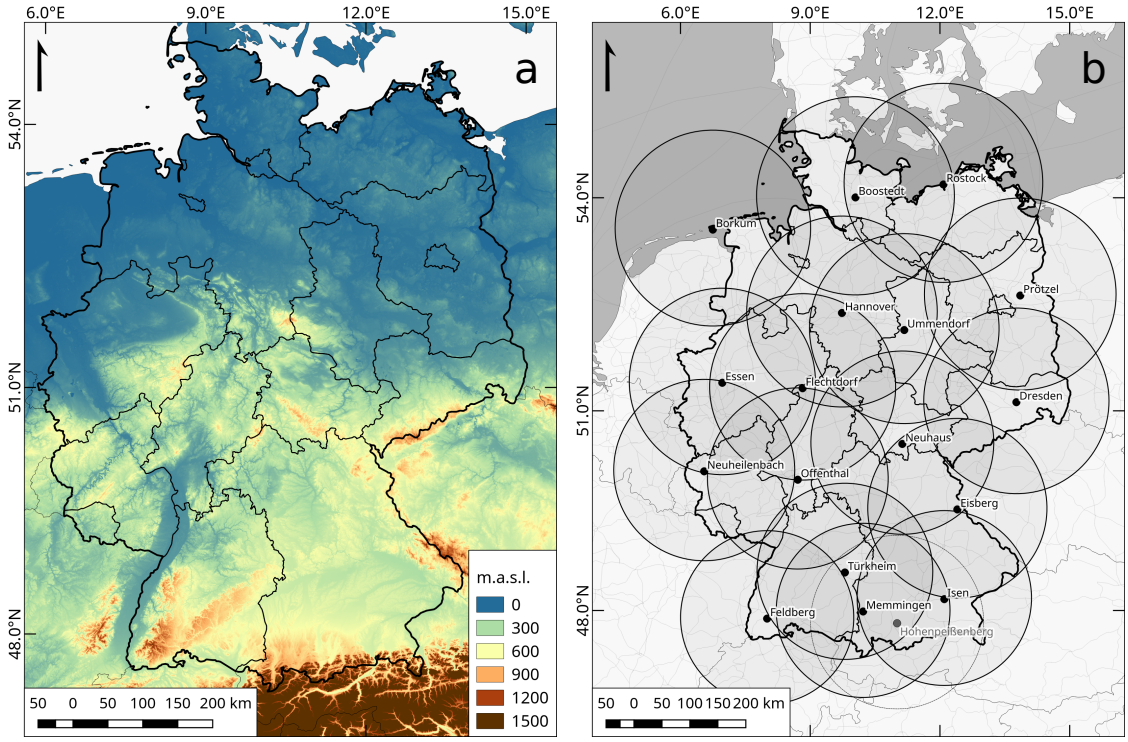

Figure 1. Digital elevation model of Germany based on SRTM 1 arc second data (**a**) and the observational network of weather radar stations contributing to the RADOLAN dataset (**b**).

Assumptions on the drop size distribution and droplet count are necessary for the deduction of precipitation [54]. For RADOLAN, an extended Z-R relationship is utilized, as opposed to solely using standardized values from the literature. The relationship takes the absolute reflectivity, as well as horizontal gradients into account to distinguish typical convective and stratiform droplet distributions [48]. Furthermore, potential overshooting effects in wintertime due to lower cloud heights are considered with a seasonally-dependent correction via a regression analysis. However, a general linear correction scheme does not fulfill the requirements of DWD due to erroneous adaptation of single extreme events, e.g., intensive convective cells that occur regularly throughout Germany in the summer. Therefore, a multiple polynomial regression is calculated to generate the correction factors for every pixel. This accounts for the respective scanning height class, day of year, and reflectivity [54]. The enhancements concerning dual-polarization radar relevant Z-R relationships were not integrated in the online adjustment routine at the time of data acquisition.

Nevertheless, for a realistic estimation of the quantity of precipitation, measurements of approximately 1300 conventional stations are used for the operational hourly gauge adjustment routine [55]. These sensors (Ott PLUVIO) basically work according to "Hellmann" ombrometers [57], which obey the standards of the World Meteorological Organization [58]. The appliance of a weighing principle and surrounding temperature-dependent heating sets the PLUVIO apart from conventional measurement systems and allows capturing solid and fluid precipitation alike [48]. A subset of the

gauge stations is used in the generation of the monthly Global Precipitation Climatology Centre (GPCC) product.

The precipitation product is available at a temporal, spatial, and intensity resolution of 1 h, 1 km, and 0.1 mm. A dimension of 900 × 900 pixels allows the polar-stereographic composite grid with the center point at 9.0°E 51.0°N to cover the whole state territory of Germany [47,48]. Throughout this study, the dataset will be referred to as "RADOLAN".

3.1.2. Satellite Data

The GPM IMERG Version 5 final precipitation half hourly dataset with 0.1-degree spatial resolution is compared to the aforementioned radar precipitation dataset. The GPM Core Satellite is equipped with a multi-channel, dual-polarization Passive Microwave sensor (PMW) and an active scanning radar. Improvements to the predecessor TRMM satellite include increased orbital inclination from 35° to 65° for improved coverage, upgraded radar to two frequencies, as well as additional "high-frequency" channels in the PMW, both allowing for and facilitating the detection of light and solid precipitation, respectively [12,13]. In Version 5, the research-level "final" dataset is adjusted monthly to the extensive GPCC gauge-based dataset, which is available at 1.0° × 1.0° spatial resolution [59]. In the study, the dataset will be addressed as "GPM".

3.1.3. Preprocessing of Datasets

In order to make the datasets spatially and temporally comparable, the RADOLAN dataset was reprojected from the DWD-specific stereographic projection to WGS84, remapped, and aggregated to the GPM grid. Remapping routines using bilinear interpolation or high-order finite-differencing techniques may lead to unexpected behavior, e.g., higher local maxima, and are non-conservative; hence, they behave inconsistent with regard to precipitation sums in the original and regridded dataset [60,61]. Furthermore, bilinear remapping schemes produce significant changes especially to categorical skill scores [62]. Therefore, the ideal regridding scheme to use for precipitation data, being discontinuous over space and time, is the area conservative regridding, which calculates fractional contributions of grid cells from the original data and hence maintains the same area-averaged rainfall before and after the remapping [63]. Thus, the specifically-applied spatial averaging procedure to remap the finer RADOLAN grid data to the coarser GPM grid utilizes the first order conservative remapping scheme from Jones [64], comprised in the Climate Data Operators software (CDO), which applies the SCRIP algorithm (Spherical Coordinate Remapping and Interpolation Package) [65,66]. This technique is widely applied in other studies dealing with precipitation data [67–69]. The area-averaged precipitation quantity $\bar{F}_k$ at the destination grid is calculated as follows:

$$\bar{F}_k = \frac{1}{A_k} \int_{A_k} f dA \quad (1)$$

where A_k denotes the area of the destination grid cell k and f is the precipitation quantity in the original grid, which has an overlapping area with the destination grid [64].

Furthermore, the GPM data were aggregated temporally to match RADOLAN's hourly resolution. Both datasets were clipped to the extent of the state territory of Germany.

3.2. Methodology

The GPM satellite precipitation dataset was statistically compared to RADOLAN weather radar data. Generally, in investigations like this, quality checks of the involved data are critical to produce meaningful results in the end. In this study, 55 weather radar hourly grids are reported as missing, representing solely 0.17% of the considered time steps. The GPM time series is complete. Furthermore, visual interpretation of the radar images for the time span under review indicates no erroneous data

concerning typical radar-related errors like beam blockage and artifacts, which occurred in the first versions of the distributed RADOLAN data at the beginning of the recording period.

To determine whether the datasets show seasonally-dependent dissimilar behavior, due to different precipitation schemes and the higher prevalence of snowfall in winter, the statistical analysis was split into the four meteorological seasons winter (DJF), spring (MAM), summer (JJA), and fall (SON). Overall, statistical comparisons of precipitation sums and means have been carried out. Pixel-by-pixel difference and correlation analyses were conducted additionally to provide a spatial representation of the level of compliance of the RADOLAN and GPM datasets. Pearson's r was used as the correlation measure.

$$r = \frac{cov(P_{\mathrm{GPM}}, P_{\mathrm{RADOLAN}})}{\sigma_{P_{\mathrm{GPM}}} \sigma_{P_{\mathrm{RADOLAN}}}} \tag{2}$$

Furthermore, the overall unconditional bias B was calculated for the data with the following formula.

$$B = \frac{\sum_{i=1}^{N} P_{\mathrm{GPM}_i}}{\sum_{i=1}^{N} P_{\mathrm{RADOLAN}_i}} \tag{3}$$

A perfect linearity of precipitation measurement amounts in GPM and RADOLAN results in a value of 1.

To represent the average magnitude of the error, the Mean Absolute Error (MAE) is used:

$$\mathrm{MAE} = \frac{\sum_{i=1}^{N} |P_{\mathrm{GPM}_i} - P_{\mathrm{RADOLAN}_i}|}{N} \tag{4}$$

The Root Mean Squared Error (RMSE) with greater weight for larger errors than the aforementioned MAE is also part of the statistical evaluation:

$$\mathrm{RMSE} = \sqrt{\frac{1}{N} \sum_{i=1}^{N} (P_{\mathrm{GPM}_i} - P_{\mathrm{RADOLAN}_i})^2} \tag{5}$$

where P_{GPM} and P_{RADOLAN} are the satellite and weather radar precipitation estimates, respectively, i denotes the ith hourly event in the case of the pixel-by-pixel calculation, and the ith element (all pixels over all time steps) for the overall calculation. In the same way, N stands for observed hourly values per pixel or the product of the count of pixels and the count of hourly values, respectively.

Furthermore, the ability to ascertain wet days with precipitation amounts greater than 1 mm was examined to allow for inferences to be made about the detection rates of the two precipitation datasets. Therefore, the count of these days and the respective mean precipitation sum have been evaluated for the datasets on a seasonal basis.

Additionally, categorical indices are calculated to further the knowledge about detection performance. They allow the evaluation of the binary accordance of the precipitation datasets, meaning to see if events are captured uniformly in both datasets. This has been done for the spatially-aggregated datasets, as well as on a pixel-by-pixel basis. For these calculations, the contingency grid shown in Table 1 is used, where a, b, c, and d represent the total count of data pairs matching the requested criteria. RADOLAN is chosen as reference due to the originally higher spatial resolution and the higher temporal frequency in adjusting to gauge measurements. For further information on the metrics used, please refer to, e.g., Woodcock [70], Doswell et al. [71], Schaefer [72].

Table 1. Contingency table for the calculation of categorical indices.

		RADOLAN	
		Rain	**No Rain**
GPM	**rain**	a	b
	no rain	c	d

The Probability Of Detection (POD) for GPM measurements over Germany in the reported time period can be written as:

$$\mathrm{POD} = \frac{a}{(a+c)}, \tag{6}$$

and gives a measure of how effective the satellite observations detect a rain event compared to RADOLAN with the perfect score being 1.

The opposite case, where precipitation is erroneously indicated by GPM, is assessed with the False Alarm Ratio (FAR):

$$\mathrm{FAR} = \frac{b}{(a+b)}, \tag{7}$$

where the perfect score is 0.

The Frequency Bias Index (FBI) is the ratio of the total count of precipitation events of the two datasets. The values range from 0 to ∞, with a perfect score of 1:

$$\mathrm{FBI} = \frac{(a+b)}{(a+c)}. \tag{8}$$

This complements the similar measure of the unconditional bias in that the amounts of precipitation are left out and only temporal and spatial similarities in the occurrence of such events are taken into consideration.

The Critical Success Index (CSI) combines the information of FAR and POD. Thus, it shows how well the correctly-detected precipitation events from GPM conform to all the recorded precipitation events, making the CSI a very balanced measure, with the best score being 1:

$$\mathrm{CSI} = \frac{a}{(a+b+c)}. \tag{9}$$

Finally, the Heidke Skill Score (HSS) was calculated for the datasets. This metric answers the question on accuracy against random guessing. For a perfect measurement, the value will be 1. Performance equal to or worse than random guessing results in $-1 \leq \mathrm{HSS} \leq 0$:

$$\mathrm{HSS} = \frac{2 \times (a \times d - b \times c)}{((a+c) \times (c+d) + (a+b) \times (b+d))}. \tag{10}$$

A threshold of 0.1 mm/h is defined to delineate a precipitation event for the calculation of the above indices. This is in agreement with both datasets' intensity resolution. Hourly pixel values below this threshold are treated as noise and therefore are omitted.

4. Results

4.1. Statistical Analysis

4.1.1. Overall

Figure 2a,b shows the yearly mean precipitation of the two datasets. The plots serve clearly as evidence for the different recording techniques and their initially different spatial properties. The topographic characteristics of Germany can be traced from the RADOLAN data, which, although

spatially aggregated, reveal the inherited higher spatial variability. In contrast, the yearly mean precipitation measured by the GPM constellation appears smoother. The overall pattern indicates a similar precipitation distribution across Germany with high divergence in the level of detail. Both datasets agreed on the foothills of the Alps as the rain-laden region and eastern Germany as the driest sub-region in the state territory. The difference of GPM's and RADOLAN's precipitation amounts over the whole period under review again demonstrates the differences in spatial variability of the datasets. Furthermore, GPM in many parts of Germany overestimated the quantity of precipitation. Yet, over areas of secondary mountain ranges and alpine regions, the satellite data indicated lower precipitation amounts than the gauge-adjusted weather radar (Figure 2c).

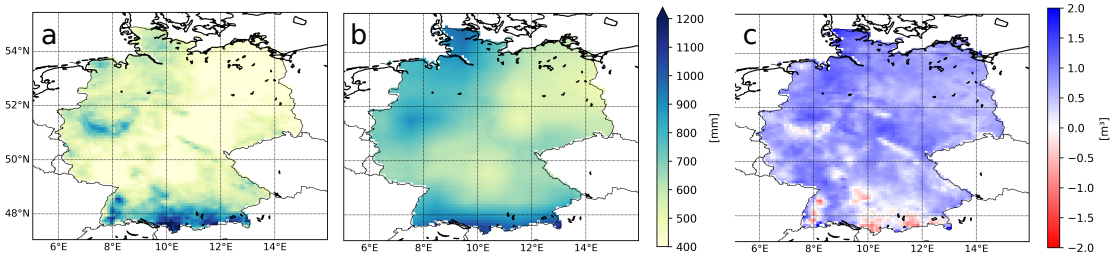

Figure 2. Yearly mean precipitation sum over Germany from RADOLAN (**a**) and GPM (**b**) data and the overall difference (GPM − RADOLAN) calculated for the period under review (**c**).

The monthly precipitation sums averaged over entire Germany show a clear pattern (Figure 3). Across all winter months in the reporting period, GPM's QPE clearly exceeded those of RADOLAN with a maximum monthly mean surplus per pixel of >20 mm. In summer months, the collected data coincided.

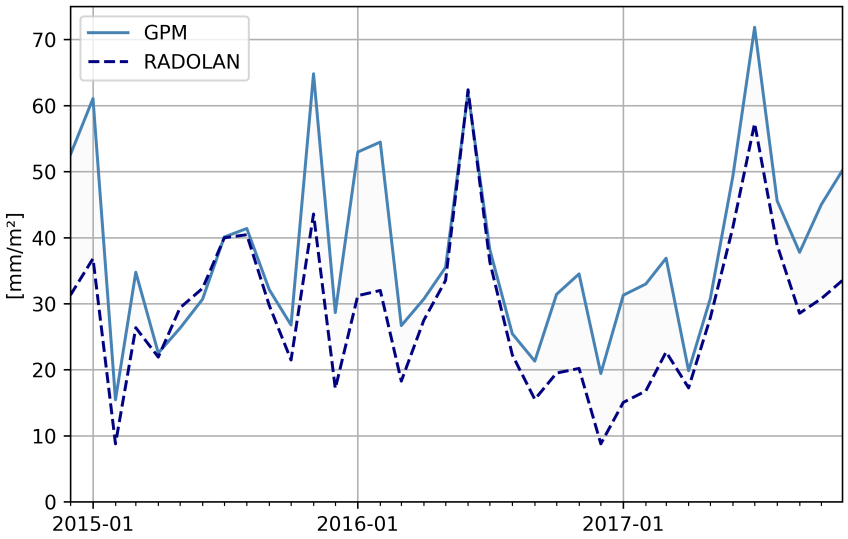

Figure 3. Spatially-averaged monthly precipitation sums in the GPM and RADOLAN datasets.

The evaluation of the unconditional bias upholds previous findings by also indicating a general overestimation of the precipitation amount by the GPM data compared to RADOLAN's QPE with $B = 1.31$.

4.1.2. Seasonal Analysis

The analysis of seasonal aggregated data was used to further reveal differences in precipitation patterns and the respective detection by the GPM and RADOLAN datasets. The absolute differences per season over the whole reporting period are shown in Figure 4. Besides the again prominent existence of differences due to spatial variability, the differences are diverse across seasons and conform to Figure 3. In fall and winter months (SON, DJF; Figure 4), GPM data showed higher precipitation values than RADOLAN in most areas. In the other two seasons, the satellite QPE were generally more on par with the weather radar data. However, in the southern part of the study area, RADOLAN showed higher values in spring (MAM) and especially in the summer season (JJA).

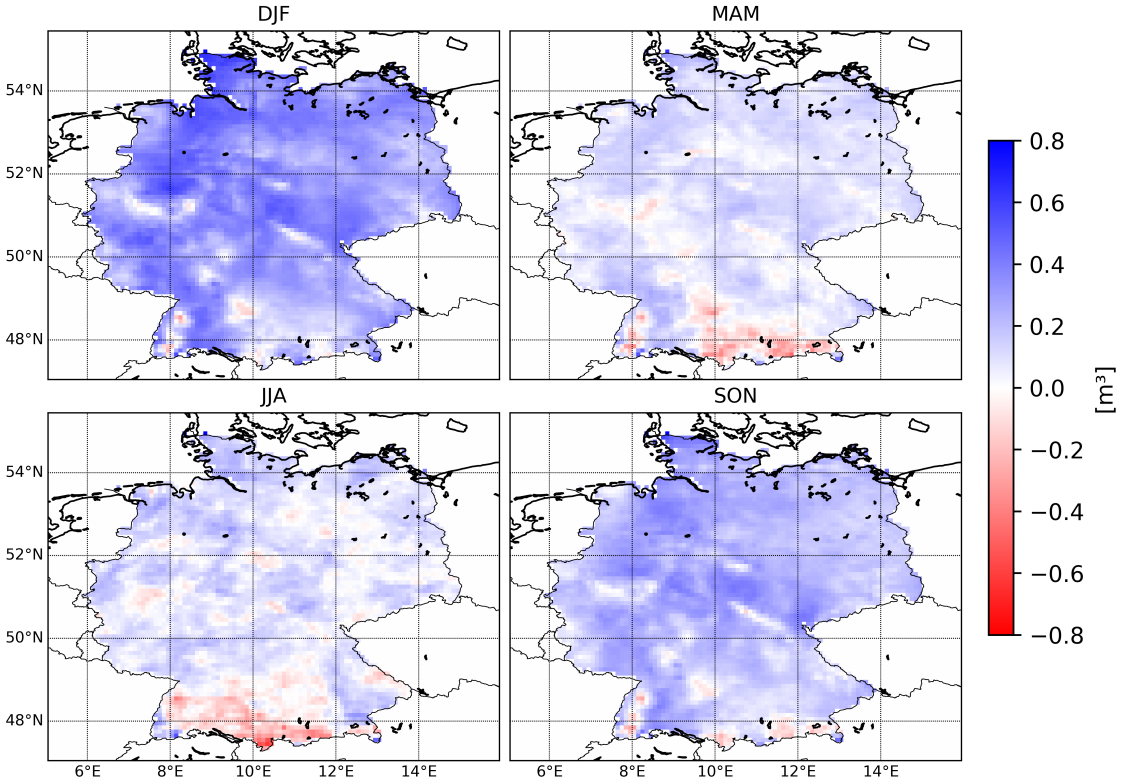

Figure 4. Differences in precipitation sums from GPM-RADOLAN datasets for seasons DJF, MAM, JJA, and SON over the reporting period.

These findings are further supported by the mean precipitation sums per season across the territory of Germany, which are shown in Figure 5a. An overestimation of the precipitation amount by GPM data occurred in all seasons. However, wintertime with a surplus of 76% needs to be emphasized.

Pearson's R value was utilized to calculate the correlation between GPM and RADOLAN precipitation. Additionally, the measure was applied on a pixel-by-pixel basis to evaluate the GPM and RADOLAN data's spatial agreement. Therefore, for every location in every seasonal data subset, the correlation was calculated. The overall correlation was 0.49, where for the single seasons, the values differed greatly, resulting in a value of 0.38 for DJF-, 0.55 for MAM-, 0.54 for JJA-, and 0.57 for SON-season. These results were backed by the spatial representations shown in Figure 6. All seasons besides DJF showed moderate correlation throughout the state territory of Germany. In the winter season, however, great shares of the southeastern parts of the study region showed very low correlation values around 0.1 to 0.2 with the minimum being 0.07.

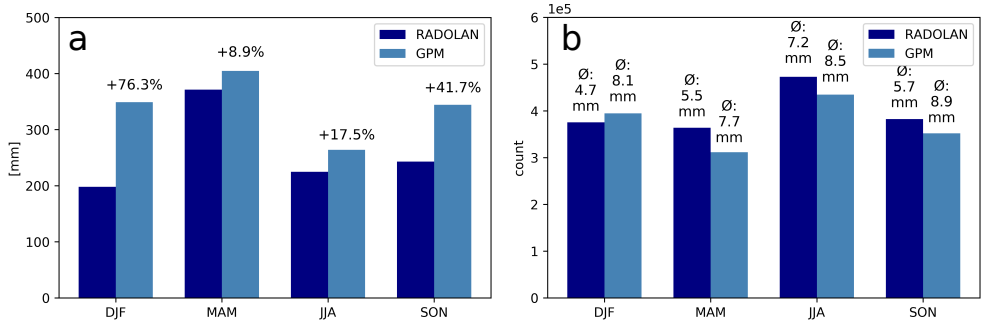

Figure 5. Mean of seasonal precipitation sums (**a**) and seasonal count and mean precipitation of "wet days" (**b**) of the GPM and RADOLAN datasets.

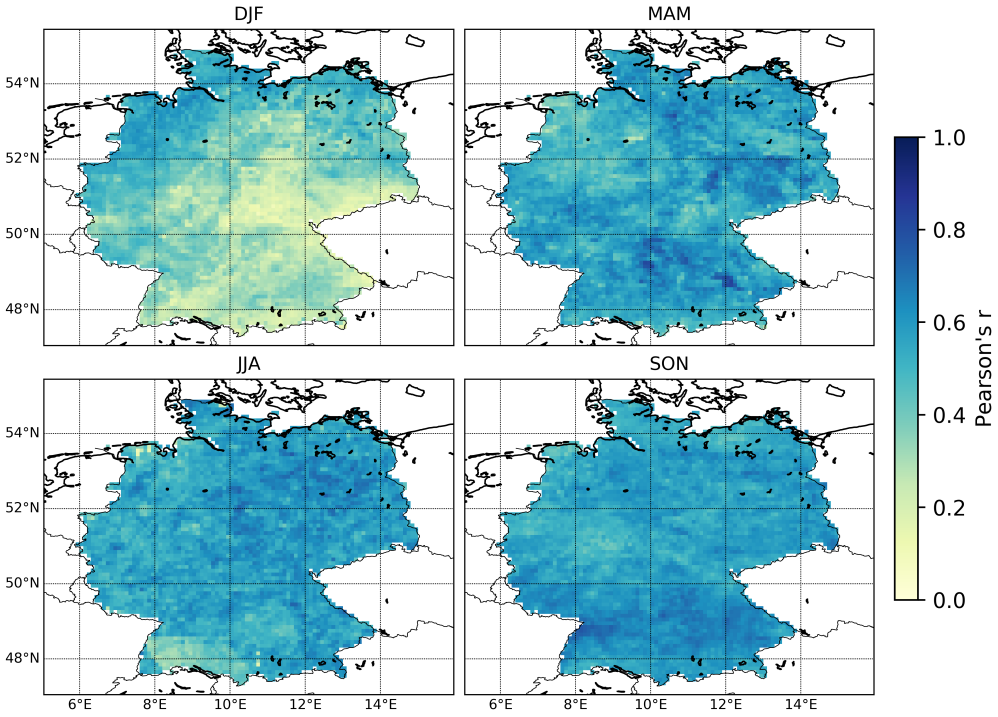

Figure 6. Pixel-by-pixel correlation of precipitation from GPM and RADOLAN datasets for seasons DJF, MAM, JJA, and SON.

4.2. Categorical Performance

The amount of wet days with a daily precipitation sum greater than 1 mm varied between the datasets (see Figure 5b). Besides the winter season, RADOLAN captured significantly more rain events than GPM. In the spring season, this accounted for up to 50,000 pixel hours within the reporting period. Yet, also in accordance with previous results, the mean precipitation amount per wet day measured by GPM was higher than the respective RADOLAN value in all seasons. Although GPM showed a lower detection rate for wet days, the surplus of precipitation amount compensated this effect, allowing the aforementioned results concerning the satellite measurements to be positively biased compared to RADOLAN to still be valid.

Diverse categorical indices have been calculated to obtain knowledge about the dataset-specific detection capabilities concerning precipitation events (see Section 3.2). These were again calculated for

Remote Sens. **2018**, *10*, 2029

the whole datasets, as well as for seasonal subsets. Furthermore, a spatial representation calculated on a pixel basis may be found in Figures 7 and 8.

The capability of the GPM dataset to capture every precipitation event was moderate with an overall value of 0.53 (see Table 2). Regions with high relief energy showed the lowest POD values throughout all the seasons. The highest amounts of erroneously-detected precipitation events showed up in the eastern part of Germany, demarcated most clearly in the SON and DJF seasons. This demarcation is related directly to the FBI being strongly positive in that region in the same seasons. Still, more events per pixels across Germany were detected by RADOLAN in all seasons, resulting in values of FBI ranging from 0.68 to 0.90 with an overall value of 0.78.

A different temporal pattern can be found in the error indices MAE and RMSE. However, due to the aforementioned topography related concern, the spatial shortcomings of GPM versus RADOLAN in representing precipitation still persisted. Besides the winter season, also in the summer, high error values throughout most of Germany were present. Nevertheless, alpine regions have to be highlighted as specific region, as the error values clearly exceeded the error values from the rest of Germany.

Table 2. Categorical indices per season.

Season	All	DJF	MAM	JJA	SON
Probability Of Detection (POD)	0.53	0.38	0.51	0.67	0.56
False Alarm Ratio (FAR)	0.32	0.48	0.25	0.25	0.32
Critical Success Index (CSI)	0.42	0.28	0.43	0.55	0.44
Heidke Skill Score (HSS)	0.56	0.39	0.57	0.68	0.58
Frequency Bias Index (FBI)	0.78	0.72	0.68	0.90	0.83
Mean Absolute Error (MAE)	0.11	0.12	0.08	0.12	0.10
Root Mean Square Error (RMSE)	0.59	0.66	0.47	0.67	0.52

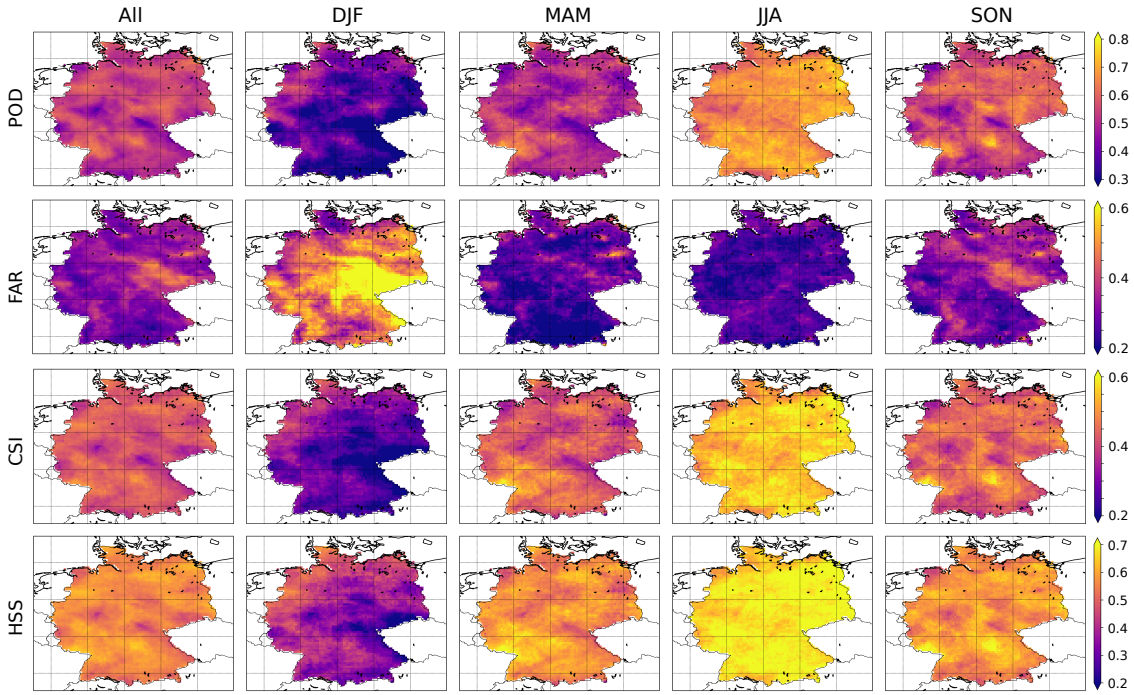

Figure 7. Categorical indices POD, FAR, CSI, and HSS for the total review period, DJF, MAM, JJA, and SON seasons.

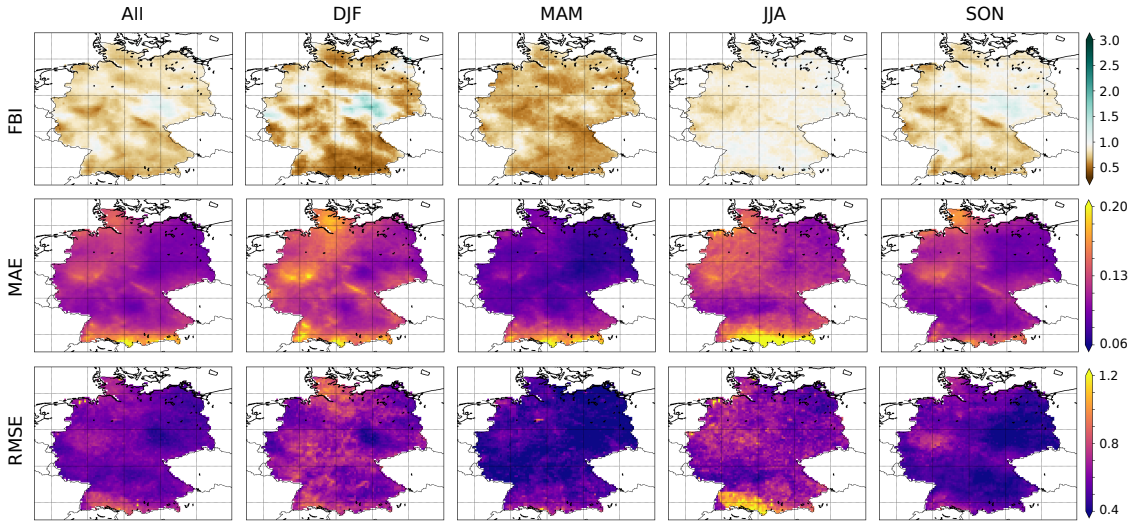

Figure 8. FBI, MAE, and RMSE for for total review period, DJF, MAM, JJA, and SON seasons.

5. Discussion

The single most marked observation to emerge from the data comparison is the strong discrepancy of the GPM and RADOLAN dataset concerning precipitation estimation for the winter season. Correlation between the satellite observation and weather radar data is low for this time period and seems to show an inversely proportional relation to continentality. Combined with low POD values, uncertainty arises with respect to the applicability of the dataset in, e.g., hydrological modeling. The problems of GPM dealing with solid precipitation have to be considered as one rationale behind the low detection rate, yet highly overestimated precipitation amounts in the winter season compared to the weather radar. GPM IMERG data being positively and negatively biased in cold environments is consistent with previous findings in the literature reported from [22,36], respectively. He et al. [18] even excluded winter months from their study as both satellite and gauge measurements are error prone in the detection of solid precipitation. Kochendorfer et al. [73] also stated that weighing precipitation gauges is highly error prone, especially when wind speeds exceed 5 ms^{-1}. In this case, less than 50% of the actual amount of solid precipitation may be collected. For the type of measurement gauges mainly used in Germany, Boudala et al. [74] reported an undercatch with a ratio of 0.57 for solid precipitation. Different filter algorithms are applied to the gauge measurements by the DWD. However, wind effects may still alter the measurements [48].

In the current study, GPM was positively biased compared with RADOLAN throughout all seasons. Biased precipitation estimation of the satellite dataset has been published by several authors [17,18,22,44], however, for both positive and negative directions. Furthermore, the already mentioned results of quantitative overestimation, particularly in winter and partly caused by false alarms, account for the shift in the precipitation amounts. The very high FAR and FBI values in eastern Germany in winter (see Figures 7 and 8), where lakes and big rivers (Elbe, Havel, Mulde) are abundant lead to an assumption of these landscapes and their inherent water cycle influencing the retrieval. Although, there is a high discrepancy in the number of events, there is no sign of excessive overestimation of the quantity of precipitation compared to the surrounding regions. Thus, e.g., ground fog, possibly not detected by RADOLAN though overrepresented in GPM, could be taken into consideration as an explanation for the disagreement of both datasets. Furthermore, solid precipitation in winter could be the reason for the discrepancies, although other areas throughout Germany are definitely more prone to snowfall. Moreover, the region is located in the lee of a secondary mountain range. Erroneously-detected precipitation in areas of rain shadow is reported for GPM estimates by Prakash et al. [21]. The performance of GPM considering light rain and solid particle detection

increased compared to its predecessor TRMM [11], yet the present case demonstrates like other studies that the need to further improve the algorithm still exists.

Furthermore, the detection of orographic precipitation is erroneous in GPM, which has already been covered by several studies [18,21,22]. The inability to capture topography-induced convective precipitation clearly becomes evident in this study by most categorical indices and the overall difference image signifying these areas (see Figures 2c, 7 and 8). Therefore, existing high rainfall intensities along the Alps naturally lead to high error values in MAE and RMSE. The grainy nature of RMSE in the summer season JJA (see Figure 8) and high error values in southwest Germany can certainly be attributed to the nature of the metric itself and hence to the sensitivity towards high intensity precipitation events, which commonly occur in these regions throughout summer. Due to the RADOLAN's inherent shorter scanning interval and thus, after aggregation to hourly data, still existing higher probability to detect a high intensity rainfall happening on a short temporal scale, great discrepancies in the RMSE may arise from a missed precipitation event by GPM, particularly in the summer season.

General caution has to be applied when datasets with originally different spatial resolution are compared. Although the applied conservative remapping scheme as described in Section 3.1.3 is widely appreciated as very suitable for regridding precipitation data, other techniques (e.g., bilinear, bicubic, iterative curvature-based interpolation) may slightly alter the findings of this study. However, the authors compared the results from the highly unequal non-conservative bilinear interpolation (data not shown) and the applied conservative interpolation scheme, finding that the changes in the results were very small and did not change the statement of the results. However, we recommend that future studies should consider an in depth analysis of the impact of the different interpolation schemes on the comparison of different precipitation datasets. Moreover, a transferability of the results can only be given to regions that share similar boundary conditions. Therefore, the case study over Germany is well suited, as it represents various topographical conditions, as well as several precipitation regimes to test the performance of GPM.

Further processing could include temporal aggregation to and comparison of daily values as precipitation data often are used on this temporal scale as input for other applications, e.g., in hydrologic modeling. It has to be noted that both institutes, NASA and DWD, provide additional products of the respective family (GPM and RADOLAN), which are calculated with a modified algorithm or are based on a subset of sensors. However, the specific purpose of this study was to compare the respective final community-ready precipitation datasets GPM IMERG v05 final and RADOLAN RW, which fully incorporate all data gathered for the respective mission.

Lastly, it has to be noted that the identified performance-related discrepancies profoundly become popular, as the two data sets cannot be considered entirely independent. GPM IMERG utilizes data from the GPCC network on a monthly basis for calibration. Parts of the involved gauges are also used in the hourly online adjustment routine of the RADOLAN dataset. This issue has been accepted by the authors as the calibration for both datasets takes place on a totally different temporal scale.

6. Conclusions

This study conducted a statistical comparison of two QPE products, namely the GPM IMERG half hourly Version 5 final satellite and RADOLAN RW weather radar dataset. Standard metrics like RMSE, MAE, and bias have been applied and categorical indices used to identify the strengths and shortcomings in the ability to detect single precipitation events. Additionally, a pixel-by-pixel analysis of these measures allows drawing conclusions on the spatial distribution of the inherent event identification capabilities of the GPM and RADOLAN datasets.

The results provide considerable insight into the different properties and indicate extensive discrepancies in some parts of the study. Four key findings are revealed by the analysis: (i) the GPM dataset shows low responsivity for the topographically-induced spatial variability of precipitation over Germany compared to the RADOLAN data (see Figure 2); (ii) the precipitation amounts measured by

the satellite product exceed the weather radar data on a territory scale in all seasons, especially in winter (see Figure 3), whereas over spatial subsets with high relief energy, RADOLAN is on par or generates a surplus in precipitation quantity (see Figure 4 and MAE and RMSE in Figure 8); (iii) RADOLAN captures a higher amount of low intensity events (see the high FBI in Figure 8); and (iv) substantial differences in winter season have to be reported, in terms of low correlation (see Figure 6) and high FAR values, yet low POD and CSI/HSS success statistics (see Figure 7). These outcomes lead to the conclusion that caution and awareness of the peculiarities of the dataset have to be applied when using GPM data over Germany and thus also over parts of Europe. However, this protective measure extends to every dataset, which is attributed to being a reference or used in a similar manner.

Author Contributions: Conceptualization, T.R.; Methodology and Formal Analysis, T.R.; Writing—Original Draft Preparation, T.R.; Writing—Review & Editing, T.R., T.W. and P.M.; Visualization, T.R.; Project Administration, P.M.

Funding: The project leading to this application has received funding from the European Union's Horizon 2020 research and innovation program under Grant Agreement No. 687320.

Acknowledgments: Thomas Ramsauer is truly thankful for the inspiration, ideas, and support that Alexander Loew has given to him.

Conflicts of Interest: The authors declare no conflict of interest.

References

1. GCOS. *The Global Observing System for Climate: Implementation Needs*. WMO Pub GCOS-200; GCOS: Geneva, Switzerland, 2016.
2. Kidd, C.; Becker, A.; Huffman, G.J.; Muller, C.L.; Joe, P.; Skofronick-Jackson, G.; Kirschbaum, D.B. So, How Much of the Earth's Surface Is Covered by Rain Gauges? *Bull. Am. Meteorol. Soc.* **2017**, *98*, 69–78. [CrossRef]
3. Tarpanelli, A.; Massari, C.; Ciabatta, L.; Filippucci, P.; Amarnath, G.; Brocca, L. Exploiting a constellation of satellite soil moisture sensors for accurate rainfall estimation. *Adv. Water Resour.* **2017**, *108*, 249–255. [CrossRef]
4. Román-Cascón, C.; Pellarin, T.; Gibon, F.; Brocca, L.; Cosme, E.; Crow, W.; Fernández-Prieto, D.; Kerr, Y.H.; Massari, C. Correcting satellite-based precipitation products through SMOS soil moisture data assimilation in two land-surface models of different complexity: API and SURFEX. *Remote Sens. Environ.* **2017**, *200*, 295–310. [CrossRef]
5. Crow, W.; van Den Berg, M.; Huffman, G.; Pellarin, T. Correcting rainfall using satellite-based surface soil moisture retrievals: The Soil Moisture Analysis Rainfall Tool (SMART). *Water Resour. Res.* **2011**, *47*. [CrossRef]
6. Ciabatta, L.; Brocca, L.; Massari, C.; Moramarco, T.; Puca, S.; Rinollo, A.; Gabellani, S.; Wagner, W. Integration of Satellite Soil Moisture and Rainfall Observations over the Italian Territory. *J. Hydrometeorol.* **2015**, *16*, 1341–1355. [CrossRef]
7. Brocca, L.; Moramarco, T.; Melone, F.; Wagner, W. A new method for rainfall estimation through soil moisture observations. *Geophys. Res. Lett.* **2013**, *40*, 853–858. [CrossRef]
8. Crow, W.T.; Huffman, G.J.; Bindlish, R.; Jackson, T.J. Improving Satellite-Based Rainfall Accumulation Estimates Using Spaceborne Surface Soil Moisture Retrievals. *J. Hydrometeorol.* **2009**, *10*, 199–212. [CrossRef]
9. Beck, H.E.; Vergopolan, N.; Pan, M.; Levizzani, V.; van Dijk, A.I.J.M.; Weedon, G.; Brocca, L.; Pappenberger, F.; Huffman, G.J.; Wood, E.F. Global-scale evaluation of 23 precipitation datasets using gauge observations and hydrological modeling. *Hydrol. Earth Syst. Sci. Discuss.* **2017**, *2017*, 1–23. [CrossRef]
10. Simpson, J.; Adler, R.F.; North, G.R. A proposed tropical rainfall measuring mission (TRMM) satellite. *Bull. Am. Meteorol. Soc.* **1988**, *69*, 278–295. [CrossRef]
11. Skofronick-Jackson, G.; Petersen, W.A.; Berg, W.; Kidd, C.; Stocker, E.F.; Kirschbaum, D.B.; Kakar, R.; Braun, S.A.; Huffman, G.J.; Iguchi, T.; et al. The Global Precipitation Measurement (GPM) Mission for Science and Society. *Bull. Am. Meteorol. Soc.* **2017**, *98*, 1679–1695. [CrossRef]
12. Huffman, G.J.; Bolvin, D.T.; Braithwaite, D.; Hsu, K.; Joyce, R.; Kidd, C.; Nelkin, E.J.; Sorooshian, S.; Tan, J.; Xie, P. *NASA Global Precipitation Measurement (GPM) Integrated Multi-satellitE Retrievals for GPM (IMERG) Algorithm Theoretical and Basis Document and (ATBD) and Version 5.2*; Technical Report; National Aeronautics and Space Administration: Greenbelt, MD, USA, 2018.

13. Hou, A.Y.; Kakar, R.K.; Neeck, S.; Azarbarzin, A.A.; Kummerow, C.D.; Kojima, M.; Oki, R.; Nakamura, K.; Iguchi, T. The Global Precipitation Measurement Mission. *Bull. Am. Meteorol. Soc.* **2014**, *95*, 701–722. [CrossRef]
14. Liu, Z. Comparison of Integrated Multisatellite Retrievals for GPM (IMERG) and TRMM Multisatellite Precipitation Analysis (TMPA) Monthly Precipitation Products: Initial Results. *J. Hydrometeorol.* **2016**, *17*, 777–790. [CrossRef]
15. Boluwade, A.; Stadnyk, T.; Fortin, V.; Roy, G. Assimilation of precipitation Estimates from the Integrated Multisatellite Retrievals for GPM (IMERG, early Run) in the Canadian Precipitation Analysis (CaPA). *J. Hydrol. Reg. Stud.* **2017**, *14*, 10–22. [CrossRef]
16. Tan, M.; Duan, Z. Assessment of GPM and TRMM Precipitation Products over Singapore. *Remote Sens.* **2017**, *9*, 720. [CrossRef]
17. Tan, M.L.; Santo, H. Comparison of GPM IMERG, TMPA 3B42 and PERSIANN-CDR satellite precipitation products over Malaysia. *Atmos. Res.* **2018**, *202*, 63–76. [CrossRef]
18. He, Z.; Yang, L.; Tian, F.; Ni, G.; Hou, A.; Lu, H. Intercomparisons of Rainfall Estimates from TRMM and GPM Multisatellite Products over the Upper Mekong River Basin. *J. Hydrometeorol.* **2017**, *18*, 413–430. [CrossRef]
19. Tang, G.; Ma, Y.; Long, D.; Zhong, L.; Hong, Y. Evaluation of GPM Day-1 IMERG and TMPA Version-7 legacy products over Mainland China at multiple spatiotemporal scales. *J. Hydrol.* **2016**, *533*, 152–167. [CrossRef]
20. Zhao, H.; Yang, B.; Yang, S.; Huang, Y.; Dong, G.; Bai, J.; Wang, Z. Systematical estimation of GPM-based global satellite mapping of precipitation products over China. *Atmos. Res.* **2018**, *201*, 206–217. [CrossRef]
21. Prakash, S.; Mitra, A.K.; AghaKouchak, A.; Liu, Z.; Norouzi, H.; Pai, D. A preliminary assessment of GPM-based multi-satellite precipitation estimates over a monsoon dominated region. *J. Hydrol.* **2018**, *556*, 865–876. [CrossRef]
22. Sharifi, E.; Steinacker, R.; Saghafian, B. Assessment of GPM-IMERG and Other Precipitation Products against Gauge Data under Different Topographic and Climatic Conditions in Iran: Preliminary Results. *Remote Sens.* **2016**, *8*, 135. [CrossRef]
23. Mahmoud, M.T.; Al-Zahrani, M.A.; Sharif, H.O. Assessment of global precipitation measurement satellite products over Saudi Arabia. *J. Hydrol.* **2018**, *559*, 1–12. [CrossRef]
24. Nikolopoulos, E.I.; Anagnostou, E.N.; Hossain, F.; Gebremichael, M.; Borga, M. Understanding the Scale Relationships of Uncertainty Propagation of Satellite Rainfall through a Distributed Hydrologic Model. *J. Hydrometeorol.* **2010**, *11*, 520–532. [CrossRef]
25. Li, Y.; Grimaldi, S.; Walker, J.; Pauwels, V. Application of Remote Sensing Data to Constrain Operational Rainfall-Driven Flood Forecasting: A Review. *Remote Sens.* **2016**, *8*, 456. [CrossRef]
26. Maggioni, V.; Massari, C. On the performance of satellite precipitation products in riverine flood modeling: A review. *J. Hydrol.* **2018**, *558*, 214–224. [CrossRef]
27. Mei, Y.; Anagnostou, E.N.; Shen, X.; Nikolopoulos, E.I. Decomposing the satellite precipitation error propagation through the rainfall-runoff processes. *Adv. Water Resour.* **2017**, *109*, 253–266. [CrossRef]
28. Rossi, M.; Luciani, S.; Valigi, D.; Kirschbaum, D.; Brunetti, M.; Peruccacci, S.; Guzzetti, F. Statistical approaches for the definition of landslide rainfall thresholds and their uncertainty using rain gauge and satellite data. *Geomorphology* **2017**, *285*, 16–27. [CrossRef]
29. Marra, F.; Destro, E.; Nikolopoulos, E.I.; Zoccatelli, D.; Creutin, J.D.; Guzzetti, F.; Borga, M. Impact of rainfall spatial aggregation on the identification of debris flow occurrence thresholds. *Hydrol. Earth Syst. Sci.* **2017**, *21*, 4525–4532. [CrossRef]
30. Mei, Y.; Nikolopoulos, E.; Anagnostou, E.; Zoccatelli, D.; Borga, M. Error Analysis of Satellite Precipitation-Driven Modeling of Flood Events in Complex Alpine Terrain. *Remote Sens.* **2016**, *8*, 293. [CrossRef]
31. Kugler, Z.; De Groeve, T. *The Global Flood Detection System*; JRC Scientific and Technical Reports; European Communities: Luxembourg, 2007; pp. 1–45.
32. Revilla-Romero, B.; Wanders, N.; Burek, P.; Salamon, P.; de Roo, A. Integrating remotely sensed surface water extent into continental scale hydrology. *J. Hydrol.* **2016**, *543*, 659–670. [CrossRef]
33. Revilla-Romero, B.; Thielen, J.; Salamon, P.; Groeve, T.D.; Brakenridge, G.R. Evaluation of the satellite-based Global Flood Detection System for measuring river discharge: influence of local factors. *Hydrol. Earth Syst. Sci.* **2014**, *18*, 4467–4484. [CrossRef]

34. Speirs, P.; Gabella, M.; Berne, A. A Comparison between the GPM Dual-Frequency Precipitation Radar and Ground-Based Radar Precipitation Rate Estimates in the Swiss Alps and Plateau. *J. Hydrometeorol.* **2017**, *18*, 1247–1269. [CrossRef]
35. Zhang, A.; Chen, S.; Fan, S. Comparison of Extreme Precipitation Estimation From GPM Dual-Frequency Radar and Ground-Based Radar Network in Southern China. In Proceedings of the 2017 IEEE International Geoscience and Remote Sensing Symposium (IGARSS), Fort Worth, TX, USA, 23–28 July 2017; pp. 4534–4537.
36. Gabella, M.; Speirs, P.; Hamann, U.; Germann, U.; Berne, A. Measurement of Precipitation in the Alps Using Dual-Polarization C-Band Ground-Based Radars, the GPM Spaceborne Ku-Band Radar, and Rain Gauges. *Remote Sens.* **2017**, *9*, 1147. [CrossRef]
37. Cannon, F.; Ralph, F.M.; Wilson, A.M.; Lettenmaier, D.P. GPM Satellite and Radar Measurements and of Precipitation and Freezing Level and in Atmospheric Rivers: Comparison with Ground-Based Radars and Reanalyses. *J. Geophys. Res. Atmos. Forest.* **2017**, *122*, 12747-12764. [CrossRef]
38. Gao, J.; Tang, G.; Hong, Y. Similarities and Improvements of GPM Dual-Frequency Precipitation Radar (DPR) upon TRMM Precipitation Radar (PR) in Global Precipitation Rate Estimation, Type Classification and Vertical Profiling. *Remote Sens.* **2017**, *9*, 1142. [CrossRef]
39. Biswas, S.K.; Le, M.; Chandrasekar, V. Identification of Snow from GPM-DPR observations and cross validation with S-Band Ground Radar dual polarization measurements. In Proceedings of the 32 nd URSI GASS, Montreal, QC, Canada, 19–26 August 2017.
40. Skofronick-Jackson, G.; Hudak, D.; Petersen, W.; Nesbitt, S.W.; Chandrasekar, V.; Durden, S.; Gleicher, K.J.; Huang, G.J.; Joe, P.; Kollias, P.; et al. Global Precipitation Measurement Cold Season Precipitation Experiment (GCPEX): For Measurement's Sake, Let It Snow. *Bull. Am. Meteorol. Soc.* **2015**, *96*, 1719–1741. [CrossRef]
41. You, Y.; Wang, N.Y.; Ferraro, R.; Rudlosky, S. Quantifying the Snowfall Detection Performance of the GPM Microwave Imager Channels over Land. *J. Hydrometeorol.* **2017**, *18*, 729–751. [CrossRef]
42. Casella, D.; Panegrossi, G.; Sanò, P.; Marra, A.C.; Dietrich, S.; Johnson, B.T.; Kulie, M.S. Evaluation of the GPM-DPR snowfall detection capability: Comparison with CloudSat-CPR. *Atmos. Res.* **2017**, *197*, 64–75. [CrossRef]
43. Wen, Y.; Behrangi, A.; Lambrigtsen, B.; Kirstetter, P.E. Evaluation and Uncertainty Estimation of the Latest Radar and Satellite Snowfall Products Using SNOTEL Measurements over Mountainous Regions in Western United States. *Remote Sens.* **2016**, *8*, 904. [CrossRef]
44. Sharifi, E.; Steinacker, R.; Saghafian, B. Multi time-scale evaluation of high-resolution satellite-based precipitation products over northeast of Austria. *Atmos. Res.* **2018**, *206*, 46–63. [CrossRef]
45. Rysman, J.F.; Panegrossi, G.; Sanò, P.; Marra, A.; Dietrich, S.; Milani, L.; Kulie, M. SLALOM: An All-Surface Snow Water Path Retrieval Algorithm for the GPM Microwave Imager. *Remote Sens.* **2018**, *10*, 1278. [CrossRef]
46. Gampe, D.; Ludwig, R. Evaluation of Gridded Precipitation Data Products for Hydrological Applications in Complex Topography. *Hydrology* **2017**, *4*, 53. [CrossRef]
47. *RADOLAN/RADVOR Hoch aufgelöste Niederschlagsanalyse und –Vorhersage auf der Basis Quantitativer Radar und Ombrometerdaten für and grenzüberschreitende Fluss-Einzugsgebiete von Deutschland im Echtzeitbetrieb Beschreibung des Kompositformats Version 2.4.3*; Technical Report; Deutscher Wetterdienst, Abteilung Hydrometeorologie: Offenbach, Germany, 2018.
48. Bartels, H. *Projekt RADOLAN. Routineverfahren zur Online-Aneichung der Radarniederschlagsdaten mit Hilfe von Automatischen Bodenniederschlagsstationen (Ombrometer)*; Technical Report; Deutscher Wetterdienst, Hydrometeorologie: Offenbach, Germany, 2004.
49. Meyer, H.; Kühnlein, M.; Appelhans, T.; Nauss, T. Comparison of Four Machine Learning Algorithms for Their Applicability in Satellite-Based Optical Rainfall Retrievals. *Atmos. Res.* **2016**, *169*, 424–433. [CrossRef]
50. Kühnlein, M.; Appelhans, T.; Thies, B.; Nauss, T. Improving the accuracy of rainfall rates from optical satellite sensors with machine learning—A random forests-based approach applied to MSG SEVIRI. *Remote Sens. Environ.* **2014**, *141*, 129–143. [CrossRef]
51. Bronstert, A.; Agarwal, A.; Boessenkool, B.; Crisologo, I.; Fischer, M.; Heistermann, M.; Köhn-Reich, L.; López-Tarazón, J.A.; Moran, T.; Ozturk, U.; et al. Forensic hydro-meteorological analysis of an extreme flash flood: The 2016-05-29 event in Braunsbach, SW Germany. *Sci. Total Environ.* **2018**, *630*, 977–991. [CrossRef]

52. Doycheva, K.; Horn, G.; Koch, C.; Schumann, A.; König, M. Assessment and weighting of meteorological ensemble forecast members based on supervised machine learning with application to runoff simulations and flood warning. *Adv. Eng. Inform.* **2017**, *33*, 427–439. [CrossRef]
53. Fischer, F.; Hauck, J.; Brandhuber, R.; Weigl, E.; Maier, H.; Auerswald, K. Spatio-temporal variability of erosivity estimated from highly resolved and adjusted radar rain data (RADOLAN). *Agric. For. Meteorol.* **2016**, *223*, 72–80. [CrossRef]
54. Winterrath, T.; Brendel, C.; Hafer, M.; Junghänel, T.; Klameth, A.; Walawender, E.; und Andreas Becker, E.W. *Erstellung Einer Radargestützten Niederschlagsklimatologie*; Berichte des Deutschen Wetterdienstes; Deutschen Wetterdienstes: Offenbach am Main, Germany, 2017; Volume 251, pp. 1–71.
55. Winterrath, T.; Rosenow, W.; Weigl, E. On the DWD quantitative precipitation analysis and nowcasting system for real-time application in German flood risk management. *Weather Radar Hydrol.* **2012**, *351*, 323–329.
56. Keupp, L.; Winterrath, T.; Hollmann, R. *Use of Weather Radar Data for Climate Data Records in WMO Regions IV and VI*; Technical Report, WMO CCl TT-URSDCM; WMO: Geneva, Switzerland, 2017.
57. Richter, D. *Ergebnisse methodischer Untersuchungen zur Korrektur des Systematischen Meßfehlers des Hellmann-Niederschlagmessers*; Deutschen Wetterdienstes: Offenbach am Main, Germany, 1995; Volume 194, pp. 1–93.
58. World Meteorological Organization. *Guide to Meteorological Instruments and Methods of Observation, WMO-No. 8*; World Meteorological Organization: Geneva, Switzerland, 2017.
59. Becker, A.; Finger, P.; Meyer-Christoffer, A.; Rudolf, B.; Schamm, K.; Schneider, U.; Ziese, M. A description of the global land-surface precipitation data products of the Global Precipitation Climatology Centre with sample applications including centennial (trend) analysis from 1901–present. *Earth Syst. Sci. Data* **2013**, *5*, 71–99. [CrossRef]
60. Ullrich, P.A.; Taylor, M.A. Arbitrary-Order Conservative and Consistent Remapping and a Theory of Linear Maps: Part I. *Mon. Weather Rev.* **2015**, *143*, 2419–2440. [CrossRef]
61. Chen, C.T.; Knutson, T. On the Verification and Comparison of Extreme Rainfall Indices from Climate Models. *J. Clim.* **2008**, *21*, 1605–1621. [CrossRef]
62. Accadia, C.; Mariani, S.; Casaioli, M.; Lavagnini, A.; Speranza, A. Sensitivity of precipitation forecast skill scores to bilinear interpolation and a simple nearest-neighbor average method on high-resolution verification grids. *Weather Forecast.* **2003**, *18*, 918–932. [CrossRef]
63. Chen, C.J.; Senarath, S.U.S.; Dima-West, I.M.; Marcella, M.P. Evaluation and restructuring of gridded precipitation data over the Greater Mekong Subregion. *Int. J. Climatol.* **2016**, *37*, 180–196. [CrossRef]
64. Jones, P.W. First- and Second-Order Conservative Remapping Schemes for Grids in Spherical Coordinates. *Mon. Weather Rev.* **1999**, *127*, 2204–2210. [CrossRef]
65. Jones, P.W. *A User's Guide for SCRIP: A Spherical Coordinate Remapping and Interpolation Package, Version 1.5*; Los Alamos National Laboratory: Los Alamos, NM, USA, 1998.
66. Schulzweida, U. *CDO User Guide*; Technical Report; MPI for Meteorology: Hamburg, Germany, 2018.
67. Kalognomou, E.A.; Lennard, C.; Shongwe, M.; Pinto, I.; Favre, A.; Kent, M.; Hewitson, B.; Dosio, A.; Nikulin, G.; Panitz, H.J.; et al. A Diagnostic Evaluation of Precipitation in CORDEX Models over Southern Africa. *J. Clim.* **2013**, *26*, 9477–9506. [CrossRef]
68. Diaconescu, E.P.; Gachon, P.; Laprise, R. On the Remapping Procedure of Daily Precipitation Statistics and Indices Used in Regional Climate Model Evaluation. *J. Hydrometeorol.* **2015**, *16*, 2301–2310. [CrossRef]
69. Wang, J.; Zeng, N.; Wang, M.; Jiang, F.; Chen, J.; Friedlingstein, P.; Jain, A.K.; Jiang, Z.; Ju, W.; Lienert, S.; et al. Contrasting interannual atmospheric CO_2 variabilities and their terrestrial mechanisms for two types of El Niños. *Atmos. Chem. Phys.* **2018**, *18*, 10333–10345. [CrossRef]
70. Woodcock, F. The evaluation of yes/no forecasts for scientific and administrative purposes. *Mon. Weather Rev.* **1976**, *104*, 1209–1214. [CrossRef]
71. Doswell, C.A.; Davies-Jones, R.; Keller, D.L. On summary measures of skill in rare event forecasting based on contingency tables. *Weather Forecast.* **1990**, *5*, 576–585. [CrossRef]
72. Schaefer, J.T. The critical success index as an indicator of warning skill. *Weather Forecast.* **1990**, *5*, 570–575. [CrossRef]

73. Kochendorfer, J.; Rasmussen, R.; Wolff, M.; Baker, B.; Hall, M.E.; Meyers, T.; Landolt, S.; Jachcik, A.; Isaksen, K.; Brækkan, R.; et al. The quantification and correction of wind-induced precipitation measurement errors. *Hydrol. Earth Syst. Sci.* **2017**, *21*, 1973–1989. [CrossRef]
74. Boudala, F.S.; Isaac, G.A.; Filman, P.; Crawford, R.; Hudak, D.; Anderson, M. Performance of Emerging Technologies for Measuring Solid and Liquid Precipitation in Cold Climate as Compared to the Traditional Manual Gauges. *J. Atmos. Ocean. Technol.* **2017**, *34*, 167–185. [CrossRef]

2.2 Article II: RADOLAN_API: An Hourly Soil Moisture Data Set Based on Weather Radar, Soil Properties and Reanalysis Temperature Data

---

Journal: Remote Sensing **Status**: published **IF**: 5.349

Reference: Ramsauer, T., Weiß, T., Löw, A. & Marzahn, P. (2021): RADOLAN_API: An Hourly Soil Moisture Data Set Based on Weather Radar, Soil Properties and Reanalysis Temperature Data. *Remote Sensing*. 13 (9), 1712. DOI: 10.3390/rs13091712

Scope and Context:

After having compared the precipitation data sets, the second publication now utilizes the German weather radar data set RADOLAN RW to retrieve soil moisture values. Precipitation is the most important driver of soil moisture in Germany. The specific weather radar data set (RW) is quality controlled and gauge adjusted. Therefore, it is used although temporal even higher resolution data is available from German Weather Service (DWD). With additional information on soil properties and ambient temperature a high quality soil moisture estimation based on an extended antecedent precipitation index is created in this study. Validation efforts utilizing in situ measurement data from openly available soil moisture networks and self-conducted field campaigns demonstrate a good fit of the modeled data.

The presented work builds on the precipitation data set comparison in article I and utilized the therein presented weather radar data set which shows superior performance for the domain of Germany. The high precipitation detection ability of weather radar translates to respectively high temporal resolution soil moisture data, which unambiguously captures soil moisture upsurges and shows high agreement with validation data.

remote sensing

MDPI

Article

RADOLAN_API: An Hourly Soil Moisture Data Set Based on Weather Radar, Soil Properties and Reanalysis Temperature Data

Thomas Ramsauer *, Thomas Weiß, Alexander Löw and Philip Marzahn

Department of Geography, Ludwig-Maximilians-Universität München, Luisenstraße 37, 80333 Munich, Germany; t.weiss@iggf.geo.uni-muenchen.de (T.W.); alexander.loew@lmu.de (A.L.); p.marzahn@iggf.geo.uni-muenchen.de (P.M.)

* Correspondence: t.ramsauer@iggf.geo.uni-muenchen.de

Abstract: Soil moisture is a key variable in the terrestrial water and energy system. This study presents an hourly index that provides soil moisture estimates on a high spatial and temporal resolution (1 km × 1 km). The long established Antecedent Precipitation Index (API) is extended with soil characteristic and temperature dependent loss functions. The Soilgrids and ERA5 data sets are used to provide the controlling variables. Precipitation as main driver is provided by the German weather radar data set RADOLAN. Empiric variables in the equations are fitted in a optimization effort using 23 in-situ soil moisture measurement stations from the Terrestial Environmental Observatories (TERENO) and a separately conducted field campaign. The volumetric soil moisture estimation results show error values of 3.45 Vol% mean *ubRMSD* between RADOLAN_API and station data with a high temporal accordance especially of soil moisture upsurge. Further potential of the improved API algorithm is shown with a per-station calibration of applied empirical variables. In addition, the RADOLAN_API data set was spatially compared to the ESA CCI soil moisture product where it altogether demonstrates good agreement. The resulting data set is provided as open access data.

Keywords: soil moisture; high resolution; weather radar; hourly; API; soil properties; Soilgrids; TERENO; ESA CCI SM; RADOLAN

Citation: Ramsauer, T.; Weiß, T.; Löw, A.; Marzahn, P. RADOLAN_API: An Hourly Soil Moisture Data Set Based on Weather Radar, Soil Properties and Reanalysis Temperature Data. *Remote Sens.* **2021**, *13*, 1712. https://doi.org/10.3390/rs13091712

Academic Editor: Teodosio Lacava

Received: 1 April 2021
Accepted: 23 April 2021
Published: 28 April 2021

1. Introduction

Soil moisture plays a key role in the interaction of different land surface processes and energy fluxes [1–3]. It controls processes like evaporation, infiltration and runoff, hence the fundamentals of the hydrological cycle [4,5]. Therefore, soil moisture influences hazards of different sorts, e.g., the extent or magnitude of floods [6]. But also temperature or precipitation extremes relate to soil moisture state and memory [7]. Soil moisture further is the main governing resource in relation to ecosystem function and form as it provides water for nutrient uptake and transpiration [8]. With that, net biome productivity and hence CO_2 fluxes are strongly linked to soil moisture variability [9]. Consequently, soil moisture has been classified as an essential climate variable (ECV) by the World Meteorological Organization's Global Climate Observing System (WMO, GCOS) [10].

Today, measurement techniques for soil moisture are available across scales. Divers approaches allow measurement of soil moisture on point scale, e.g., gravimetric measurements, Time Domain Reflectometry (TDR) and Frequency Domain Reflectometry (FDR) but also using the attenuation of the Global Positioning System's (GPS) signal [11,12]. Ground penetrating radar [13,14] or cosmic-ray neutron measurements, that cover bigger footprints, may also be used in mobile sampling applications and hence bridge the gap to field scale measurements of the available subsurface soil water storage [11]. Sparse station measurements combined with modeling allows for regional scale soil moisture estimations [15]. In a great effort, the International Soil Moisture Network (ISMN) collects, harmonizes

and provides such sparse soil moisture measurements consisting of data streams from a multitude of individually operating networks [16].

Besides these on-site measurements, remote sensing offers retrieval opportunities for large scale spatially distributed soil moisture estimates. Imagery ranges in spatial coverage and resolution from regional UAV based sensing [17] to satellite based global soil moisture products at one single acquisition date [18,19]. Various constellations including thermal infrared, optical and microwave satellite sensor systems can be utilized to retrieve soil moisture [20–23]. Optical and thermal remote sensing allows for soil moisture estimations via the thermal-optical triangle method (TOTRAM), that interpretes the combination of pixel-based values of land surface temperature and a vegetation index, or the optical trapezoid model (OPTRAM), that utilizes the physical relationship of shortwave infrared transformed reflectance and soil moisture instead [21]. However, given the limitations regarding cloud cover a continuous stream of satellite sensed soil moisture is only possible with active and passive microwave sensors like the Advanced Scatterometer (ASCAT) [24] or the Soil Moisture Active Passive (SMAP) Mission [25,26]. Various algorithms for these platforms have been developed [18,27–32]. The spatial resolution of such data sets and retrieval algorithms usually is rather coarse with tens of kilometers [26]. Several years after the launch of the Sentinel-1 satellites, operationally provided data sets utilize the high resolution active microwave data and soil moisture data sets with higher spatial resolution of up to 1 km $\times$ 1 km are available [33,34]. The temporal resolution however depends on the revisit time of the satellites which allows for daily or half-daily data points only [26]. Yet, soil moisture data at very high resolution is sought after by different scientific communities [26]. Sub-daily data is needed to account for the highly volatile nature of soil moisture [35]. So far mostly point measurements can provide this level of temporal resolution. An hourly, continuously available spatial data set at high resolution is lacking.

In comparison, spatially distributed measurements of precipitation are available in high temporal resolution. Precipitation is the main driver for soil moisture changes in the majority of biomes [36]. There is a multitude of different precipitation measurement options [37]. Ground-based estimates range from the long established procedure of direct point measurements using rain gauges to more sophisticated methods like weather radar estimates which also deliver spatially distributed precipitation amounts [38,39]. From that, gridded precipitation products based on gauge measurements alone are developed to deliver spatial coverage [40], e.g., the global land-surface precipitation products of the Global Precipitation Climatology Centre (GPCC) [41,42]. Furthermore, mostly on national scale, ground-based weather radar precipitation data is further improved via coupling with point measurements in the effort to derive an improved, gauge-adjusted version of the spatial precipitation data set [43–46]. For several decades also satellite systems have been used for atmospheric observations [37]. Geostationary satellites carrying visible/IR sensors and low earth orbit platforms that utilize active and passive microwave imaging systems are in use [37,47]. These data sets mostly comprise a whole constellation of satellites, e.g., NASA's Global Precipitation Measurement Mission (GPM) [48] or the PERSIANN-Climate Data Record (CDR) program which aggregates different satellite data streams and the Global Precipitation Climatology Project (GPCP) using artificial neural networks [49,50]. Reanalysis data sets like the fifth generation reanalysis data set by the European Center for Medium Range Weather Forecast (ECMWF, ERA5) [51] and sophisticated merging schemes like the Multi-Source Weighted-Ensemble Precipitation (MSWEP) [52] strive to further improve quality of gridded precipitation data sets. Still, there are flaws and weaknesses in all estimation and aggregation methods. Direct measurements of rainfall are error-prone concerning wind effects [53] and most regions lack or lose a sufficient amount of rain gauges [54]. Sun et al. [37] also demonstrate big differences and hence uncertainty in satellite and reanalysis data sets.

Still, precipitation values from such data sets correlate with change in soil moisture [55]. Considering the need for sub-daily soil moisture estimates at relatively high spatial and temporal resolution, this study introduces a precipitation based soil mois-

ture data set. For that, we employ the German gauge-adjusted weather radar system RADOLAN [44] to derive a modified version of the Antecedent Precipitation Index (API) that directly can be used as soil moisture data set. This allows exploitation of the high sampling rate of the weather radar and also provides spatial distributed, quality controlled precipitation estimates.

Kohler and Linsley [56] introduced the concept of the API to link runoff to antecedent soil moisture conditions, which since then has been applied in varying form in several studies: research on natural hazards consults the API for different applications, e.g., in linking antecedent moisture conditions to bush fires in Australia [57] or investigating the effect of antecedent precipitation on landslides [58]. The API is still used to supplement rainfall-runoff transformation modeling [59–61], and subsequently it is used to support flash flood warning at ungauged locations using radar precipitation data in France [62] and Morocco [63]. But the API is not only utilized to estimate surface discharge but also to help with soil moisture assessments via exploiting the relationship to precipitation. Crow et al. [64] and Crow [65] show that errors in precipitation estimates can be evaluated with the API and also that soil moisture retrievals can be improved using the dependence of the two variables. Zhao et al. [66] discuss supplementing relative soil moisture estimates with the API. Recent studies suggest using the API directly or in conjunction with geostatistical methods to derive soil moisture estimates [67–69]. The API algorithm used in this study expands upon the work of Pellarin et al. [70] who in recent studies used the API in an assimilation scheme to provide a near-realtime precipitation product [71]. The proposed improved API algorithm additionally incorporates temperature data and information on soil texture composition to allow for individual dry-down rates at distinct locations. Together with higher temporal and spatial resolution precipitation input data the authors aspire to better match local traits of the course of soil moisture in terms of dry-down rates and volatility after rainfall events. The API is calculated in a temperate region in this study, as compared to previous investigations that mostly apply the idea in more arid environments [68,70]. This increases the complexity since modeling the seasonality of soil moisture does not allow for a full dry-down of the soil column in a dry season like it has been demonstrated in these other studies.

In this article we answer the question if this improved empirical soil moisture index based on the antecedent precipitation index (RADOLAN_API) is capable to resemble the course of local soil moisture measurements throughout Germany. The detection of timely upsurge of soil moisture and dry-down rates as well as depicting the seasonality with for the temperate region typical summerly depletion is of high interest in this regard. Specifically, we investigate if the proposed hourly soil moisture product matches local measurements within defined but disputed error margins of 4 Vol% soil moisture [10,72]. Furthermore, we test a version of the developed RADOLAN_API data set with local fitted empirical variables against the soil moisture station data using the same threshold of 4 Vol% defined by GCOS.

The characteristics and capabilities of the RADOLAN_API are assessed statistically on different time scales by evaluation against in-situ measurements and spatial comparisons against the ESA CCI soil moisture product. We calculate performance and error metrics in terms of correlation, bias and differences between RADOLAN_API time series and station data. Moreover, we compare the API with the satellite product on a pixel-by-pixel basis and lay out our findings in the upcoming sections. This article also serves as file descriptor for the RADOLAN_API data set, which is openly available [73]. Appendix A Table A1 provides a summary table on the file characteristics.

2. Materials and Methods

2.1. Data Sets

2.1.1. Precipitation Data Set

Precipitation data forms the fundamental base for the calculation of the proposed soil moisture data set and heavily impacts the final product. Therefore, this study uses

quality controlled weather radar data of the German Weather Service (DWD, Deutscher Wetter Dienst) for the years 2015 to 2019. Specifically, the publicly available RADOLAN RW (Radar Online Adjustment) product is consulted, to meet the requirements of high spatial, temporal and radiometric resolution [74,75].

This weather radar data set holds precipitation estimates that are adjusted with gauge measurements [74]. The quality controlled precipitation sums are available at temporal, spatial, and intensity resolution of 1 h, 1 km, and 0.1 mm [44]. With that, RADOLAN delivers input and reference data for high-resolution hydrological modeling [76], rain type modeling [77], estimation of spatio-temporal variability of soil erosion [78] and (flash) flood modeling [79,80] as well as ground truth data for machine learning applications [81]. The polar-stereographic composite grid with the center point at 9.0°E 51.0°N covers the whole state territory of Germany [75,82].

All of the included C-Band weather radar stations operate on scanning intervals of 5 min and an approximate coverage of each device of a radius of 150 km. Significant overlap within the dense network ensures accurate retrievals by minimizing problems due to dampening in the signal that occur with increased distance from each sensor [83]. Furthermore, within the automatic calibration procedure, rain intensity-adapted Z-R relationships (empirical formula to estimate rainfall rates from radar reflectivity signal strength) are applied. The correction for radar artifacts contains filtering for statistical clutter and consideration of orographic shadowing effects [74,75].

Nevertheless, for a realistic estimation of the quantity of precipitation, measurements of approximately 1300 conventional stations are used for the operational hourly gauge adjustment routine [84]. These sensors basically work according to "Hellmann" ombrometers [85], which obey the standards of the World Meteorological Organization [86]. The appliance of a weighing principle and surrounding temperature-dependent heating sets the utilized devices apart from conventional measurement systems and allows capturing solid and fluid precipitation alike [75].

To derive precipitation from radar backscatter values assumptions on the drop size distribution and droplet count are necessary [83]. RADOLAN uses an extended Z-R relationship, that considers the absolute reflectivity and horizontal gradients to distinguish between typical convective and stratiform droplet distributions [75]. In wintertime, the effects of overshooting due to lower cloud heights become more prominent in weather radar systems. These shortcomings are accounted for with a seasonally-dependent correction via a regression analysis. In order to mitigate erroneous adaptation at single extreme precipitation events, e.g., intensive convective cells that occur regularly throughout Germany in summer, DWD applies a multiple polynomial regression to generate the correction factors for every pixel. Respective scanning height class, day of year, and reflectivity are therefore taken into account [83]. The weather radar data shows good agreement with NASA's Integrated Multi-satellitE Retrievals for the Global Precipitation Measurement Mission (IMERG, GPM) satellite precipitation data set for the vegetation period [39]. This makes the data set a very good candidate as input data for the calculation of the soil moisture index with a high potential of transferability. Throughout this study, the data set will be referred to as "RADOLAN".

2.1.2. Soil Properties

Data from the Soilgrids project [87], released by the International Soil Reference and Information Center (ISRIC), provides the information on soil properties in this study. Local clay and sand content are utilized to shape the dry-down rates of the modeled soil moisture at any given pixel. Soilgrids is a global complete soil information data set with 250 m spatial resolution and 6 layers. Based on machine learning driven algorithms that account for environmental co-variables and soil profile data, the Soilgrids data set predicts soil type and a multitude of physical and bio-chemical soil properties, e.g., distribution of soil compartments, bulk density, pH [87,88]. Soilgrid data is adapted widely by the scientific

community, e.g., for generating European and global soil hydraulic databases [89–91] and as auxiliary variables in downscaling algorithms [91].

2.1.3. Temperature Data Set

This study uses the ERA5 single level air temperature data set (t2m) generated by the ECMWF published by the Copernicus Climate Change Service Climate Data Store (CDS) [51,92]. The ERA5 atmospheric reanalysis data set provides climate variables at hourly resolution on global scale currently covering the period from 1979 to present and as preliminary back extension from 1950 onward. Therefore, observation data is combined with model data by the technique of data assimilation in a consistent manner respecting the laws of physics [92]. For the provision at CDS the ERA5 data is interpolated to a regular $0.25^\circ \times 0.25^\circ$ grid, which for this study was further bilinearly interpolated to the RADOLAN grid. Albergel et al. [93] show that using ERA5 data as atmospheric forcing in land surface model simulations significantly improves the representation of land surface variables when compared to the predecessor ERA-Interim. Furthermore, other studies find a systematically reduced bias in ERA5 temperature and precipitation data when compared to the previous version [94,95] and indicate the high usability of the reanalysis data set in high-accuracy and high-resolution modeling scenarios [96,97].

2.1.4. Calibration and Validation Data Sets

Different data sets are used to calibrate and validate the RADOLAN_API data set. Soil moisture data from TERENO networks and a self-conducted field campaign at the Wallerfing test site is used for calibration of the necessary variables in the API equation and for validation on point data. The ISMN database provides data from the TERENO Eiffel/Lower Rhine Valley (TERENO-Rur) site [11,16,98,99]. To increase the number and diversity of in-situ measurement stations in terms of soil composition, stations from the TERENO Northeast German Lowland Observatory (TERENO-NE) site are incorporated in this study [100]. Furthermore, the self conducted field campaign holds data for six measurement stations on agricultural fields throughout the growing period of 2017. The data at each site (A2, A4, A6, P2, P4, P6) represents the respective average of five Echo EC-5 probes in 5cm depth that was corrected for diurnal cycle fluctuations.

So, for calibration and validation a total of 23 measurement stations are used. Figure 1 shows (a) the individual soil composition information derived from Soilgrids data and (b) the location of the test sites. Table 1 gives information on the station's setup and their assignment to calibration and validation classes. The stations represent the typical portfolio of soil compartment distribution of Germany.

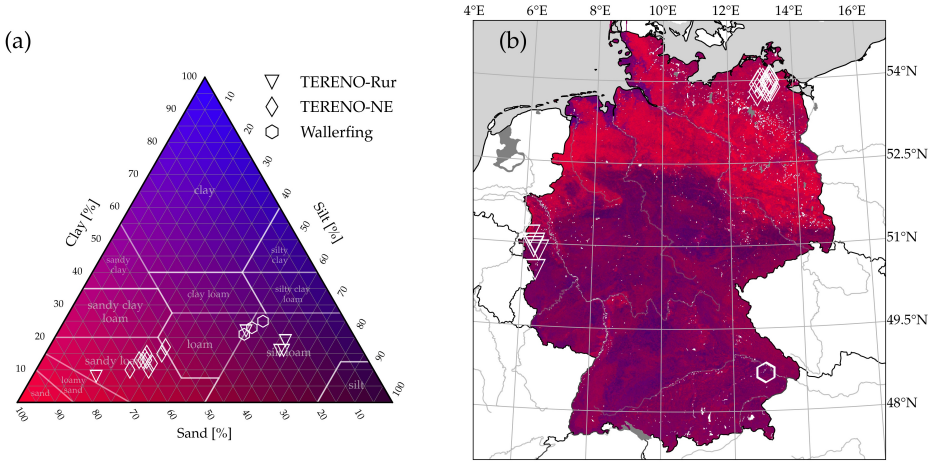

Figure 1. Soil composition for the test sites (**a**) and similarly color coded soil map for Germany (**b**), derived from Soilgrid's data top layer sand and clay content [87].

For spatial evaluation of the RADOLAN_API data set the study uses the European Space Agency's Climate Change Initiative (ESA CCI SM) combined data set in version 4.7 [101–103]. The combined data set is derived through a multi-sensor merging approach that uses both active and passive publicly available Level 2 satellite products [102]. The authors chose this data set as evaluation reference because of its wide usage in the scientific community. That makes it well-established and strengths and weaknesses are well-known [104–109]. The ESA CCI SM data set is bilinearly interpolated to the RADOLAN grid for interoperability and comparability.

Table 1. Overview of soil moisture measurement stations that are used in calibration and validation procedure. Cal/Val set states the assignment to the respective random calibration and validation set.

Station	Network	Cal/Val Set	Coordinates	Sand [%]	Clay [%]	Available Time Period
Beestland	TERENO-NE	I	53.9255°N, 12.9180°E	60	10	20111107–20191010
Boeken	TERENO-NE	II	53.9971°N, 13.3124°E	58	15	20111107–20190523
Goermin	TERENO-NE	I	53.9828°N, 13.2579°E	54	15	20111107–20191010
Grosszastrow	TERENO-NE	II	54.0170°N, 13.2733°E	59	14	20111107–20191106
Heydenhof	TERENO-NE	II	53.8682°N, 13.2686°E	52	17	20130206–20191106
Neu Tellin	TERENO-NE	I	53.8598°N, 13.2121°E	61	13	20111107–20191010
Rustow	TERENO-NE	II	53.9581°N, 13.0786°E	60	13	20111107–20191106
Sanzkow	TERENO-NE	II	53.8810°N, 13.1243°E	65	10	20111107–20191106
Sommersdorf	TERENO-NE	II	53.7899°N, 12.9021°E	58	12	20151020–20191010
Toitz	TERENO-NE	II	53.9725°N, 12.9906°E	59	14	20111107–20190910
Voelschow	TERENO-NE	I	53.8712°N, 13.3459°E	59	14	20130128–20190619
Zarrenthin	TERENO-NE	I	53.9425°N, 13.2857°E	59	13	20111107–20191107
Gevenich	TERENO-Rur	II	50.9892°N, 6.32355°E	22	16	20110804–20190403
Merzenhausen	TERENO-Rur	II	50.9303°N, 6.29747°E	21	16	20111103–20190103
Schoeneseiffen	TERENO-Rur	I	50.5149°N, 6.37559°E	28	22	20100222–20190425
Selhausen	TERENO-Rur	II	50.8691°N, 6.44954°E	19	19	20130424–20161029
Wildenrath	TERENO-Rur	II	51.1327°N, 6.16918°E	75	8	20120416–20181004
Wallerfing_A2	Wallerfing	I	48.6953°N, 12.8673°E	22	25	20160422–20161026
Wallerfing_A4	Wallerfing	I	48.6969°N, 12.8673°E	22	25	20160422–20161026
Wallerfing_A6	Wallerfing	I	48.6891°N, 12.8722°E	26	23	20160422–20161026
Wallerfing_P2	Wallerfing	I	48.6907°N, 12.8746°E	26	23	20160422–20161026
Wallerfing_P4	Wallerfing	II	48.7028°N, 12.8966°E	29	21	20160422–20161026
Wallerfing_P6	Wallerfing	I	48.7037°N, 12.8989°E	29	21	20160422–20161026

2.2. Antecedent Precipitation Index

The basic idea of the antecedent precipitation index (API) is to take a certain number of preceding time steps and include the respective rainfall amount in the current time step with a time dependent diminishing factor. Equation (1) shows the basic idea of the API formulated by Kohler and Linsley [56], with API being the index value at time step t and $t-1$ respectively, γ being the diminishing factor and P_t representing the precipitation amount at the current time step t.

$$API_t = \gamma \times API_{t-1} + P_t \tag{1}$$

Derivations of this formula exist in manifold ways that allow using the API as soil moisture proxy. Crow et al. [64] e.g., apply a simple cosine based loss function that controls the summerly depletion overhead as replacement for γ. However, several single processes contribute to the reduction of soil water content represented by this diminishing factor. In this study, the antecedent precipitation index algorithm proposed by Pellarin et al. [70] is extended with additional dampening factors in the attempt to improve the empirical representation of local dominant processes that control the soil moisture loss. Temperature values from the ERA5 reanalysis data set [51,92] is used as proxy information for the upwards water loss in the soil column through evapotranspiration (Equation (3)). With that, sub-daily variations in water loss can be attributed instead of e.g., applying seasonal varying loss factors. Including this extra amount of data might be considered as immoderate contribution to a simple soil moisture index. However, this procedure will provide a

better guidance in temporal scales of multiple days or weeks and hence allows e.g., for hot dry spells in summer or earlier onset of winter to be better accounted for. Local saturation state and soil properties control the amount of gravity driven drainage of soil moisture to the lower soil compartments through the process of percolation (Equation (4)). Together, factors a and b reduce the amount of soil water from time step $t-1$ to yield the current state soil moisture index API at time step t:

$$API_t = a \times b \times API_{t-1} + (\theta_{sat} - API_{t-1}) \times \left[1 - e^{-\frac{P_t}{d}}\right] \quad (2)$$

with

$$a = 1 - \left[\frac{T}{\alpha} \times e^{-\beta \times clay}\right] \quad (3)$$

and

$$b = e^{-\left(\frac{API_{t-1} - \theta_{res}}{\theta_{sat} - \theta_{res}}\right)^{\gamma}} \quad (4)$$

where θ_{sat} = maximum saturation, θ_{res} = residual saturation, P_t = precipitation [mm], d = depth [mm], T = temperature, α = temperature scaling factor, $clay$ = clay content [%], β = clay scaling factor and $\gamma \geq 1$ regulating the peak outflow. Figure 2 shows a graphical representation of the loss scaling factors a and b for different overall settings. For this study β is fixed to 0.05 due to computational restrictions.

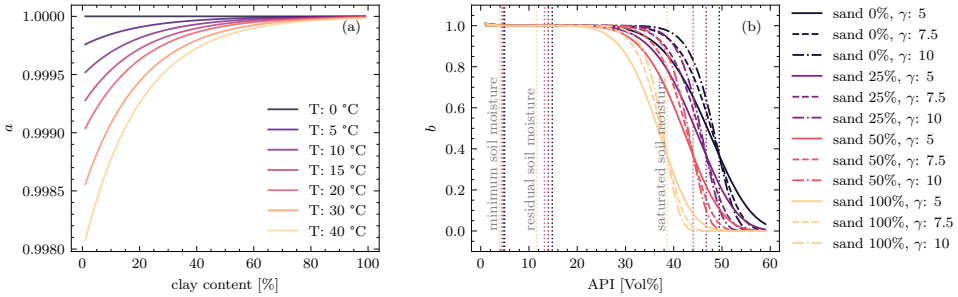

Figure 2. Soil moisture loss factors a, depending on clay content and temperature (**a**) and b depending on sand content and saturation state (**b**) for the applied α and γ values.

The saturation state in Equation (4) calculates from maximum saturation θ_{sat} and residual saturation θ_{res}. The respective values are specifically derived based on empirical relationships of the Interaction Soil Biosphere Atmosphere (ISBA) model [110,111] with

$$\theta_{sat} = 0.1 \times (-1.08 \times (sand) + 494.31) \quad (5)$$

$$\theta_{res} = 0.3 \times \theta_{sat} \quad (6)$$

incorporating local *sand* content. Information on soil texture composition is derived from the Soilgrids [87] data sets. The intent behind factor a is to allow quick outflow if the soil is near saturation. Loss factor b is responsible for loss due to temperature but takes clay content and an empirical scaling factor into account. In this study, we differentiate between the API, which uses empirical scaling factors optimized for all station data, and the local API (lAPI) that uses per-station optimized empirical scaling factors α and γ. Both indices take the respective local soil characteristics and temperature data into account.

2.3. Calibration and Validation Procedure

The coupling of precipitation information from the RADOLAN weather radar with distributed soil information and temperature data makes the retrieval of spatio-temporal API values possible. The empirical approach of the calculation implies that the variables α and γ contributing to the loss factors a and b need to be adjusted for best results. Due to the lack of a valid spatially distributed ground-truth data set and computational limits the

respective parameters are set constant throughout space and time for the three dimensional API calculation, which is the data represented in the RADOLAN_API data set. However, to highlight the general capacities of the advanced API algorithm itself, a local optimization of the empirical parameters (lAPI) for the single calibration sites is conducted as well. These lAPI realisations on point scale also include local temperature and soil information data but furthermore individually adjusted α and γ values (Table A2).

Three main measures are used for the evaluation of the proposed data set: bias, unbiased root mean square difference ($ubRMSD$) and Pearson's R linear correlation coefficient.

$$bias = \frac{1}{N}\sum_{i=1}^{N}(x_i - y_i) \tag{7}$$

$$\text{RMSD} = \sqrt{\frac{1}{N}\sum_{i=1}^{N}(x_i - y_i)^2} \tag{8}$$

$$\text{ubRMSD} = \sqrt{RMSD^2 - bias^2} \tag{9}$$

$$R = \frac{\sigma_{xy}}{\sigma_x \sigma_y} \tag{10}$$

Quality flags of ISMN and TERENO data sets are respected for calibration and cross-validation. ESA CCI SM data also ships with quality flags. Such, that indicate snow or cold temperatures are used for all data sets in the point scale evaluation (API, station measurement data and ESA CCI SM data) and also for the spatial evaluation of the RADOLAN_API against ESA CCI SM data. Therefore, a seven day rolling window is additionally applied to help with excluding days after or in between freezing. Remaining quality flags concerning the data quality of ESA CCI SM data itself are only applied to the satellite data set.

Soil moisture data of the TERENO network and the conducted field campaign is used to calibrate the empirical parameters of the API formula that determine the effect of loss factors a and b in Equation (2). The respective stations only provide data for a specific time span and hence calibration was done for the particular available period while omitting a 14 day warm-up period.

Calibration of the respective empirical variables of the API demanded for iteratively calculating the described hourly soil moisture index for each of the 23 single reference stations. Depths of measurement and local soil composition of each installation therefore is taken into account. The applied optimization procedure evaluates the calculations against measured soil moisture station data. In case of the API (RADOLAN_API) version, the minimization target is defined as the mean $RMSD$ across all stations against the measured data. The empirical variables α and γ are optimized iteratively and finally selected based on the outcome of the procedure. For the individually optimized lAPI on point scale, the variables are optimized on a per-station basis. In both variants, the whole available time series was used at each point with no masking besides respecting the warm-up period. The Nelder-Mead algorithm is used for minimization of the respective target variable (mean) $RMSE$ [112]. Gao and Han [113] state that this is the most widely applied direct search method for unconstrained optimization problems and further improved the algorithm for solving problems more efficiently in high dimensions.

For validation purposes the soil moisture stations are randomly split and assigned to two sets, I and II (Table 1), to carry out a standard cross-validation. Hence, the calibration approach described above is repeated for the respective calibration subset of stations and the resulting empirical variables are used to validate the remaining subset against the appropriate soil moisture station data. Table A2 gives an overview of respective α and γ values for the overall and local individual optimization as well as the calibration sets.

This study also evaluates the API spatially against ESA CCI data on a pixel-by-pixel basis. Additional to the overall comparison, a monthly and seasonal summary is conducted to provide insights in the temporal dependence of the performance. Furthermore, the local

calibrated lAPI time series at the measurement sites are compared to the measurements. The results aim to show the adaptability of the API to local circumstances.

3. Results

3.1. Calibration and Evaluation

The calibration for RADOLAN_API resulted in a mean *ubRMSD* of 3.37 Vol% with a standard deviation of 1.93 Vol% between the calculated API on point scale and respective reference measurements. Table 3 summarizes the evaluation metrics. The spatial distributed API data set RADOLAN_API is published as CC-BY-SA in form of a netCDF file [73]. The hourly resolution and 1 km × 1 km spatial resolution add up to a data set with dimensions 692 × 1188 × 43,824 (latitude, longitude, time) and a file size of 20.9 GBs that covers the years 2015 to 2019. A summary of the file characteristics is presented in Table A1. In the following "API" refers to the variant of the index included in this soil moisture data set.

The evaluation of the proposed API against ESA CCI SM data and station data respects masking based on the ESA CCI SM flags as described in Section 2.3. Hence, values of metrics in the evaluation differ to the ones obtained in the calibration process itself. This is done to allow the calibration of the empiric variables to also account for seasonality in terms of rising soil moisture in fall and higher soil moisture values after winter. However, for a fair comparison and comparability, the flagged time spans, highlighted in grey in Figure 3, are excluded for the remaining evaluation. That figure shows the best and worst performing station of each network relating to *RMSD* between API and measurement. Further insight in the exact metrics is given in Table 2 where also metrics for ESA CCI SM versus measurements and ESA CCI SM versus API are included.

Table 2. Evaluation of the overall and locally optimized API and ESA CCI SM data against local measurements; and evaluation of ESA CCI SM against overall optimized API; masks are applied as described in the text; the asterisk (*) indicate lower (*ub*)*RMSD* and higher *R* values of the API respectively in comparison to ESA CCI SM data when benchmarked against the local measurements.

	***RMSD* [Vol%]**				***ubRMSD* [Vol%]**				***R***			
		In-Situ		CCI		**In-Situ**		**CCI**		**In-Situ**		**CCI**
Station	**API**	**lAPI**	**CCI**	**API**	**API**	**lAPI**	**CCI**	**API**	**API**	**lAPI**	**CCI**	**API**
Beestland	2.29 *	2.02 *	5.19	5.77	2.16 *	2.02 *	3.26	3.27	0.69 *	0.69 *	0.56	0.55
Boeken	2.19 *	1.76 *	4.34	4.58	1.88 *	1.76 *	4.32	4.36	0.60 *	0.71 *	0.42	0.40
Goermin	2.83 *	2.29 *	4.34	4.41	2.78 *	2.29 *	4.30	4.30	0.64 *	0.77 *	0.50	0.44
Grosszastrow	3.09 *	2.67 *	5.19	4.76	3.09 *	2.67 *	4.87	4.51	0.60 *	0.71 *	0.36	0.28
Heydenhof	2.93 *	2.03 *	4.49	4.28	2.15 *	2.02 *	4.01	4.28	0.67 *	0.71 *	0.53	0.44
Neu Tellin	1.84 *	1.72 *	4.26	4.62	1.84 *	1.71 *	3.37	3.80	0.77 *	0.80 *	0.59	0.41
Rustow	2.67 *	2.29 *	3.79	3.99	2.30 *	2.28 *	3.78	3.69	0.59 *	0.63 *	0.48	0.49
Sanzkow	4.04	2.28 *	3.87	4.12	2.72 *	2.28 *	3.77	3.51	0.70 *	0.79 *	0.55	0.59
Sommersdorf	2.01 *	1.81 *	4.21	4.32	2.00 *	1.81 *	2.82	3.25	0.76 *	0.80 *	0.71	0.60
Toitz	2.59 *	1.55 *	3.07	3.91	1.55 *	1.55 *	3.06	3.25	0.72 *	0.71 *	0.63	0.57
Voelschow	3.21*	1.74 *	4.27	4.48	2.03*	1.73*	4.07	4.34	0.61 *	0.76 *	0.52	0.43
Zarrenthin	2.96 *	2.87 *	4.72	4.24	2.91*	2.83*	4.56	4.21	0.32	0.32	0.33	0.41
Gevenich	7.94 *	4.51 *	8.84	3.74	7.35	4.51 *	6.67	2.61	0.62	0.84 *	0.69	0.59
Merzenhausen	8.09	6.51 *	7.12	4.30	7.84	6.50	5.76	3.84	0.05	0.57	0.68	0.21
Schoeneseiffen	8.90	3.87 *	6.99	4.30	7.20	3.87 *	6.80	2.52	0.54	0.88 *	0.59	0.47
Selhausen	5.91	4.15 *	4.21	3.56	5.62	4.15 *	4.21	3.04	0.51	0.77	0.81	0.42
Wildenrath	8.87 *	5.01 *	11.54	4.80	6.96	5.00 *	6.42	2.60	0.44	0.77 *	0.57	0.54
Wallerfing_A2	4.29 *	3.14 *	6.33	3.46	3.31	3.12	2.92	1.98	0.51	0.65	0.70	0.47
Wallerfing_A4	4.89 *	4.01 *	6.64	3.46	4.00	3.99	3.38	1.98	0.40	0.45	0.68	0.47
Wallerfing_A6	7.52 *	2.75 *	9.24	2.46	2.73 *	2.70 *	2.76	1.68	0.76 *	0.73	0.75	0.65
Wallerfing_P2	5.19 *	2.75 *	6.85	2.50	2.76 *	2.68 *	2.77	1.67	0.76 *	0.74	0.75	0.65
Wallerfing_P4	4.30 *	1.80 *	7.12	3.32	2.15 *	1.80 *	2.54	1.56	0.81 *	0.86 *	0.72	0.65
Wallerfing_P6	8.72 *	2.03 *	11.26	2.92	2.10 *	2.03 *	2.63	1.57	0.81 *	0.81 *	0.63	0.65
Mean	4.66 *	2.85 *	5.99	4.01	3.45 *	2.84 *	4.05	3.12	0.60	0.72 *	0.60	0.49
Standard dev.	2.47	1.27 *	2.36	0.77	2.01	1.27 *	1.30	1.02	0.18	0.13	0.13	0.12

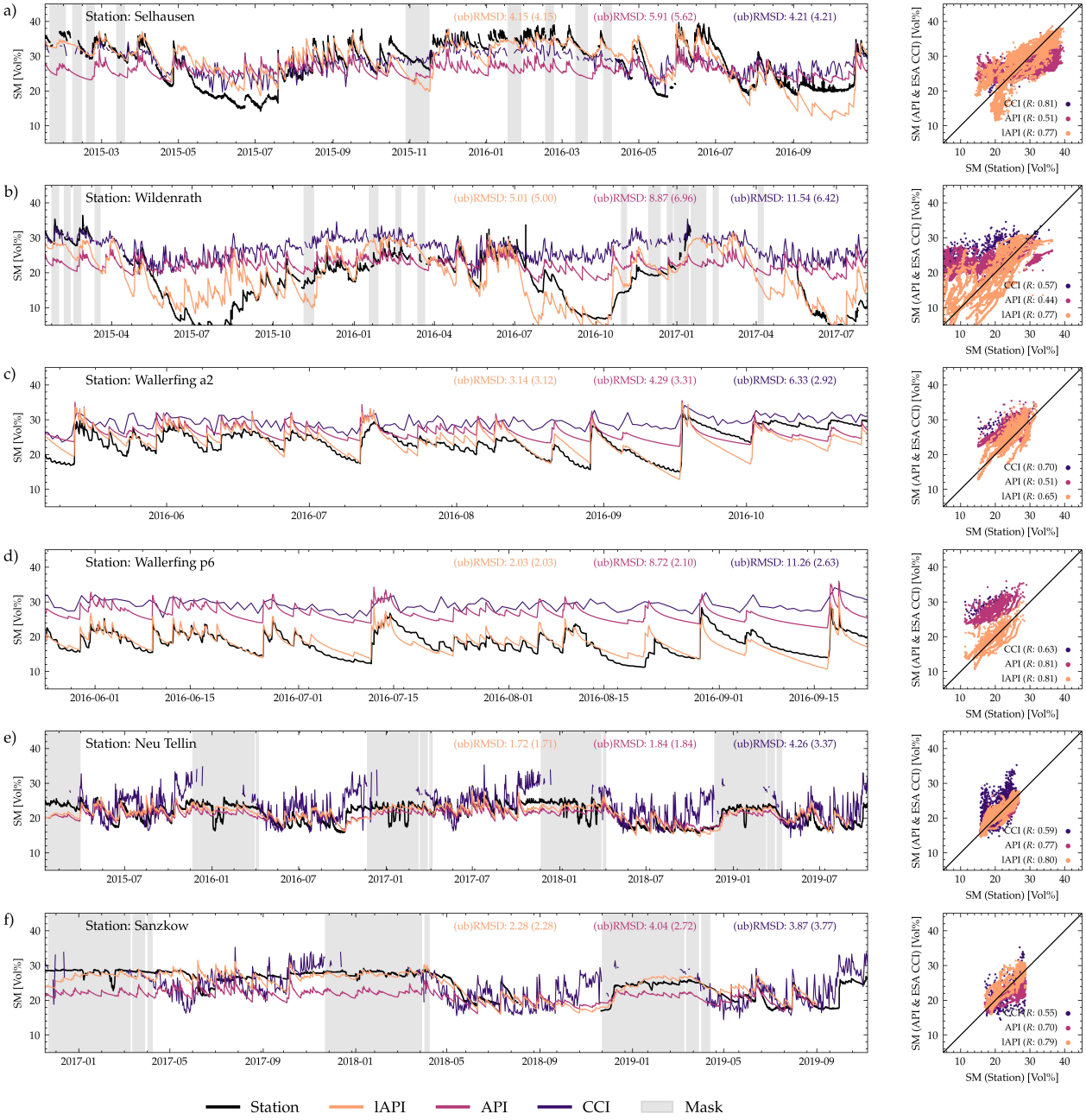

Figure 3. Soil moisture measurement, API, lAPI and ESA CCI SM data and respective scatterplots for selected stations Selhausen (**a**), Wildenrath (**b**), Wallerfing a2 (**c**), Wallerfing p6 (**d**), Neu Tellin (**e**) and Sanzkow (**f**).

The overall optimized API shows a mean *RMSD* of 4.66 Vol% and *ubRMSD* of 3.45 Vol% with a respective standard deviation across the 23 point results of 2.47 Vol% and 2.01 Vol% when compared to in-situ station measurements. With that, the differences to measurement data are smaller than for the ESA CCI SM data set in the same comparison (5.99 Vol% and 4.05 Vol% respectively). However, the API shows wider spread and deviation in both *RMSD* and *ubRMSD*. The API data set reaches the highest mismatch in *RMSD* and *ubRMSD* to the station Wildenrath with 8.87 Vol% and 6.96 Vol% respectively. This station shows extremely low soil moisture values during summer (Figure 3b) which can be traced back to the high sand and low clay content at that site (Table 1). Lowest

difference is reached at station Neu Tellin with 1.84 Vol% (*RMSD*) and for unbiased comparison station Toitz with 1.55 Vol% (*ubRMSD*). Generally, the sandier sites of the TERENO-NE site perform noticeable better than stations from the other networks.

Overall, the API is similarly correlated to the in-situ measurements like the ESA CCI SM data is, with a mean correlation coefficient of 0.60. Here again, the API shows a higher standard deviation of 0.18 compared to 0.13 of ESA CCI SM data. Expectedly, the lAPI shows increased correlation to the soil moisture measurements with a mean of 0.72 and maximum of 0.88. This higher accordance is shown clearly in Figure 3 where the lAPI distinctly follows the summerly depletion for TERENO-Rur and TERENO-NE time series. The scatterplots demonstrate the improvements accordingly. For Wallerfing sites where there is no seasonality or summerly depletion to follow, the lAPI shows higher and prolonged outflow. This results in a difference in *RMSD* of −1.15 Vol% and −6.69 Vol% and also lowered *ubRMSD* that is reduced by 0.16 Vol% and 0.07 Vol% for the stations Wallerfing A2 and Wallerfing P6 respectively. The temporal accuracy and dynamic of the API and lAPI do match the measurement data very well which also the Wallerfing plots (Figure 3b,c) demonstrate clearly. This is the direct effect of the high resolution of the RADOLAN product that directly propagates into a rise in soil moisture.

3.2. Two-Fold Cross-Validation

The stations are randomly assigned to two groups I and II for the cross-validation (CV) procedure. Table 1 gives the respective affiliation. Each group is used as calibration and validation group respectively. Run I of the CV uses stations of set I as calibration data and stations of set II as validation data and vice versa for run II. Overall, the cross validation shows in average very similar evaluation metrics like the overall calibration that uses all stations at once (Table 3). The mean *RMSD* only increases by 0.07 Vol% to 4.72 Vol% where the standard deviation in the combined validation data set even declines.

Table 3. Calibration results of API depletion factors and averaged evaluation metrics for overall calibration and calibration in the cross-validation scheme (no masking applied).

Run	***RMSD* [Vol%]**	***ubRMSD* [Vol%]**	***R***
Overall Calibration	mean: 4.65 stdev: 2.37	mean: 3.37 stdev: 1.93	mean: 0.61 stdev: 0.15
Avg. of Cross-Validation	mean: 4.72 stdev: 2.29	mean: 3.38 stdev: 1.93	mean: 0.61 stdev: 0.16
Run I: Validation Set	mean: 4.48 stdev: 2.13	mean: 2.59 stdev: 1.28	mean: 0.66 stdev: 0.12
Run II: Validation Set	mean: 4.99 stdev: 2.43	mean: 4.25 stdev: 2.13	mean: 0.55 stdev: 0.17

In run I the *RMSD* drops whereas in run II the *RMSD* with 4.99 Vol% is higher than in the overall calibration. The correlation coefficient behaves similar: the *R* of both validation sets combined does not change compared to the overall calibration, however run I validation set outperforms the run II validation set. This difference becomes more prominent for the *ubRMSD*. Both validation sets combined, the error metric does not significantly change compared to the overall calibration with 4.72 Vol% and 4.65 Vol%. But validation in the cross-validation run I outperforms run II validation with 2.59 Vol% *ubRMSD* compared to 4.25 Vol% *ubRMSD*. Standard deviation values increase in run II validation accordingly. Figure 4 clearly presents this fact. Whereas *RMSD* and *R* do not deviate much from the average distribution, the *ubRMSD* values for run I and II distinctly differ with a wide spread (standard deviation of 2.13 Vol%) of the metric for the validation set in run II and a compact distribution of *ubRMSD* for run I (standard deviation 1.28 Vol%). The disparity is to be attributed to the random partition of stations in the two sets: every group got a majority of a distinctive set of soil types (Table 1). Run I with stations of group II as validation stations holds many of the better performing stations, when calibrated separately, mostly of the TERENO-NE site.

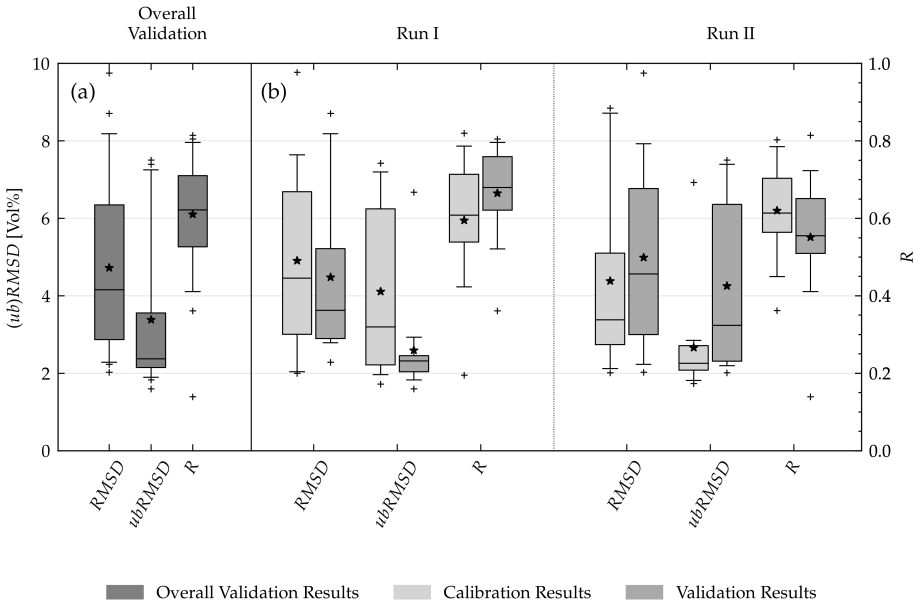

Figure 4. Results of the two-fold cross-validation showing spread of *RMSD*, *ubRMSD* and *R* in validation stations of (**a**) both runs combined and (**b**) in respective calibration and validation stations from each run. Outliers (+) are defined exceeding 2.7 σ, asterisks (*) show the mean of the respective distribution. Summary of values listed in Table 3.

3.3. Comparison with ESA CCI Soil Moisture Data

The API was compared to ESA CCI SM data on a pixel by pixel basis. Figure 5 shows the *ubRMSD*, bias and correlation coefficient *R* for three seasons MAM, JJA, SON and the mean over all three of them. It becomes apparent that in the spring season MAM the differences are highest with *ubRMSD* values exceeding 4 Vol% in central Germany. Similar patterns are observable for seasons JJA and SON where these are not as pronounced. Outlines of the low mountain range in the central part of Germany e.g., the Harz Mountains (51.7°N, 10.7°E) or Pfälzerwald (49.3°N, 7.9°E) are reflected in the *ubRMSD*. Most prominently however, the errors are highest in the east of the Rothhaargebirge (~51.0°N, 9.0°E) which is justified with a monthly unsteady bias ranging from negative to positive values in the MAM season (Figure A1). In the northeastern part of Germany dissimilarity of the API and ESA CCI SM data is prevalent. At the TERENO sites in this region the API outperformed the ESA CCI SM product (Table 2). A clear reflection of soil types is not to be seen in the error values (Figure 1).

Overall a negative bias of the API compared to the ESA CCI SM product exists, which similarly was present in the per-station comparison. The negative bias of the API in the spatial comparison is most noticeable along river Elbe (52.5°N, 11.7°E) and in north western Germany (East Frisia, 53.5°N, 7.9°E). In the Harz Mountains the API values are positivly biased which can possibly be attributed to higher precipitation amounts due to orographic rainfall.

Correlation between the ESA CCI SM and the API data set ranges between a *R* value of 0.4 and 0.8 with lower values in the MAM season. Figure 6 depicts the spatially aggregated evaluation between ESA CCI SM an and API on a monthly basis. It has to be noted, that for masking reasons only about half of the amount of grid cells are available for the winter period (Figure A2). The monthly evaluation supports the statement of low correlation (with high standard deviation) and higher bias in wintertime where the overall optimized API does not deliver soil moisture values as high as ESA CCI SM does. The monthly mean *ubRMSD* in the MAM season ranges from 1.0 to 2.0 Vol% (Figure 6 and Figure A1) which does not reflect the strong deviation from the seasons JJA and SON as shown in Figure 5 due to the discussed shift in bias.

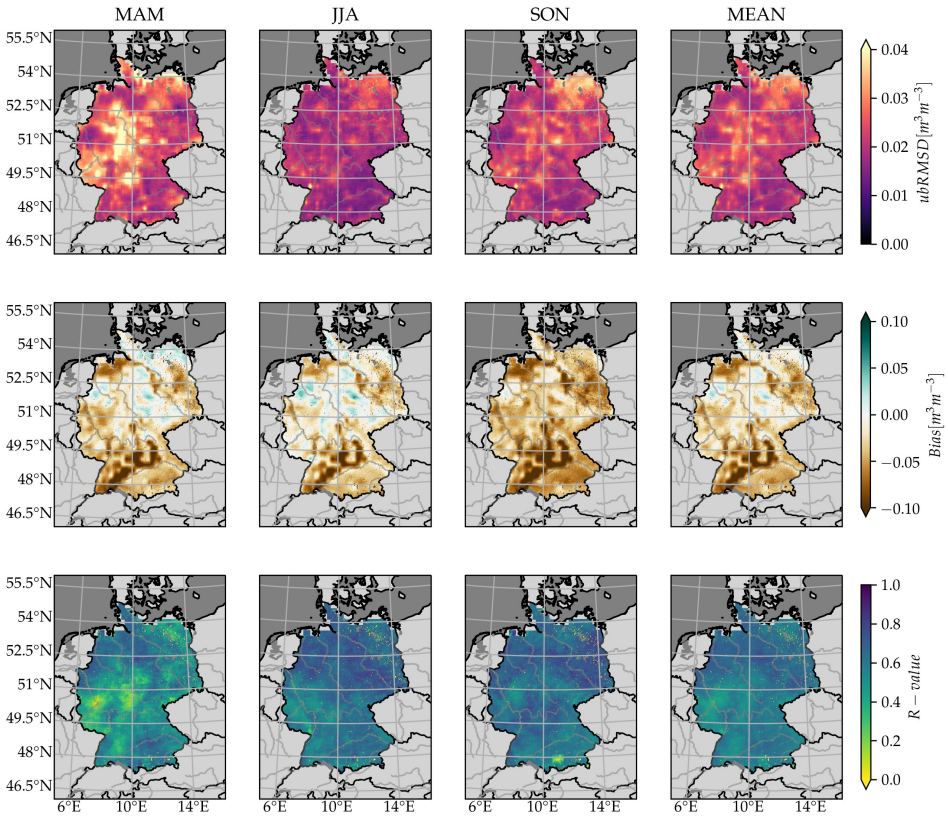

Figure 5. *ubRMSD*, *bias*, and *R* between API and ESA CCI SM data for seasons MAM, JJA, SON and mean of the seasonal measures.

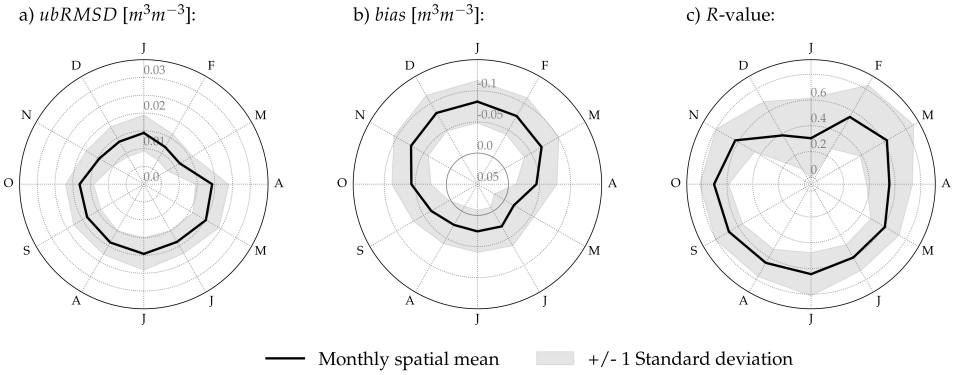

Figure 6. Polar plots of the monthly (**a**) *ubRMSD*, (**b**) *bias* & (**c**) *R* between the mean daily API and ESA CCI SM.

4. Discussion

The introduced RADOLAN_API data set shows very good agreement with local soil moisture measurements in terms of volumetric soil moisture estimation with a mean *ubRMSD* of 3.45 Vol% and mean *RMSD* of 4.66 Vol% in the evaluation against 23 measurement stations. The unbiased error values of the hourly soil moisture data set fulfill the criteria of GCOS which proclaims an error threshold of 4 Vol% for soil moisture estimations. With that, RADOLAN_API shows lower mean *ubRMSD* and lower mean *RMSD* values than ESA CCI SM (4.05 Vol% and 5.99 Vol%) at the utilized soil moisture measurement stations (Table 2). An especially strong argument for the weather radar based API is the

timely increase of modeled soil moisture that clearly hits the measured upsurge. This is perfectly visible in comparison to station measurements in Figure 3c,d. Delivering this high accuracy in the change signal is a very valuable characteristic and often sought after in the modeling community [26]. Consequently, on point scale, the API outperforms ESA CCI SM data at 16 of 23 stations with regard to *ubRMSD* against measurement data. This might be explained with the higher spatial and temporal resolution in the original data set than the merged satellite product. Also vegetation influence is reasonably handled in the empiric loss functions of the proposed API.

Additionally, we introduced a locally optimized API (lAPI), that similarly considers soil information and temperature but empirical scaling variables are locally adjusted. Seasonalities of highly volatile soil moisture time series can be even better represented with the lAPI than the overall optimized API. This is convincingly presented in the exemplary station plots in Figure 3. The correlation between modeled data and measurements increases accordingly from a R value of 0.60 (API) to 0.72 (lAPI, Table 2).

The cross-validation procedure of the API shows little differences in validation results of the two respective sets. This means that on the one hand the API formula is robust. On the other hand the need for a local, more individual adjustment based e.g., on relationships between soil properties and actually applied values of the depletion variables is evident. Accordingly, Table 2 shows improvements in all averaged metrics $RMSD$, $ubRMSD$ and R for the lAPI compared to the API.

Investigation on different temporal resolutions by showing monthly and seasonal aggregates of error and correlation metrics is necessary to get unambiguous results [72]. This approach allowed the authors to identify a local non-stationary bias in the western part of Germany conducting the spatial comparison of the API and ESA CCI SM data.

A dominant pattern of negative biased API values in the southern part of Germany is prevalent. For these regions, the ESA CCI SM data set shows strikingly high mean soil moisture estimates (Figure A3). Missing sensor data in the constellation contributing to ESA CCI SM data can lead to differences in soil moisture estimates [101]. In this regard, an accumulation of acquisitions that use a specific sensor combination while featuring the distinct bias pattern, could however not be confirmed as possible reason (Figure A3). These high values in the ESA CCI SM data set coincide with occurrences of Leptosols and Cambisols from material derived from limestone, marlstone and dolomite weathering [114]. In the same region the hydrogeology is dominated by karstified or fissured jurassic calcareous fazies in the base rock [115]. The attributed low air capacity of the effective root zone and indicated low soil moisture at field capacity for this area does not fit the behaviour of the ESA CCI SM data [116,117]. Wagner [118] discusses unexpected backscatter effects in microwave satellite data. Increased surface roughness of dry soils containing rock fragments in the top layer might be the explanation for the very high soil moisture values in these regions [118].

Many processes and properties on earth's surface that affect the water and energy fluxes are not directly included in the proposed empirical API model that seeks to avoid the input data overhead. The two most obvious of these factors might be soil organic carbon (SOC) and vegetation cover: predominantly in dry conditions, SOC explains variance better than soil texture [119]. Furthermore, de la Torre et al. [120] show that vegetation strongly influences soil dry-down rates through evapotranspiration. Empirically modeling the manifold effects that vegetation related processes have on soil moisture in the API formula certainly holds error potential. Yet, the results at the single measurement station sites indicate that the diverse interactions were well mimicked with the applied loss functions at least for grasslands and agricultural sites.

Still, uncertainties in the utilized data sets propagate and introduce errors in the soil moisture estimation. Tifafi et al. [121] e.g., point out spatial representativeness errors in the Soilgrids data set, specifically however for the modeled soil organic carbon. Also, inaccuracies in the RADOLAN data set directly propagate into the API values. Good overall agreement of the weather radar data with the renowned GPM data set has been shown

but seasonal differences in performance may be the reasoning for the higher negative bias values in the eastern part of Germany [39]. An investigation of the effects of such input data inherent deficiencies has not been carried out by the authors and is not in the scope of this article. Usage of further downscaled soil texture information as shown by Marzahn and Meyer [122] can guide the way of the proposed API towards field scale soil moisture estimations.

5. Conclusions

This study introduces the hourly weather radar data, temperature and soil information based soil moisture data set RADOLAN_API. The utilized empirical variables in the API formula are once optimized to be used in the spatial API data set RADOLAN_API, but also on a per-station basis to evaluate the adjustability of the improved API algorithm to given specific circumstances concerning interplay of soil characteristics and natural surroundings. Evaluation of the modeled soil moisture data was conducted on different temporal resolutions, covering daily, monthly and seasonal aggregations.

The API generally shows good agreement with measured data especially for timely detection of the onset of soil moisture increase. This characteristic is taken from the high temporal resolution of the RADOLAN weather radar data input. Also, performance of the RADOLAN_API in terms of error metrics against in-situ soil moisture data is very good with a mean $ubRMSD$ of 3.45 Vol% across 23 stations and hence complies with the GCOS threshold of 4 Vol%. The local adjusted API accomplishes an $ubRMSD$ of 2.84 Vol% against said stations, mostly because the individual seasonality can be better depicted on different soils with local optimization of the empirical parameters in the API algorithm.

Thus, the API is capable of rendering the soil moisture development on point scale and spatially distributed with a focus on detection of rapid moisture change. It has been shown that the per-station optimized API data set greatly benefits from a local optimization of the empirical variables and allows for better representation of seasonal variability than the overall optimized API. Hence, the authors suggest to establish a relationship between soil properties and the locally adjusted empirical loss factors through e.g., cluster analysis in further research. Usage of soil texture data of even higher spatial resolution for downscaling the API needs to be discussed. Independent of eventually investigated spatial scales, a set of distributed empirical factors regulating the soil moisture dry-down would further improve the empirical modeling of soil moisture with the API, because local prevailing soil conditions could be more individually considered.

Overall, integrating weather radar data in the soil moisture estimation scheme showed to be very beneficial. A high temporal resolution soil moisture data set option for Germany is now available to the scientific community.

Author Contributions: Conceptualization, T.R., P.M. and A.L.; methodology, T.R.; software, T.R.; validation, T.R. and T.W.; formal analysis, T.R.; investigation, T.R.; resources, T.R. and T.W.; data curation, T.R.; writing–original draft preparation, T.R.; writing–review and editing, T.R., T.W. and P.M.; visualization, T.R.; supervision, A.L. and P.M.; project administration, P.M. and A.L.; funding acquisition, A.L. All authors have read and agreed to the published version of the manuscript.

Funding: The project leading to this application has received funding from the European Union's Horizon 2020 research and innovation program under Grant Agreement No. 687320.

Data Availability Statement: The data set presented in this study is openly available at Zenodo, https://doi.org/10.5281/zenodo.4588904 (accessed on 27 April 2021), reference number [73].

Acknowledgments: The authors thank every institution (DWD, ISMN, ESA, ECMWF, ISRIC, TERENO) for funding or providing the utilized data sets as open access. Thomas Ramsauer is truly grateful to Alexander Löw († 2 July 2017) for the initial trust and inspiration that paved the way for this research.

Conflicts of Interest: The authors declare no conflict of interest.

Abbreviations

The following abbreviations are used in this manuscript:

API	Antecedent Precipitation Index
ASCAT	Advanced Scatterometer
CDS	Climate Data Store
CV	Cross Validation
DJF	December, January, February (Season)
DWD	Deutscher Wetterdienst (German weather service)
ECMWF	European Center for Medium-Range Weather Forecasts
ECV	Essential Climate Variable
ERA5	ECMWF Reanalysis v5
ESA CCI SM	European Space Agency's Climate Change Initiative Soil Moisture Product
FDR	Frequency Domain Reflectometry
GCOS	Global Climate Observing System
GPCC	Global Precipitation Climatology Centre
GPCP	Global Precipitation Climatology Project
GPM	Global Precipitation Measurement (mission)
GPS	Global Positioning System
IMERG	Integrated Multi-satellitE Retrievals for the GPM Mission
ISMN	International Soil Moisture Network
ISRIC	International Soil Reference and Information Center
JJA	June, July, August (Season)
lAPI	local optimized Antecedent Precipitation Index
MAM	March, April, May (Season)
NASA	National Aeronautics and Space Administration
OPTRAM	Optical Trapezoid Model
PERSIANN-CDR	Precipitation Estimation from Remotely Sensed Information using an Artificial Neural Network-Climate Data Record
RADOLAN	RAdar OnLine ANeichung (radar online adjustment)
RMSD	Root Mean Square Difference
SMAP	Soil Moisture Active Passive (mission)
SOC	Soil Organic Carbon
SON	September, October, November (Season)
TDR	Time Domain Reflectometry
TERENO	Terrestrial Environmental Observatories
TOTRAM	Thermal-Optical Triangle Method
ubRMSD	unbiased Root Mean Square Difference
UAV	Unmanned Aerial Vehicle
WMO	World Meteorological Organization

Remote Sens. **2021**, *13*, 1712

Appendix A

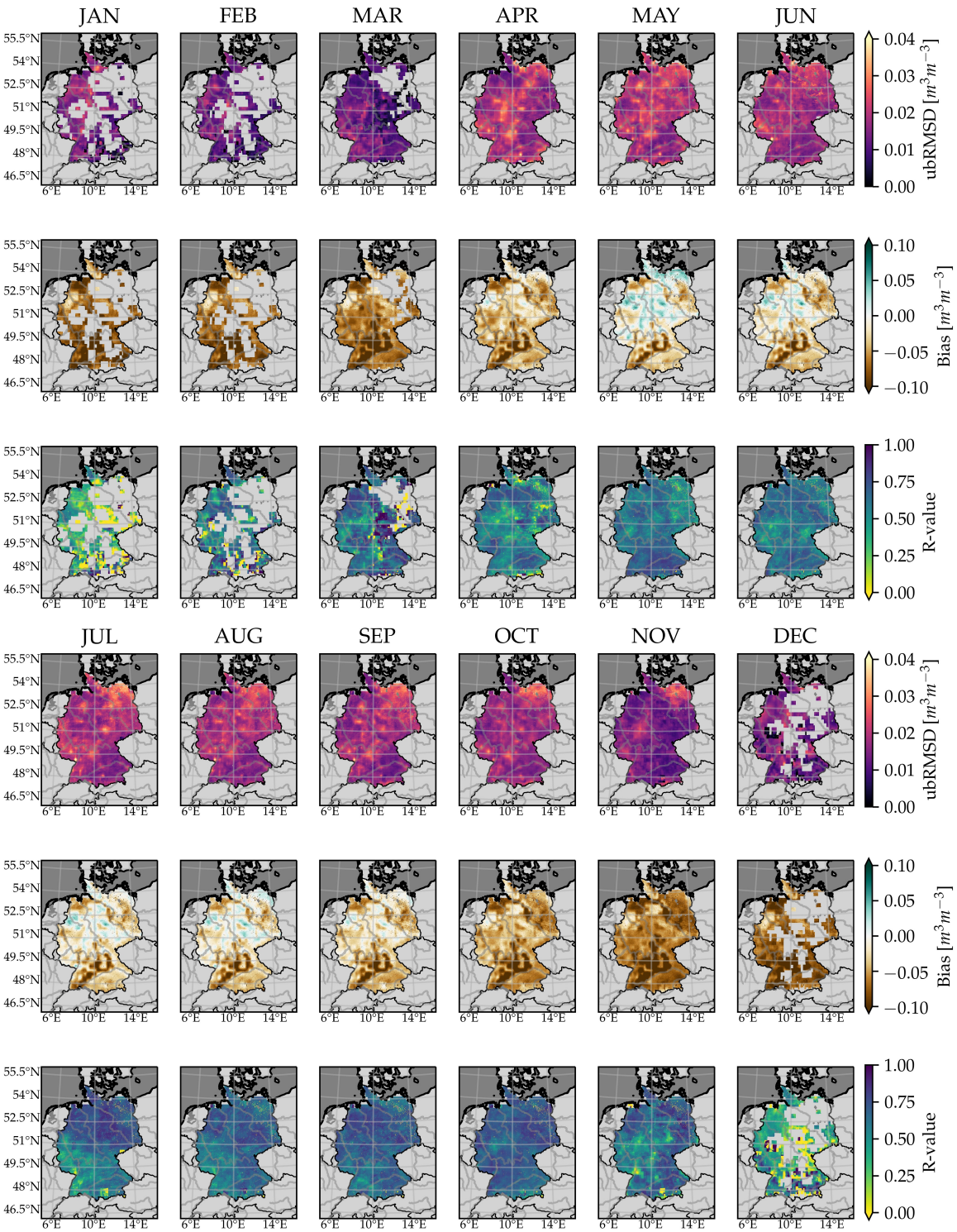

Figure A1. Monthly *ubRMSD*, *bias*, and *R* between API and ESA CCI SM data.

Remote Sens. **2021**, *13*, 1712

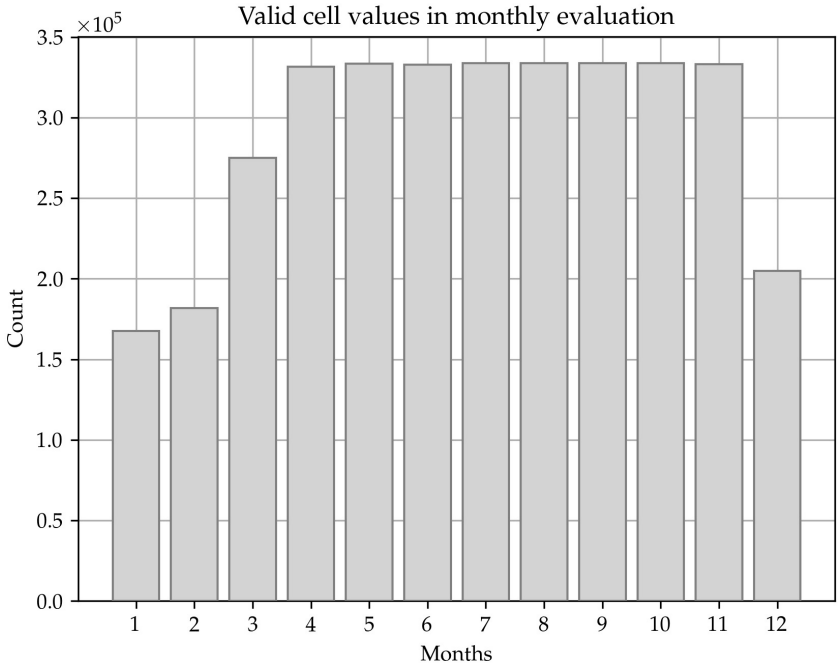

Figure A2. Count of valid unmasked grid cells available for monthly comparison of API and ESA CCI SM data.

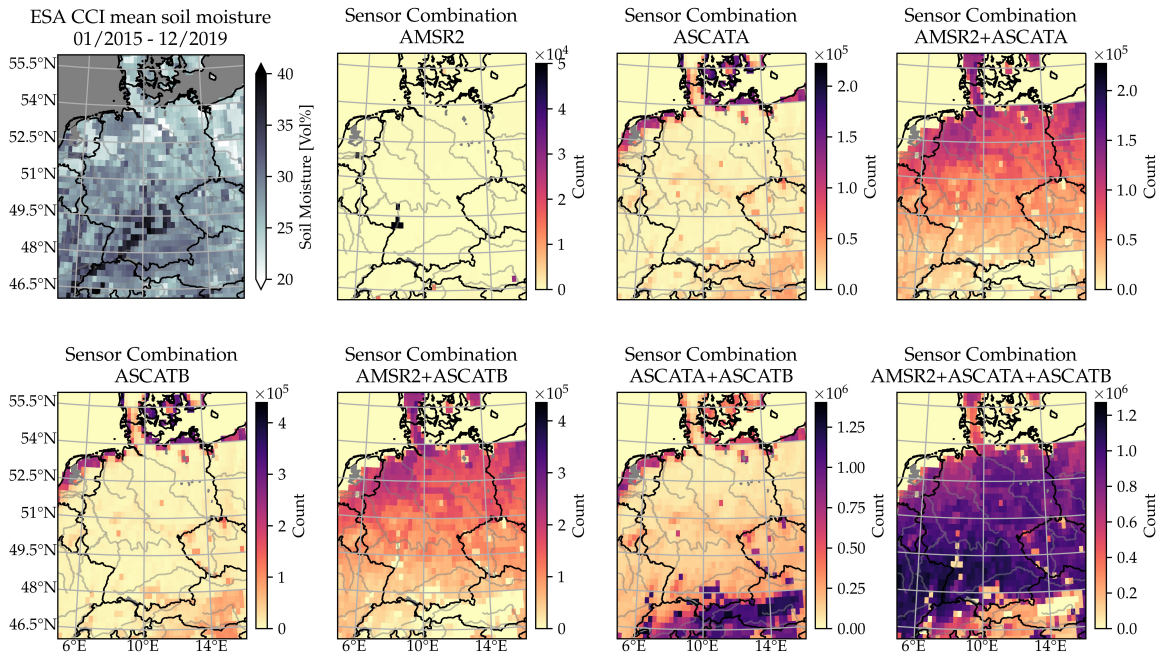

Figure A3. Mean soil moisture from ESA CCI SM for the period of 01/2015 to 12/2019 and counts of different sensor combinations contributing to the merged product. For respective combinations see ESA CCI SM product info.

Table A1. RADOLAN_API data set description.

Filename	RADOLAN_API_v1.0.0.nc
Filetype	NetCDF4
Version	1.0.0
License	CC-BY-SA
URL	https://doi.org/10.5281/zenodo.4588904 (accessed on 27 April 2021)
File Size	20.9 GB
Dimensions	692 × 1188 × 43,824 (latitude, longitude, time)
Spatial Resolution	1 km × 1 km
Spatial Coverage	Territory of Germany
Temporal Coverage	01.01.2015–31.12.2019

Table A2. Values of variables α and γ for overall and individual (local) optimization and variable values in the respective cross validation class (rounded).

	Overall Opt.		Local Opt.		CV Class I Calibration		CV Class II Calibration	
Station	α	γ	α	γ	α	γ	α	γ
Beestland	19,768.0102	6.9960	25,888.4543	6.7393	-	-	23,704.3638	7.0166
Boeken	19,768.0102	6.9960	15,459.5184	8.6683	-	-	23,704.3638	7.0166
Goermin	19,768.0102	6.9960	13,407.3887	8.9687	-	-	23,704.3638	7.0166
Grosszastrow	19,768.0102	6.9960	13,103.0731	8.7054	16,265.6752	7.0217	-	-
Heydenhof	19,768.0102	6.9960	13,002.0141	10.3239	-	-	23,704.3638	7.0166
Neu Tellin	19,768.0102	6.9960	17,048.6849	7.9655	16,265.6752	7.0217	-	-
Rustow	19,768.0102	6.9960	18,155.6516	8.7882	16,265.6752	7.0217	-	-
Sanzkow	19,768.0102	6.9960	15,280.2734	12.2186	-	-	23,704.3638	7.0166
Sommersdorf	19,768.0102	6.9960	15,931.4899	7.4929	16,265.6752	7.0217	-	-
Toitz	19,768.0102	6.9960	26,363.4512	8.3422	-	-	23,704.3638	7.0166
Zarrenthin	19,768.0102	6.9960	24,362.5183	6.5954	-	-	23,704.3638	7.0166
Gevenich	19,768.0102	6.9960	3238.0722	11.7320	16,265.6752	7.0217	-	-
Merzenhausen	19,768.0102	6.9960	3399.5669	14.6008	16,265.6752	7.0217	-	-
Schoeneseiffen	19,768.0102	6.9960	4502.4258	36.9911	16,265.6752	7.0217	-	-
Selhausen	19,768.0102	6.9960	4390.2302	15.1374	16,265.6752	7.0217	-	-
Wildenrath	19,768.0102	6.9960	4129.9100	13.6303	-	-	23,704.3638	7.0166
Wallerfing_A2	19,768.0102	6.9960	2991.0367	7.0635	16,265.6752	7.0217	-	-
Wallerfing_A4	19,768.0102	6.9960	4604.2422	6.2033	16,265.6752	7.0217	-	-
Wallerfing_A6	19,768.0102	6.9960	3552.1796	4.0507	-	-	23,704.3638	7.0166
Wallerfing_P2	19,768.0102	6.9960	3009.0580	5.6143	16,265.6752	7.0217	-	-
Wallerfing_P6	19,768.0102	6.9960	3115.7178	3.3863	-	-	23,704.3638	7.0166
Wallerfing_P4	19,768.0102	6.9960	3612.4949	5.8123	-	-	23,704.3638	7.0166

References

1. Legates, D.R.; Mahmood, R.; Levia, D.F.; DeLiberty, T.L.; Quiring, S.M.; Houser, C.; Nelson, F.E. Soil moisture: A central and unifying theme in physical geography. *Prog. Phys. Geogr. Earth Environ.* **2010**, *35*, 65–86. [CrossRef]
2. Miralles, D.G.; van den Berg, M.J.; Teuling, A.J.; de Jeu, R.A.M. Soil moisture-temperature coupling: A multiscale observational analysis. *Geophys. Res. Lett.* **2012**, *39*. [CrossRef]
3. McPherson, R.A. A review of vegetation—atmosphere interactions and their influences on mesoscale phenomena. *Prog. Phys. Geogr. Earth Environ.* **2007**, *31*, 261–285. [CrossRef]
4. Babaeian, E.; Sadeghi, M.; Franz, T.E.; Jones, S.; Tuller, M. Mapping soil moisture with the OPtical TRApezoid Model (OPTRAM) based on long-term MODIS observations. *Remote Sens. Environ.* **2018**, *211*, 425–440. [CrossRef]
5. Al-Yaari, A.; Wigneron, J.P.; Dorigo, W.; Colliander, A.; Pellarin, T.; Hahn, S.; Mialon, A.; Richaume, P.; Fernandez-Moran, R.; Fan, L.; et al. Assessment and inter-comparison of recently developed/reprocessed microwave satellite soil moisture products using ISMN ground-based measurements. *Remote Sens. Environ.* **2019**, *224*, 289–303. [CrossRef]
6. Chifflard, P.; Kranl, J.; zur Strassen, G.; Zepp, H. The significance of soil moisture in forecasting characteristics of flood events. A statistical analysis in two nested catchments. *J. Hydrol. Hydromech.* **2018**, *66*, 1–11. [CrossRef]
7. Hirschi, M.; Seneviratne, S.I.; Alexandrov, V.; Boberg, F.; Boroneant, C.; Christensen, O.B.; Formayer, H.; Orlowsky, B.; Stepanek, P. Observational evidence for soil-moisture impact on hot extremes in southeastern Europe. *Nat. Geosci.* **2010**, *4*, 17–21. [CrossRef]
8. Robinson, D.A.; Campbell, C.S.; Hopmans, J.W.; Hornbuckle, B.K.; Jones, S.B.; Knight, R.; Ogden, F.; Selker, J.; Wendroth, O. Soil Moisture Measurement for Ecological and Hydrological Watershed-Scale Observatories: A Review. *Vadose Zone J.* **2008**, *7*, 358–389. [CrossRef]
9. Green, J.K.; Seneviratne, S.I.; Berg, A.M.; Findell, K.L.; Hagemann, S.; Lawrence, D.M.; Gentine, P. Large influence of soil moisture on long-term terrestrial carbon uptake. *Nature* **2019**, *565*, 476–479. [CrossRef] [PubMed]
10. GCOS. *The Global Observing System for Climate: Implementation Needs;* WMO Pub GCOS-200: Geneva, Switzerland, 2016.

11. Dorigo, W.A.; Wagner, W.; Hohensinn, R.; Hahn, S.; Paulik, C.; Xaver, A.; Gruber, A.; Drusch, M.; Mecklenburg, S.; van Oevelen, P.; et al. The International Soil Moisture Network: A data hosting facility for global in situ soil moisture measurements. *Hydrol. Earth Syst. Sci.* **2011**, *15*, 1675–1698. [CrossRef]
12. Koch, F.; Schlenz, F.; Prasch, M.; Appel, F.; Ruf, T.; Mauser, W. Soil Moisture Retrieval Based on GPS Signal Strength Attenuation. *Water* **2016**, *8*, 276. [CrossRef]
13. Zhou, L.; Yu, D.; Wang, Z.; Wang, X. Soil Water Content Estimation Using High-Frequency Ground Penetrating Radar. *Water* **2019**, *11*, 1036. [CrossRef]
14. Lombardi, F.; Lualdi, M. Step-Frequency Ground Penetrating Radar for Agricultural Soil Morphology Characterisation. *Remote Sens.* **2019**, *11*, 1075. [CrossRef]
15. Crow, W.T.; Berg, A.A.; Cosh, M.H.; Loew, A.; Mohanty, B.P.; Panciera, R.; de Rosnay, P.; Ryu, D.; Walker, J.P. Upscaling sparse ground-based soil moisture observations for the validation of coarse-resolution satellite soil moisture products. *Rev. Geophys.* **2012**, *50*. [CrossRef]
16. Dorigo, W.; Xaver, A.; Vreugdenhil, M.; Gruber, A.; Hegyiová, A.; Sanchis-Dufau, A.; Zamojski, D.; Cordes, C.; Wagner, W.; Drusch, M. Global Automated Quality Control of In Situ Soil Moisture Data from the International Soil Moisture Network. *Vadose Zone J.* **2013**, *12*. [CrossRef]
17. Wu, K.; Rodriguez, G.A.; Zajc, M.; Jacquemin, E.; Clément, M.; Coster, A.D.; Lambot, S. A new drone-borne GPR for soil moisture mapping. *Remote Sens. Environ.* **2019**, *235*, 111456. [CrossRef]
18. Wagner, W. Evaluation of the agreement between the first global remotely sensed soil moisture data with model and precipitation data. *J. Geophys. Res.* **2003**, *108*. [CrossRef]
19. Wang, Y.; Leng, P.; Peng, J.; Marzahn, P.; Ludwig, R. Global assessments of two blended microwave soil moisture products CCI and SMOPS with in-situ measurements and reanalysis data. *Int. J. Appl. Earth Obs. Geoinf.* **2021**, *94*, 102234. [CrossRef]
20. Babaeian, E.; Sadeghi, M.; Jones, S.B.; Montzka, C.; Vereecken, H.; Tuller, M. Ground, Proximal, and Satellite Remote Sensing of Soil Moisture. *Rev. Geophys.* **2019**, *57*, 530–616. [CrossRef]
21. Sadeghi, M.; Babaeian, E.; Tuller, M.; Jones, S.B. The optical trapezoid model: A novel approach to remote sensing of soil moisture applied to Sentinel-2 and Landsat-8 observations. *Remote Sens. Environ.* **2017**, *198*, 52–68. [CrossRef]
22. Piles, M.; Petropoulos, G.P.; Sánchez, N.; González-Zamora, Á.; Ireland, G. Towards improved spatio-temporal resolution soil moisture retrievals from the synergy of SMOS and MSG SEVIRI spaceborne observations. *Remote Sens. Environ.* **2016**, *180*, 403–417. [CrossRef]
23. Ghilain, N.; Arboleda, A.; Batelaan, O.; Ardö, J.; Trigo, I.; Barrios, J.M.; Gellens-Meulenberghs, F. A New Retrieval Algorithm for Soil Moisture Index from Thermal Infrared Sensor On-Board Geostationary Satellites over Europe and Africa and Its Validation. *Remote Sens.* **2019**, *11*, 1968. [CrossRef]
24. Bartalis, Z.; Wagner, W.; Naeimi, V.; Hasenauer, S.; Scipal, K.; Bonekamp, H.; Figa, J.; Anderson, C. Initial soil moisture retrievals from the METOP-A Advanced Scatterometer (ASCAT). *Geophys. Res. Lett.* **2007**, *34*. [CrossRef]
25. Entekhabi, D.; Njoku, E.G.; O'Neill, P.E.; Kellogg, K.H.; Crow, W.T.; Edelstein, W.N.; Entin, J.K.; Goodman, S.D.; Jackson, T.J.; Johnson, J.; et al. The Soil Moisture Active Passive (SMAP) Mission. *Proc. IEEE* **2010**, *98*, 704–716. [CrossRef]
26. Peng, J.; Albergel, C.; Balenzano, A.; Brocca, L.; Cartus, O.; Cosh, M.H.; Crow, W.T.; Dabrowska-Zielinska, K.; Dadson, S.; Davidson, M.W.; et al. A roadmap for high-resolution satellite soil moisture applications – confronting product characteristics with user requirements. *Remote Sens. Environ.* **2021**, *252*, 112162. [CrossRef]
27. Merzouki, A.; McNairn, H.; Powers, J.; Friesen, M. Synthetic Aperture Radar (SAR) Compact Polarimetry for Soil Moisture Retrieval. *Remote Sens.* **2019**, *11*, 2227. [CrossRef]
28. Choker, M.; Baghdadi, N.; Zribi, M.; Hajj, M.E.; Paloscia, S.; Verhoest, N.; Lievens, H.; Mattia, F. Evaluation of the Oh, Dubois and IEM Backscatter Models Using a Large Dataset of SAR Data and Experimental Soil Measurements. *Water* **2017**, *9*, 38. [CrossRef]
29. Ochsner, T.E.; Cosh, M.H.; Cuenca, R.H.; Dorigo, W.A.; Draper, C.S.; Hagimoto, Y.; Kerr, Y.H.; Larson, K.M.; Njoku, E.G.; Small, E.E.; et al. State of the Art in Large-Scale Soil Moisture Monitoring. *Soil Sci. Soc. Am. J.* **2013**, *77*, 1888–1919. [CrossRef]
30. Kerr, Y.; Waldteufel, P.; Wigneron, J.P.; Martinuzzi, J.; Font, J.; Berger, M. Soil moisture retrieval from space: The Soil Moisture and Ocean Salinity (SMOS) mission. *IEEE Trans. Geosci. Remote Sens.* **2001**, *39*, 1729–1735. [CrossRef]
31. Naeimi, V.; Scipal, K.; Bartalis, Z.; Hasenauer, S.; Wagner, W. An Improved Soil Moisture Retrieval Algorithm for ERS and METOP Scatterometer Observations. *IEEE Trans. Geosci. Remote Sens.* **2009**, *47*, 1999–2013. [CrossRef]
32. Owe, M.; de Jeu, R.; Walker, J. A methodology for surface soil moisture and vegetation optical depth retrieval using the microwave polarization difference index. *IEEE Trans. Geosci. Remote Sens.* **2001**, *39*, 1643–1654. [CrossRef]
33. Das, N.N.; Entekhabi, D.; Dunbar, R.S.; Chaubell, M.J.; Colliander, A.; Yueh, S.; Jagdhuber, T.; Chen, F.; Crow, W.; O'Neill, P.E.; et al. The SMAP and Copernicus Sentinel 1A/B microwave active-passive high resolution surface soil moisture product. *Remote Sens. Environ.* **2019**, *233*, 111380. [CrossRef]
34. Bauer-Marschallinger, B.; Paulik, C.; Hochstöger, S.; Mistelbauer, T.; Modanesi, S.; Ciabatta, L.; Massari, C.; Brocca, L.; Wagner, W. Soil Moisture from Fusion of Scatterometer and SAR: Closing the Scale Gap with Temporal Filtering. *Remote Sens.* **2018**, *10*, 1030. [CrossRef]
35. Vereecken, H.; Huisman, J.; Pachepsky, Y.; Montzka, C.; van der Kruk, J.; Bogena, H.; Weihermüller, L.; Herbst, M.; Martinez, G.; Vanderborght, J. On the spatio-temporal dynamics of soil moisture at the field scale. *J. Hydrol.* **2014**, *516*, 76–96. [CrossRef]

36. Sehler, R.; Li, J.; Reager, J.T.; Ye, H. Investigating Relationship Between Soil Moisture and Precipitation Globally Using Remote Sensing Observations. *J. Contemp. Water Res. Educ.* **2019**, *168*, 106–118. [CrossRef]
37. Sun, Q.; Miao, C.; Duan, Q.; Ashouri, H.; Sorooshian, S.; Hsu, K.L. A Review of Global Precipitation Data Sets: Data Sources, Estimation, and Intercomparisons. *Rev. Geophys.* **2018**, *56*, 79–107. [CrossRef]
38. New, M.; Todd, M.; Hulme, M.; Jones, P. Precipitation measurements and trends in the twentieth century. *Int. J. Climatol.* **2001**, *21*, 1889–1922. [CrossRef]
39. Ramsauer, T.; Weiß, T.; Marzahn, P. Comparison of the GPM IMERG Final Precipitation Product to RADOLAN Weather Radar Data over the Topographically and Climatically Diverse Germany. *Remote Sens.* **2018**, *10*, 2029. [CrossRef]
40. Legates, D.R.; Willmott, C.J. Mean seasonal and spatial variability in gauge-corrected, global precipitation. *Int. J. Climatol.* **1990**, *10*, 111–127. [CrossRef]
41. Schamm, K.; Ziese, M.; Becker, A.; Finger, P.; Meyer-Christoffer, A.; Schneider, U.; Schröder, M.; Stender, P. Global gridded precipitation over land: A description of the new GPCC First Guess Daily product. *Earth Syst. Sci. Data* **2014**, *6*, 49–60. [CrossRef]
42. Becker, A.; Finger, P.; Meyer-Christoffer, A.; Rudolf, B.; Schamm, K.; Schneider, U.; Ziese, M. A description of the global land-surface precipitation data products of the Global Precipitation Climatology Centre with sample applications including centennial (trend) analysis from 1901–present. *Earth Syst. Sci. Data* **2013**, *5*, 71–99. [CrossRef]
43. Todini, E. A Bayesian technique for conditioning radar precipitation estimates to rain-gauge measurements. *Hydrol. Earth Syst. Sci.* **2001**, *5*, 187–199. [CrossRef]
44. Winterrath, T.; Brendel, T.; Junghänel, T.; Klameth, A.; Lengfeld, K.; Walawender, E.; Weigl, E.; Hafer, M.; Becker, A. An overview of the new radar-based precipitation climatology of the Deutscher Wetterdienst—data, methods, products. In *Rainfall Monitoring, Modelling and Forecasting in Urban Environment. UrbanRain18: 11th International Workshop on Precipitation in Urban Areas. Conference Proceedings*; ETH Zurich, Institute of Environmental Engineering: Zürich, Switzerland, 2019. [CrossRef]
45. Sebastianelli, S.; Russo, F.; Napolitano, F.; Baldini, L. On precipitation measurements collected by a weather radar and a rain gauge network. *Nat. Hazards Earth Syst. Sci.* **2013**, *13*, 605–623. [CrossRef]
46. Foehn, A.; Hernández, J.G.; Schaefli, B.; Cesare, G.D. Spatial interpolation of precipitation from multiple rain gauge networks and weather radar data for operational applications in Alpine catchments. *J. Hydrol.* **2018**, *563*, 1092–1110. [CrossRef]
47. Kidd, C.; Levizzani, V. Status of satellite precipitation retrievals. *Hydrol. Earth Syst. Sci.* **2011**, *15*, 1109–1116. [CrossRef]
48. Skofronick-Jackson, G.; Petersen, W.A.; Berg, W.; Kidd, C.; Stocker, E.F.; Kirschbaum, D.B.; Kakar, R.; Braun, S.A.; Huffman, G.J.; Iguchi, T.; et al. The Global Precipitation Measurement (GPM) Mission for Science and Society. *Bull. Am. Meteorol. Soc.* **2017**, *98*, 1679–1695. [CrossRef] [PubMed]
49. Adler, R.F.; Huffman, G.J.; Chang, A.; Ferraro, R.; Xie, P.P.; Janowiak, J.; Rudolf, B.; Schneider, U.; Curtis, S.; Bolvin, D.; et al. The Version-2 Global Precipitation Climatology Project (GPCP) Monthly Precipitation Analysis (1979–Present). *J. Hydrometeorol.* **2003**, *4*, 1147–1167. [CrossRef]
50. Ashouri, H.; Hsu, K.L.; Sorooshian, S.; Braithwaite, D.K.; Knapp, K.R.; Cecil, L.D.; Nelson, B.R.; Prat, O.P. PERSIANN-CDR: Daily Precipitation Climate Data Record from Multisatellite Observations for Hydrological and Climate Studies. *Bull. Am. Meteorol. Soc.* **2015**, *96*, 69–83. [CrossRef]
51. Hersbach, H.; de Rosnay, P.; Bell, B.; Schepers, D.; Simmons, A.; Soci, C.; Abdalla, S.; Alonso-Balmaseda, M.; Balsamo, G.; Bechtold, P.; et al. Operational global reanalysis: Progress, future directions and synergies with NWP. In *ERA Report Series*; ECMWF: Reading, UK, 2018. [CrossRef]
52. Beck, H.E.; van Dijk, A.I.J.M.; Levizzani, V.; Schellekens, J.; Miralles, D.G.; Martens, B.; de Roo, A. MSWEP: 3-hourly 0.25° global gridded precipitation (1979–2015) by merging gauge, satellite, and reanalysis data. *Hydrol. Earth Syst. Sci.* **2017**, *21*, 589–615. [CrossRef]
53. Kochendorfer, J.; Rasmussen, R.; Wolff, M.; Baker, B.; Hall, M.E.; Meyers, T.; Landolt, S.; Jachcik, A.; Isaksen, K.; Brækkan, R.; et al. The quantification and correction of wind-induced precipitation measurement errors. *Hydrol. Earth Syst. Sci.* **2017**, *21*, 1973–1989. [CrossRef]
54. Kidd, C.; Becker, A.; Huffman, G.J.; Muller, C.L.; Joe, P.; Skofronick-Jackson, G.; Kirschbaum, D.B. So, How Much of the Earth's Surface Is Covered by Rain Gauges? *Bull. Am. Meteorol. Soc.* **2017**, *98*, 69–78. [CrossRef] [PubMed]
55. Shrivastava, S.; Kar, S.C.; Sharma, A.R. Soil moisture variations in remotely sensed and reanalysis datasets during weak monsoon conditions over central India and central Myanmar. *Theor. Appl. Climatol.* **2016**, *129*, 305–320. [CrossRef]
56. Kohler, M.A.; Linsley, R.K. *Predicting the Runoff from Storm Rainfall*; U.S. Department of Commerce, Weather Bureau: Washington, DC, USA, 1951.
57. Kala, J.; Evans, J.P.; Pitman, A.J. Influence of antecedent soil moisture conditions on the synoptic meteorology of the Black Saturday bushfire event in southeast Australia. *Q. J. R. Meteorol. Soc.* **2015**, *141*, 3118–3129. [CrossRef]
58. Zhao, B.; Dai, Q.; Han, D.; Dai, H.; Mao, J.; Zhuo, L.; Rong, G. Estimation of soil moisture using modified antecedent precipitation index with application in landslide predictions. *Landslides* **2019**, *16*, 2381–2393. [CrossRef]
59. Brocca, L.; Melone, F.; Moramarco, T. On the estimation of antecedent wetness conditions in rainfall–runoff modelling. *Hydrol. Process.* **2008**, *22*, 629–642. [CrossRef]
60. Ali, S.; Ghosh, N.; Singh, R. Rainfall-runoff simulation using a normalized antecedent precipitation index. *Hydrol. Sci. J.* **2010**, *55*, 266–274. [CrossRef]

61. Song, S.; Wang, W. Impacts of Antecedent Soil moisture on the Rainfall–Runoff Transformation Process Based on High-Resolution Observations in Soil Tank Experiments. *Water* **2019**, *11*, 296. [CrossRef]
62. Javelle, P.; Fouchier, C.; Arnaud, P.; Lavabre, J. Flash flood warning at ungauged locations using radar rainfall and antecedent soil moisture estimations. *J. Hydrol.* **2010**, *394*, 267–274. [CrossRef]
63. Tramblay, Y.; Bouaicha, R.; Brocca, L.; Dorigo, W.; Bouvier, C.; Camici, S.; Servat, E. Estimation of antecedent wetness conditions for flood modelling in northern Morocco. *Hydrol. Earth Syst. Sci.* **2012**, *16*, 4375–4386. [CrossRef]
64. Crow, W.T.; Huffman, G.J.; Bindlish, R.; Jackson, T.J. Improving Satellite-Based Rainfall Accumulation Estimates Using Spaceborne Surface Soil Moisture Retrievals. *J. Hydrometeorol.* **2009**, *10*, 199–212. [CrossRef]
65. Crow, W.T. A Novel Method for Quantifying Value in Spaceborne Soil Moisture Retrievals. *J. Hydrometeorol.* **2007**, *8*, 56–67. [CrossRef]
66. Zhao, Y.; Wei, F.; Yang, H.; Jiang, Y. Discussion on Using Antecedent Precipitation Index to Supplement Relative Soil Moisture Data Series. *Procedia Environ. Sci.* **2011**, *10*, 1489–1495. [CrossRef]
67. Schoener, G.; Stone, M.C. Impact of antecedent soil moisture on runoff from a semiarid catchment. *J. Hydrol.* **2019**, *569*, 627–636. [CrossRef]
68. Schoener, G.; Stone, M.C. Monitoring soil moisture at the catchment scale—A novel approach combining antecedent precipitation index and radar-derived rainfall data. *J. Hydrol.* **2020**, *589*, 125155. [CrossRef]
69. Ochsner, T.E.; Linde, E.; Haffner, M.; Dong, J. Mesoscale Soil Moisture Patterns Revealed Using a Sparse In Situ Network and Regression Kriging. *Water Resour. Res.* **2019**, *55*, 4785–4800. [CrossRef]
70. Pellarin, T.; Louvet, S.; Gruhier, C.; Quantin, G.; Legout, C. A simple and effective method for correcting soil moisture and precipitation estimates using AMSR-E measurements. *Remote Sens. Environ.* **2013**, *136*, 28–36. [CrossRef]
71. Pellarin, T.; Román-Cascón, C.; Baron, C.; Bindlish, R.; Brocca, L.; Camberlin, P.; Fernández-Prieto, D.; Kerr, Y.H.; Massari, C.; Panthou, G.; et al. The Precipitation Inferred from Soil Moisture (PrISM) Near Real-Time Rainfall Product: Evaluation and Comparison. *Remote Sens.* **2020**, *12*, 481. [CrossRef]
72. Gruber, A.; Lannoy, G.D.; Albergel, C.; Al-Yaari, A.; Brocca, L.; Calvet, J.C.; Colliander, A.; Cosh, M.; Crow, W.; Dorigo, W.; et al. Validation practices for satellite soil moisture retrievals: What are (the) errors? *Remote Sens. Environ.* **2020**, *244*, 111806. [CrossRef]
73. Ramsauer, T.; Weiß, T.; Marzahn, P. *RADOLAN_API—A Soil Moisture Data Set Derived from Weather Radar Data*; Zenodo: Geneve, Switzerland, 2021. [CrossRef]
74. Winterrath, T.; Brendel, C.; Hafer, M.; Junghänel, T.; Klameth, A.; Lengfeld, K.; Walawender, E.; Weigl, E.; Becker, A. *RADKLIM Version 2017.002: Reprocessed Gauge-Adjusted Radar Data, One-Hour Precipitation Sums (RW)*; DWD: Offenbach, Germany, 2018. [CrossRef]
75. Bartels, H. *Projekt RADOLAN. Routineverfahren zur Online-Aneichung der Radarniederschlagsdaten mit Hilfe von Automatischen Bodenniederschlagsstationen (Ombrometer)*; Technical Report; Deutscher Wetterdienst, Hydrometeorologie: Offenbach, Germany, 2004.
76. Fersch, B.; Senatore, A.; Adler, B.; Arnault, J.; Mauder, M.; Schneider, K.; Völksch, I.; Kunstmann, H. High-resolution fully-coupled atmospheric-hydrological modeling: A cross-compartment regional water and energy cycle evaluation. *Hydrol. Earth Syst. Sci.* **2019**. [CrossRef]
77. Benoit, L.; Vrac, M.; Mariethoz, G. Accounting for rain type non-stationarity in sub-daily stochastic weather generators. *Hydrol. Earth Syst. Sci. Discuss.* **2019**. [CrossRef]
78. Fischer, F.; Hauck, J.; Brandhuber, R.; Weigl, E.; Maier, H.; Auerswald, K. Spatio-temporal variability of erosivity estimated from highly resolved and adjusted radar rain data (RADOLAN). *Agric. For. Meteorol.* **2016**, *223*, 72–80. [CrossRef]
79. Hänsel, P.; Langel, S.; Schindewolf, M.; Kaiser, A.; Buchholz, A.; Böttcher, F.; Schmidt, J. Prediction of Muddy Floods Using High-Resolution Radar Precipitation Forecasts and Physically-Based Erosion Modeling in Agricultural Landscapes. *Geosciences* **2019**, *9*, 401. [CrossRef]
80. Bronstert, A.; Agarwal, A.; Boessenkool, B.; Crisologo, I.; Fischer, M.; Heistermann, M.; Köhn-Reich, L.; López-Tarazón, J.A.; Moran, T.; Ozturk, U.; et al. Forensic hydro-meteorological analysis of an extreme flash flood: The 2016-05-29 event in Braunsbach, SW Germany. *Sci. Total Environ.* **2018**, *630*, 977–991. [CrossRef] [PubMed]
81. Meyer, H.; Kühnlein, M.; Appelhans, T.; Nauss, T. Comparison of Four Machine Learning Algorithms for Their Applicability in Satellite-Based Optical Rainfall Retrievals. *Atmos. Res.* **2016**, *169*, 424–433. [CrossRef]
82. DWD. *RADOLAN/RADVOR Hoch Aufgelöste Niederschlagsanalyse und–Vorhersage auf der Basis Quantitativer Radar und Ombrometerdaten für and Grenzüberschreitende Fluss-Einzugsgebiete von Deutschland im Echtzeitbetrieb Beschreibung des Kompositformats Version 2.4.3*; Technical Report; Deutscher Wetterdienst, Abteilung Hydrometeorologie: Offenbach, Germany, 2018.
83. Winterrath, T.; Brendel, C.; Hafer, M.; Junghänel, T.; Klameth, A.; Walawender, E.; und Andreas Becker, E.W. Erstellung einer radargestützten Niederschlagsklimatologie. In *Berichte des Deutschen Wetterdienstes*; Deutscher Wetterdienst: Offenbach, Germany, 2017; Volume 251.
84. Winterrath, T.; Rosenow, W.; Weigl, E. On the DWD quantitative precipitation analysis and nowcasting system for real-time application in German flood risk management. *Weather Radar Hydrol.* **2012**, *351*, 323–329.
85. Richter, D. Ergebnisse methodischer Untersuchungen zur Korrektur des systematischen Meßfehlers des Hellmann-Niederschlagmessers. In *Berichte des Deutschen Wetterdienstes*; Deutscher Wetterdienst: Offenbach, Germany, 1995; Volume 1995.
86. World Meteorological Organization. *Guide to Meteorological Instruments and Methods of Observation, WMO-No. 8*; World Meteorological Organization: Geneva, Switzerland, 2017.

87. Hengl, T.; de Jesus, J.M.; Heuvelink, G.B.M.; Gonzalez, M.R.; Kilibarda, M.; Blagotić, A.; Shangguan, W.; Wright, M.N.; Geng, X.; Bauer-Marschallinger, B.; et al. SoilGrids250m: Global gridded soil information based on machine learning. *PLoS ONE* **2017**, *12*, e0169748. [CrossRef] [PubMed]
88. Hengl, T.; Leenaars, J.G.B.; Shepherd, K.D.; Walsh, M.G.; Heuvelink, G.B.M.; Mamo, T.; Tilahun, H.; Berkhout, E.; Cooper, M.; Fegraus, E.; et al. Soil nutrient maps of Sub-Saharan Africa: Assessment of soil nutrient content at 250 m spatial resolution using machine learning. *Nutr. Cycl. Agroecosyst.* **2017**, *109*, 77–102. [CrossRef] [PubMed]
89. Tóth, B.; Weynants, M.; Pásztor, L.; Hengl, T. 3D soil hydraulic database of Europe at 250 m resolution. *Hydrol. Process.* **2017**, *31*, 2662–2666. [CrossRef]
90. Ross, C.W.; Prihodko, L.; Anchang, J.; Kumar, S.; Ji, W.; Hanan, N.P. HYSOGs250m, global gridded hydrologic soil groups for curve-number-based runoff modeling. *Sci. Data* **2018**, *5*. [CrossRef] [PubMed]
91. Wu, X.; Lu, G.; Wu, Z.; He, H.; Zhou, J.; Liu, Z. An Integration Approach for Mapping Field Capacity of China Based on Multi-Source Soil Datasets. *Water* **2018**, *10*, 728. [CrossRef]
92. Hersbach, H.; Bell, B.; Berrisford, P.; Biavati, G.; Horányi, A.; Muñoz Sabater, J.; Nicolas, J.; Peubey, C.; Radu, R.; Rozum, I.; et al. Copernicus Climate Change Service (C3S). In *ERA5: Fifth Generation of ECMWF Atmospheric Reanalyses of the Global Climate*; Climate Change Service Climate Data Store (CDS), 2018. [CrossRef]
93. Albergel, C.; Dutra, E.; Munier, S.; Calvet, J.C.; Munoz-Sabater, J.; de Rosnay, P.; Balsamo, G. ERA-5 and ERA-Interim driven ISBA land surface model simulations: Which one performs better? *Hydrol. Earth Syst. Sci.* **2018**, *22*, 3515–3532. [CrossRef]
94. Tarek, M.; Brissette, F.P.; Arsenault, R. Evaluation of the ERA5 reanalysis as a potential reference dataset for hydrological modelling over North America. *Hydrol. Earth Syst. Sci.* **2020**, *24*, 2527–2544. [CrossRef]
95. Betts, A.K.; Chan, D.Z.; Desjardins, R.L. Near-Surface Biases in ERA5 Over the Canadian Prairies. *Front. Environ. Sci.* **2019**, *7*. [CrossRef]
96. Zhang, W.; Zhang, H.; Liang, H.; Lou, Y.; Cai, Y.; Cao, Y.; Zhou, Y.; Liu, W. On the suitability of ERA5 in hourly GPS precipitable water vapor retrieval over China. *J. Geod.* **2019**, *93*, 1897–1909. [CrossRef]
97. Mahto, S.S.; Mishra, V. Does ERA-5 Outperform Other Reanalysis Products for Hydrologic Applications in India? *J. Geophys. Res. Atmos.* **2019**, *124*, 9423–9441. [CrossRef]
98. Bogena, H.; Montzka, C.; Huisman, J.; Graf, A.; Schmidt, M.; Stockinger, M.; von Hebel, C.; Hendricks-Franssen, H.; van der Kruk, J.; Tappe, W.; et al. The TERENO-Rur Hydrological Observatory: A Multiscale Multi-Compartment Research Platform for the Advancement of Hydrological Science. *Vadose Zone J.* **2018**, *17*, 180055. [CrossRef]
99. Zacharias, S.; Bogena, H.; Samaniego, L.; Mauder, M.; Fuß, R.; Pütz, T.; Frenzel, M.; Schwank, M.; Baessler, C.; Butterbach-Bahl, K.; et al. A Network of Terrestrial Environmental Observatories in Germany. *Vadose Zone J.* **2011**, *10*, 955–973. [CrossRef]
100. Heinrich, I.; Balanzategui, D.; Bens, O.; Blasch, G.; Blume, T.; Böttcher, F.; Borg, E.; Brademann, B.; Brauer, A.; Conrad, C.; et al. Interdisciplinary Geo-ecological Research across Time Scales in the Northeast German Lowland Observatory (TERENO-NE). *Vadose Zone J.* **2018**, *17*, 180116. [CrossRef]
101. Gruber, A.; Scanlon, T.; van der Schalie, R.; Wagner, W.; Dorigo, W. Evolution of the ESA CCI Soil Moisture climate data records and their underlying merging methodology. *Earth Syst. Sci. Data* **2019**, *11*, 717–739. [CrossRef]
102. Dorigo, W.; Wagner, W.; Albergel, C.; Albrecht, F.; Balsamo, G.; Brocca, L.; Chung, D.; Ertl, M.; Forkel, M.; Gruber, A.; et al. ESA CCI Soil Moisture for improved Earth system understanding: State-of-the art and future directions. *Remote Sens. Environ.* **2017**, *203*, 185–215. [CrossRef]
103. Gruber, A.; Dorigo, W.A.; Crow, W.; Wagner, W. Triple Collocation-Based Merging of Satellite Soil Moisture Retrievals. *IEEE Trans. Geosci. Remote Sens.* **2017**, *55*, 6780–6792. [CrossRef]
104. Pan, N.; Wang, S.; Liu, Y.; Zhao, W.; Fu, B. Global Surface Soil Moisture Dynamics in 1979–2016 Observed from ESA CCI SM Dataset. *Water* **2019**, *11*, 883. [CrossRef]
105. Ma, H.; Zeng, J.; Chen, N.; Zhang, X.; Cosh, M.H.; Wang, W. Satellite surface soil moisture from SMAP, SMOS, AMSR2 and ESA CCI: A comprehensive assessment using global ground-based observations. *Remote Sens. Environ.* **2019**, *231*, 111215. [CrossRef]
106. Raoult, N.; Delorme, B.; Ottlé, C.; Peylin, P.; Bastrikov, V.; Maugis, P.; Polcher, J. Confronting Soil Moisture Dynamics from the ORCHIDEE Land Surface Model With the ESA-CCI Product: Perspectives for Data Assimilation. *Remote Sens.* **2018**, *10*, 1786. [CrossRef]
107. McNally, A.; Shukla, S.; Arsenault, K.R.; Wang, S.; Peters-Lidard, C.D.; Verdin, J.P. Evaluating ESA CCI soil moisture in East Africa. *Int. J. Appl. Earth Obs. Geoinf.* **2016**, *48*, 96–109. [CrossRef]
108. Chakravorty, A.; Chahar, B.R.; Sharma, O.P.; Dhanya, C. A regional scale performance evaluation of SMOS and ESA-CCI soil moisture products over India with simulated soil moisture from MERRA-Land. *Remote Sens. Environ.* **2016**, *186*, 514–527. [CrossRef]
109. An, R.; Zhang, L.; Wang, Z.; Quaye-Ballard, J.A.; You, J.; Shen, X.; Gao, W.; Huang, L.; Zhao, Y.; Ke, Z. Validation of the ESA CCI soil moisture product in China. *Int. J. Appl. Earth Obs. Geoinf.* **2016**, *48*, 28–36. [CrossRef]
110. Noilhan, J.; Lacarrère, P. GCM Grid-Scale Evaporation from Mesoscale Modeling. *J. Clim.* **1995**, *8*, 206–223. [CrossRef]
111. Noilhan, J.; Mahfouf, J.F. The ISBA land surface parameterisation scheme. *Glob. Planet. Chang.* **1996**, *13*, 145–159. [CrossRef]
112. Nelder, J.A.; Mead, R. A Simplex Method for Function Minimization. *Comput. J.* **1965**, *7*, 308–313. [CrossRef]

113. Gao, F.; Han, L. Implementing the Nelder-Mead simplex algorithm with adaptive parameters. *Comput. Optim. Appl.* **2010**, *51*, 259–277. [CrossRef]
114. Richter, A. *Bodenuebersichtskarte der Bundesrepublik Deutschland 1:1.000.000;* Bundesanstalt für Geowissenschaften und Rohstoffe (BGR): Hannover, Germany, 2013.
115. Krug, D. *Gruppen der Bodenausgangsgesteine in Deutschland 1:5000000 (BAG 5000)*; Bundesanstalt für Geowissenschaften und Rohstoffe (BGR): Hannover, Germany, 2007.
116. Duijnisveld, W.*Nutzbare Feldkapazität im Effektiven Wurzelraum in Deutschland*; Bundesanstalt für Geowissenschaften und Rohstoffe (BGR): Hannover, Germany, 2015.
117. Duijnisveld, W. *Luftkapazität der Böden im Effektiven Wurzelraum in Deutschland*; Bundesanstalt für Geowissenschaften und Rohstoffe (BGR): Hannover, Germany, 2015.
118. Wagner, W. Soil Moisture Retrieval from ERS Scatterometer Data. In *Geowissenschaftliche Mitteilungen*; Institute for Photogrammetry and Remote Sensing, Vienna University of Technology: Vienna, Austria, 1998; Volume 49
119. Manns, H.R.; Berg, A.A. Importance of soil organic carbon on surface soil water content variability among agricultural fields. *J. Hydrol.* **2014**, *516*, 297–303. [CrossRef]
120. de la Torre, A.M.; Blyth, E.; Robinson, E. Evaluation of Drydown Processes in Global Land Surface and Hydrological Models Using Flux Tower Evapotranspiration. *Water* **2019**, *11*, 356. [CrossRef]
121. Tifafi, M.; Guenet, B.; Hatté, C. Large Differences in Global and Regional Total Soil Carbon Stock Estimates Based on SoilGrids, HWSD, and NCSCD: Intercomparison and Evaluation Based on Field Data From USA, England, Wales, and France. *Glob. Biogeochem. Cycles* **2018**, *32*, 42–56. [CrossRef]
122. Marzahn, P.; Meyer, S. Utilization of Multi-Temporal Microwave Remote Sensing Data within a Geostatistical Regionalization Approach for the Derivation of Soil Texture. *Remote Sens.* **2020**, *12*, 2660. [CrossRef]

2.3 Article III: Global Soil Moisture Estimation based on GPM IMERG Data using a Site Specific Adjusted Antecedent Precipitation Index

---

Journal: International Journal of Remote Sensing **Status**: Published **IF**: 3.531

Reference: Ramsauer, T. & Marzahn, P. (2023): Global soil moisture estimation based on GPM IMERG Data Using a Site Specific Adjusted Antecedent Precipitation Index. *International Journal of Remote Sensing*. 44 (2), pp. 542–566. DOI: 10.1080/01431161.2022.2162351

Scope and Context:

Article III showcases the global surface soil moisture estimation effort based on the satellite precipitation data product of the GPM mission. Local soil characteristics from the SoilGrids project and ERA-5 temperature reanalysis data support the calculation of the advanced antecedent precipitation index. Spatially distributed, empirical dampening factors are introduced in this study. These allow for a more locally explicit and divers soil moisture retrieval. Together with temperature data and information on local soil composition the creation of valid soil moisture values across climate and vegetation zones is facilitated, meaning, that seasonal variations and local soil moisture schemes can be reproduced for different parts of the world. The GPM_API data achieves a mean ubRMSD of 4.68Vol% against the for validation utilized in situ measurement stations across the globe. In the context of this summarizing work, this third article now further develops the API related methods of article II and utilizes the second data set from the data comparison in article I, namely the GPM IMERG precipitation values.

ACCEPTED MANUSCRIPT / INT. J. REMOTE SENS.

Global Soil Moisture Estimation based on GPM IMERG Data using a Site Specific Adjusted Antecedent Precipitation Index

Thomas Ramsauer[a] and Philip Marzahn[a,b]

[a]Department of Geography, Ludwig-Maximilians-Universität München; [b]Geodesy and Geoinformatics, Faculty of Agricultural and Environmental Sciences, University of Rostock

ARTICLE HISTORY
Received 19 May 2022
Accepted 9 December 2022

NOTE
This is an Accepted Manuscript of an article published by Taylor & Francis in
INTERNATIONAL JOURNAL OF REMOTE SENSING
2023, VOL. 44, NO. 2, 542–566
available at: https://doi.org/10.1080/01431161.2022.2162351

ABSTRACT
This study presents a global, hourly surface soil moisture estimation procedure based on precipitation and temperature data. Information on soil composition further help to define the local characteristics of soil moisture development. An advanced antecedent precipitation index (API) is utilized to generate a global soil moisture product of high temporal resolution with the Global Precipitation Measurement (GPM) Missions Integrated Multi-Satellite Retrievals for GPM (IMERG) as main driver. The resulting global GPM API data set is compared against in situ measurements from the International Soil Moisture Network (ISMN) and is also evaluated against the soil moisture data set from the European Space Agency's Climate Change Initiative (ESA CCI SM). The study shows that with empirically derived dampening factors the GPM API achieves a mean ubRMSD across the utilized in situ stations in different climates and vegetation zones of 4.68 $Vol\%$ and a bias of 0.88 $Vol\%$. The data set clearly represents the local soil moisture schemes with seasonal variations. When comparing with ESA CCI SM, the GPM API does perform better at the measurement sites concerning bias, correlation and error values. The data set is in most parts negative biased compared to the ESA CCI SM, however better matches the mean soil moisture at ISMN stations. Overall, the GPM API delivers a very promising global, hourly surface soil moisture product at $0.1^\circ \times 0.1^\circ$ spatial resolution.

KEYWORDS
GPM, IMERG, soil moisture, global, precipitation, ESA, CCI, SoilGrids, ERA5, ISMN

1. Introduction

Soil moisture plays an important role in the water cycle of the earth (Robinson et al. 2008; Seneviratne et al. 2010) and has a dominant effect on the carbon cycle through its

CONTACT T. Ramsauer. Email: thomas.ramsauer@lmu.de

impact on photosynthesis (Humphrey et al. 2021) and consequently affects long-term terrestrial carbon uptake and storage (Green et al. 2019). In some regions of the world soil moisture is the limiting factor in plant transpiration and photosynthetic activity and hence impacts also energy and biogeochemical cycles (Seneviratne et al. 2010; Manning et al. 2018; Small et al. 2018; Or and Lehmann 2019). Studies show relations between soil moisture and hydroclimatic variability of variables like precipitation and evaporation (Krakauer, Cook, and Puma 2010; Hsu et al. 2017). Spatial coupling of afternoon rain over relative dry antecedent soil moisture patches (Hsu et al. 2017) and soil moisture-temperature coupling meaning higher probability of extreme warm events with the occurrence of droughts (Miralles et al. 2012; Hirschi et al. 2014) are examples.

On the other side, the connection of precipitation to soil moisture is straightforward. Only few exceptions exist for the trivial relationship, e.g. runoff generation instead of soil moisture increase if the precipitation amount surpasses the local infiltration rate or the uptake of water is hindered in other ways (Seneviratne et al. 2010; Vereecken et al. 2019). Soil moisture thereby is the most influential governing factor in controlling the rainfall-runoff response (Robinson et al. 2008).

Gridded soil moisture is used in a plentitude of hydrological modelling applications, like streamflow prediction (Alvarez-Garreton et al. 2016), forecasting characteristics of flood events (Chifflard et al. 2017) and estimation of irrigation water use (Abolafia-Rosenzweig et al. 2019). Also the state of soil moisture is a relevant condition regulating temperature extremes during heat waves and obviously an indicator for agricultural droughts as well (Hirschi et al. 2010; Sadri, Wood, and Pan 2018; Zhu et al. 2019a; Blyverket et al. 2019b). For the closely linked variables, precipitation and soil moisture data products exist on a variety of spatial scales from point measurements to global modelling and estimation from satellite imagery.

Soil moisture retrieval on global scale is only feasible by modelling or utilizing satellite imaging technology and is attempted for the last decades (Robock et al. 2000; Dirmeyer 2011; Balsamo et al. 2018). A plentitude of (also global) land surface models provide soil moisture as output (Tavakol et al. 2021). Varying complexities exist for soil moisture specific models - from a simple bucket model to fully physically based (Guswa, Celia, and Rodriguez-Iturbe 2002). Wagner (2003) state, that rising model complexity does not necessarily add to the quality of the soil moisture estimates. Also, high numbers of additional input parameters with uncertainties attached are oftentimes needed for such global land surface schemes (Lawrence et al. 2019; Vereecken et al. 2019).

Satellite remote sensing missions are also exploited to estimate surface soil moisture (SSM) on large spatial scales. Optical, thermal and active and passive microwave (MW) sensors can provide spatially explicit soil moisture estimates (Njoku and Entekhabi 1996; Kerr et al. 2001; Bartalis et al. 2007; Wagner et al. 2013; Ochsner et al. 2013; Das and Paul 2015; Sadeghi, Jones, and Philpot 2015; Petropoulos, Ireland, and Barrett 2015; Sadeghi et al. 2017; Mohanty et al. 2017; Babaeian et al. 2019). MW sensors serve as the most direct retrieval method because backscattering or emission properties of a respective soil patch are affected by the dielectric properties of the three available phases air, water and solids in the soil column (Wigneron et al. 1998; Wagner 2003; Kerr et al. 2012; Wigneron et al. 2017; Babaeian et al. 2019). Combinations of different acquisition techniques are used in several studies to increase spatial and or temporal resolution of soil moisture products and hence satisfy increasing user requirements (Peng et al. 2021), e.g. MW with optical or thermal data (Piles et al. 2011, 2016; Hajj et al. 2017; Amazirh et al. 2018; Ojha et al. 2019; Lei et al. 2020; Nguyen, Cho,

and Choi 2022), multiple MW sensors (Bauer-Marschallinger et al. 2018; Das et al. 2019; Blyverket et al. 2019a; Ebrahimi et al. 2018; Santi et al. 2018) and integration of satellite retrievals with land surface models (Reichle et al. 2011; Toride et al. 2019; Vergopolan et al. 2020; Long et al. 2019) or machine learning techniques (Santi et al. 2019; Ezzahar et al. 2019; Zeng et al. 2019; Zhang et al. 2021).

Precipitation is prominently measured on point scale, however detection using satellite sensors is operational practice as well (Kucera et al. 2013). The retrieval of precipitation from space evolved from thermal infrared imaging of cloud tops over utilizing passive microwave sensors to the first active precipitation radar onboard the Tropical Rainfall Measurement Mission (TRMM), which was capable of delivering insights to ongoing processes within clouds (Kidd and Levizzani 2011; Levizzani and Cattani 2019). Its successor, the Global Precipitation Measurement (GPM) Mission hosts multiple sensors on the core observatory and additionally aggregates information from a full fleet of other satellites into one data stream (Skofronick-Jackson et al. 2017). This allows for a high temporal resolution (half hourly) precipitation product and also an increased spatial resolution when comparing to the bulk of satellite derived global soil moisture estimates.

This study aims at exploiting the direct and obvious relationship of precipitation and soil moisture to create a global hourly resolution SSM data set fulfilling current requirements towards high resolution data (Peng et al. 2021). Incorporating information on soil composition and local temperatures allows for spatially adjusted characteristics of soil moisture development. Temperature and meteorological droughts especially affect top soil moisture values (van Hateren et al. 2021; Souza, Neto, and de Souza 2021; Manning et al. 2018; Hao et al. 2019). Such developments happen on a larger spatial scale and hence temperature values are used here to guide the regional soil moisture development. Information on soil composition however is more locally explicit and therefore used to map local differences in soil water storage and flow characteristics.

Yet, precipitation still is the main input variable that influences the development of soil moisture. With a limited amount of input variables available, indices are often used to allow for simplified state descriptions of different parts of the hydrological cycle, for example precipitation based drought indices like the standard-precipitation index (SPI) or standard precipitation-evapotranspiration index (SPEI) (Peng et al. 2020; Bezdan et al. 2019; Alsumaiei 2020; Zhu et al. 2019b). To derive global SSM, the current study uses and improves upon the extended Antecedent Precipitation Index (API) from Ramsauer et al. (2021) which also uses precipitation as main input variable. This variant builds on the basic concept of the API from Kohler and Linsley (1951), that was since used in numerous studies that use the amount of precipitation in a preceding time frame to derive general information on the current soil moisture state (Wilke and McFarland 1986; Teng, Wang, and Doraiswamy 1993; Brocca, Melone, and Moramarco 2008; Ali, Ghosh, and Singh 2010; Javelle et al. 2010; Zhao et al. 2011; Tramblay et al. 2012; Kala, Evans, and Pitman 2015). Current applications employing the principles of the API are Schoener and Stone (2019, 2020) combining the API with radar derived precipitation for soil moisture monitoring and runoff modelling, Ramsauer et al. (2021) creating a soil moisture data set for Germany based on weather radar data, Guerschman et al. (2020) establishing vegetation cover dependence on API, Zhao et al. (2019a,b) using the API derived soil moisture information in landslide prediction.

The article addresses the question of feasibility and sufficient quality of the SSM retrieved with the proposed algorithm, namely if the GPM derived API adheres to the proposed accuracy requirements for soil moisture products provided by the Global

Climate Observing System (GCOS 2016). Furthermore, the study investigates if differences in soil characteristics or climatic regions are depicted by the proposed soil moisture product through respective response of local soil moisture development and if the performance is equally good across regions and top soil compositions. Finally, a comparison is drawn to test if the product, albeit providing data in higher temporal resolution, still performs in the realms of the established ESA CCI soil moisture data set.

2. Data and Methods

2.1. *Input Data*

2.1.1. Precipitation Data

Local soil moisture highly depends on the amount of precipitation at site. Precipitation estimates from the NASA (National Aeronautics and Space Administration) and JAXA (Japan Aerospace Exploration Agency) joint Global Precipitation Measurement (GPM) mission deliver the moisture input in the current study (Skofronick-Jackson et al. 2017). The mission combines measurements from low-earth-orbiting passive microwave (PWM) and active scanning radar satellites that suffer from spatial coverage with data from global infrared (IR) imaging satellites that only deliver data at a low spatial resolution (Hou et al. 2014). Therefore, data of multiple constellation satellites from international contributing space agencies are unified and inter-calibrated, where the GPM Core Observatory (GPM CO) satellite serves as calibrator (Skofronick-Jackson et al. 2017; Hou et al. 2014). The GPM CO carries two active imaging sensors: the DPR, a dual-frequency phased array precipitation radar that operates at Ku and Ka band (13 and 35 GHz) and the GMI, a conical-scanning multi-channel (10-183 GHz) microwave imager (Hou et al. 2014). GPM CO produces the best precipitation estimates with the Combined Radar-Radiometer (CORRA-G, using GMI and DPR) configuration (Huffman et al. 2020).

The resulting merged precipitation data estimates are provided in varying form by the involved space agencies. The Integrated Multi-Satellite Retrievals for GPM (IMERG) data set is a Level 3 NASA product coming in three processing stages (*early*, *late*, *final*), giving an *early* quick estimate in near real-time and subsequently refining the product through *late* and *final* stage with more data available. The *final* run includes gauge-data from Deutscher Wetterdienst (DWD) Global Precipitation Climatology Centre (GPCC) to calibrate the satellite data and correct for bias (Schamm et al. 2014; Huffman et al. 2020). Remaining temporal and spatial gaps in the precipitation estimates from sparse microwave satellite data are filled using interpolated data from respective enclosing overpasses and data from IR sensors via data assimilation (Huffman et al. 2020). NASA's processing efforts result in a half-hourly gridded global precipitation data set with a $0.1^\circ \times 0.1^\circ$ spatial resolution that is freely available (Huffman et al. 2019).

The IMERG data set is extensively used in the scientific community, e.g. in the evaluation of kilometre-scale weather and climate models that resolve deep convective processes (Zeman et al. 2021), estimation of change in ground water storage (Ahamed et al. 2022) or via assisting large-scale ground deformation studies (Emil et al. 2021).

In this study, NASA's IMERG gridded data set in version 6, *final* run is used (Huffman et al. 2019). The resulting SSM data set uses the same spatial grid, hence no spatial aggregation or interpolation of the precipitation input data has been applied.

2.1.2. Temperature Data

Temperature is a controlling variable of evapotranspiration in a landscape. In the proposed API algorithm temperature information contributes to regulating the depletion of the surface soil water storage. The ERA5 single level air temperature data set (t2m) is a atmospheric reanalysis data set that combines observation data with model data by the technique of data assimilation in a consistent manner respecting the laws of physics (Copernicus Climate Change Service (C3S) 2017; Hersbach et al. 2018). Hourly resolution spanning the time period from 1979 to present (with a preliminary back extension from 1950 onward (Bell et al. 2021)) and global coverage fit the requirements of the current study. The ECMWF generates the utilized data set which is accessible via the Copernicus Climate Change Service Climate Data Store (CDS). At CDS the ERA5 data is available at a regular $0.25° \times 0.25°$ grid. For this study the data set was bilinearly interpolated to the GPM grid.

2.1.3. Soil Information Data

Information on soil texture is needed in the loss factors of the presented API algorithm which is gathered from the SoilGrids 2.0 data released by the International Soil Reference and Information Center (ISRIC) (Poggio et al. 2021; Hengl et al. 2017b,a). The data set provides maps of soil properties at six depths. SoilGrids provide global distribution and information on soil organic carbon content, total nitrogen, coarse fragments, pH, cation exchange capacity, bulk density and texture fractions (Poggio et al. 2021). State-of-the-art machine learning methods are fed with observational data and global covariates. With this information on environmental factors like vegetation cover, terrain morphology, climate, geology and hydrology that contribute to pedogenesis, global predictions for soil characteristics on a 250m grid are generated (Poggio et al. 2021). SoilGrids data is adapted widely by the scientific community, e.g., for generating European and global soil hydraulic databases (Tóth et al. 2017; Ross et al. 2018) and as auxiliary variables in downscaling algorithms (Wu et al. 2018).

2.2. *Calibration and Validation Data*

2.2.1. ISMN

This study utilizes data from the International Soil Moisture Network (ISMN) for calibration of empirical variables in the API algorithm on a per station basis and also for evaluation purposes of the subsequently retrieved global API data set (Dorigo et al. 2011, 2021). The ISMN provides an global in situ soil moisture reference database that contains data shared by a multitude of organizations. Furthermore, the ISMN harmonizes the data concerning units and sampling rates and performs an automatic advanced quality control before providing the data (Dorigo et al. 2011, 2013, 2021). Currently, data from 71 measurement networks and 2842 stations worldwide are available (Dorigo et al. 2021).

In-situ station data must fulfill certain criteria for application in this study. Firstly, the included automatic global quality control flags define 'good' data points. Secondly, the recorded soil moisture time series must cover at least two years worth of good data in the period covered (2015-2020). Lastly, the goal of the API data set is to provide SSM values representing the upper most soil layers only and thus, ISMN stations measuring in 5 cm depth are exclusively considered. Furthermore, individual quality control of the 188 selected stations revealed remaining errors for 81 sites although they

are flagged 'good' in the metadata. These stations were consequently also excluded. Also, after the optimization scheme (sec. 2.4) outlier stations were additionally omitted leaving 86 stations. These stations are part of soil moisture networks listed in table 1.

Table 1. List of utilized Soil Moisture Networks with station count and SREX region affiliation.

Network	Count	SREX	References
AMMA-CATCH	5	WAF	AMMA-CATCH (1990); de Rosnay et al. (2009) Mougin et al. (2009); Pellarin et al. (2009) Lebel et al. (2009); Galle et al. (2018)
FR-Aqui	2	MED	Al-Yaari et al. (2018); Wigneron et al. (2018)
SMOSMANIA	12	MED	Calvet et al. (2007); Albergel et al. (2008) Calvet et al. (2016)
SOILSCAPE	3	WNA	Moghaddam et al. (2010); Shuman et al. (2010) Moghaddam et al. (2016)
TERENO	2	CEU	Zacharias et al. (2011); Bogena et al. (2012); Bogena (2016)
USCRN	60	(W,C,E)NA	Bell et al. (2013)
iRON	2	WNA	Osenga et al. (2019); Osenga, Vano, and Arnott (2021)

The regions defined in the "Special Report on Managing the Risks of Extreme Events and Disasters to Advance Climate Change Adaptation (SREX)" (Seneviratne et al. 2012) are used for evaluation in this study. Respective region codes corresponding to the network locations are also listed in table 1.

Figure 1 shows the spatial distribution and network affiliation and figure 2 the soil composition at the utilized measurement sites. Some stations are spatially close to each other and overlap in Figure 1.

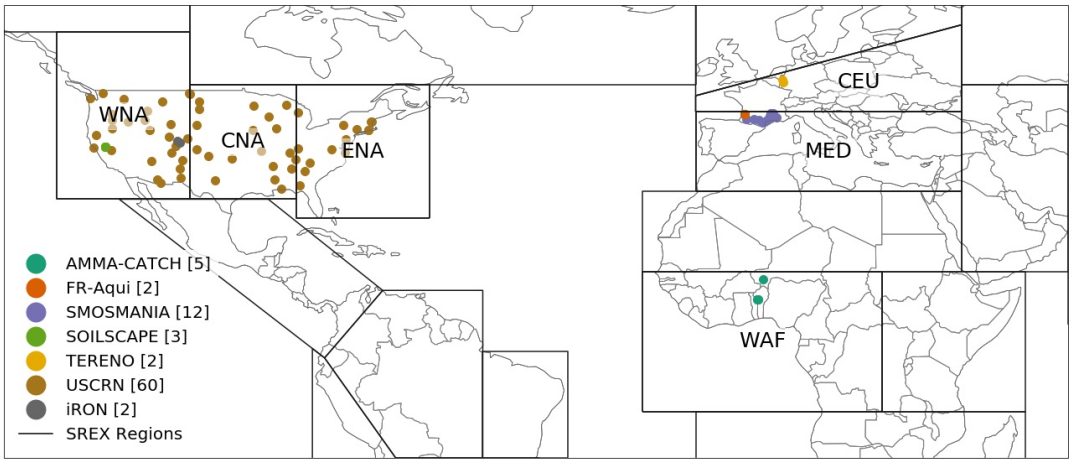

Figure 1. ISMN stations utilized for calibration and validation in this study. SREX regions are overlayed.

2.2.2. ESA CCI Soil Moisture Data

There are many global soil moisture data sets with different spatial and temporal resolution (Peng et al. 2021). ESA's Climate Change Initiative soil moisture (ESA CCI SM) merging algorithm generates long-term climate data records of soil moisture from single C-band scatterometer and multi-frequency radiometer soil moisture data sets and provides three harmonized products: an active-microwave-only, passive-microwave-only and a combined active-passive product (Dorigo et al. 2017; Gruber

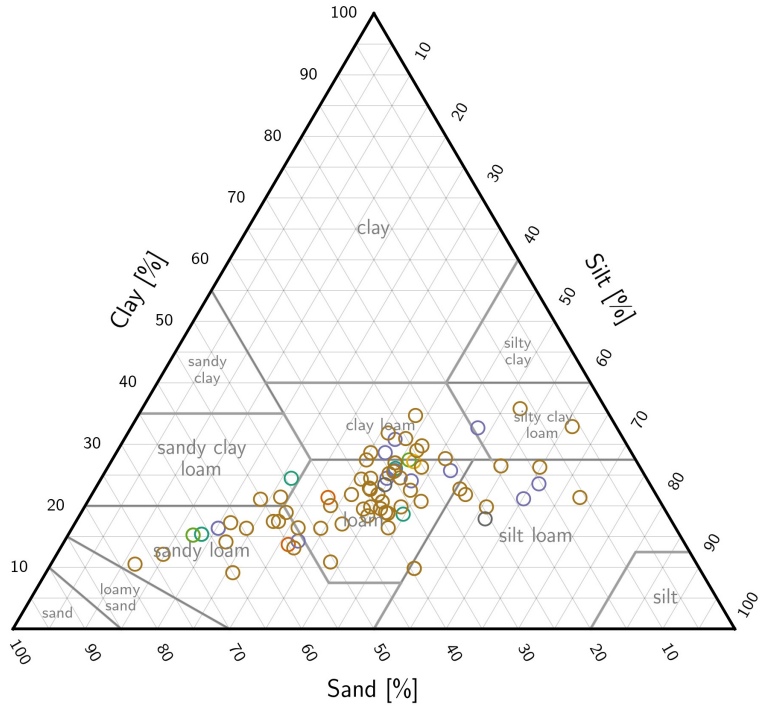

Figure 2. Soil composition at the utilized ISMN stations. Colours indicate network affiliation (see figure 1).

et al. 2019). The combined soil moisture product outperforms the single-sensor input products (Dorigo et al. 2017). The soil moisture estimates are available at daily time steps and 0.25°×0.25° spatial resolution for the time period 1978-2020. ESA CCI SM products are widely used and hence chosen as evaluation data set which the proposed global API based soil moisture data set is compared against. Specifically, version 6.1 of the combined active-passive, break-adjusted data set is utilized (Dorigo et al. 2017; Gruber et al. 2017, 2019; Preimesberger et al. 2021). To allow comparison with the API SM the ESA CCI SM data set is bilinearly interpolated to the GPM grid.

2.3. *Antecedent Precipitation Index*

The global SSM data set proposed in this study is based on the concept of the antecedent precipitation index introduced by Kohler and Linsley (1951). In the basic form the API at time step t is calculated from the value at the preceding time step API_{t-1} that is diminished by a factor, e.g. γ and increases with current precipitation P_t(eq. 1).

$$API_t = \gamma \times API_{t-1} + P_t \tag{1}$$

Subsequent studies adjust the dampening factor, e.g. utilized a cosine function for γ to account for seasonal differences in soil water losses (Crow et al. 2009). Pellarin et al. (2013) extend the algorithm for saturation dependent losses and gains to generate a more natural soil water inflow and outflow behaviour. Ramsauer et al. (2021) follow up on the basic idea of using the antecedent precipitation but further develop the algorithm to return actual soil moisture values. The proposed SSM retrieval uti-

lizes three different data inputs: precipitation data, temperature data and local soil characteristics, that is, information on sand and clay content respectively. Additional dampening factors a and b improve the empirical representation of local dominant processes that control the soil moisture variations (eq. 2). These factors account for temperature influence and locally prevailing soil conditions and control the amount of soil moisture loss from time step t to $t+1$. Spatial variability of soil water retention and outflow thereby is given with the respective input data. However, further refinements of the former API algorithm for global application are needed as the study of Ramsauer et al. (2021) focuses on the application of the API in the temperate region of Germany only, with a limited spectrum of soil composition and temperature variation. SSM in desert regions at least periodically fully depletes whereas soils in colder climates e.g. tend to show nearly no decline in moisture values in non-freezing days during wintertime at all. To account for these different characteristics in seasonality, spatially distributed dampening factors are introduced in the current study. Both empiric factors a and b represent a different loss characteristic: factor a controls the soil and temperature dependent soil moisture loss: temperature, with its influence varying spatially through the variable α, in conjunction with local clay content and current soil moisture saturation state control the regular soil moisture decline (eq. 3). Factor b on the contrary regulates peak outflow after precipitation events from the surface soil compartment through the process of percolation to lower soil layers, also considering the current saturation state (eq. 4). Spatial diversity in the magnitude of peak outflow is controlled via γ in the calculation of factor b.

$$API_t = a \times b \times API_{t-1} + (\theta_{sat} - API_{t-1}) \times \left[1 - e^{-\frac{P_t}{d}}\right] \tag{2}$$

with

$$a = 1 - \left[\frac{T}{\alpha} \times e^{-\beta \times clay} \times \left(1 - e^{-(API_{t-1} - \theta_{min})}\right)\right] \tag{3}$$

$$b = e^{-\left(\frac{API_{t-1} - \theta_{min}}{\theta_{sat} - \theta_{min}}\right)^{\gamma}} \tag{4}$$

where α and γ are empiric variables and $\beta = -0.05$, d is soil depth (for this study constant at 50 mm), T is temperature $[°C]$ (0; if $T \leq 0$), $clay$ is clay content [%]. For description of θ see equations (5)-(8). These estimations for site specific soil water holding capacity are derived following approximations from the Interaction Soil Biosphere Atmosphere (ISBA) parameterisation scheme (Noilhan and Mahfouf 1996). The ISBA model makes the following assumptions for soil moisture values at saturation (θ_{sat}, eq. 5), field capacity (θ_{fc}, eq. 6) and wilting point (θ_{wilt}, eq. 7), where the first and last variable go into the API calculation and moisture values at field capacity are used to initialize the data set.

$$\theta_{sat} = .1 * (-1.08 * sand + 494.305) \tag{5}$$

$$\theta_{fc} = 8.90467 * clay^{0.3496} \tag{6}$$

$$\theta_{wilt} = 3.71342 * \sqrt{clay} \tag{7}$$

Furthermore, θ_{min} is needed in equations 3 and 4 (see eq. 8).

$$\theta_{min} = \theta_{wilt} * .1 \tag{8}$$

The relationship between θ_{min} and θ_{wilt} in equation 8 allows for water loss beyond the permanent wilting point but avoids full drainage. Setting this threshold facilitates modelling the SSM in regions with longer dry seasons like WAF.

2.4. *Calibration Procedure*

A global soil moisture data set based on the concept of a enhanced API algorithm is proposed. The introduced approach contains variables that allow for an adjusted local characteristic of soil moisture outflow in terms of speed and decay of water loss. These empiric variables α and γ are intended to be regionalized to support and promote spatially varying water loss properties already originating from considered soil characteristics. That is, the algorithm does take sand content into account, however the regional influence thereof is regulated via the mentioned empiric variables. ISMN station data is utilized to calibrate these factors on a per station basis. Therefore, the API algorithm is run on point for every in situ station location (107 stations, sec. 2.2.1) and subsequently is compared with the available measurements in the time period of 2015-2020. The distribution of utilized stations is not optimal. All stations are located in the northern hemisphere and most of them in the United States. However, the regions sampled by these in situ stations are geologically, pedologically and also climatically divers. Thus we can ensure a broad coverage of environmental circumstances and gain confidence in the retrieved empirical variables. Utilizing an optimizing algorithm (Powell 1964), α and γ are iteratively adjusted. Optimization goal is the RMSD (eq. 10) between the generated API and local soil moisture measurement to reduce bias and obtain optimal empirical values for the specific site characteristics. The metrics bias (eq. 9), ubRMSD (eq. 11) and Pearson's R (eq. 12) are used to further assess performance of the API against in situ measurements.

$$bias = \frac{1}{N}\sum_{i=1}^{N}(x_i - y_i) \tag{9}$$

$$\text{RMSD} = \sqrt{\frac{1}{N}\sum_{i=1}^{N}(x_i - y_i)^2} \tag{10}$$

$$\text{ubRMSD} = \sqrt{RMSD^2 - bias^2} \tag{11}$$

$$R = \frac{\sigma_{xy}}{\sigma_x \sigma_y} \tag{12}$$

To generate spatially distributed representations of α and γ for global computation of the API soil moisture data set, a third grade polynomial regression between the two variables and sand content is established respectively.

Sand content is used to establish the relationship with the global representation of bespoken loss variables. Across all measurement sites used in the calibration procedure, local sand content shows the highest correlation with α and γ respectively among tested variables. Other constant environmental properties like clay content, elevation, longitude or latitude only show weaker statistical dependence (see table 2).

Table 2. Correlation matrix for empirical variables α and γ and static environmental variables of all measurement sites utilized in the calibration procedure.

	α	γ	Elevation	Latitude	Longitude	Clay	Sand
α	1	0.05	-0.17	-0.05	-0.04	-0.02	-0.23
γ	0.05	1	0.05	0.27	0.06	0.36	-0.47
Elevation	-0.17	0.05	1	0.03	-0.42	0.07	0.04
Latitude	-0.05	0.27	0.03	1	-0.18	0.31	-0.52
Longitude	-0.04	0.06	-0.42	-0.18	1	0.08	0.04
Clay	-0.02	0.36	0.07	0.31	0.08	1	-0.72
Sand	-0.23	-0.47	0.04	-0.52	0.04	-0.72	1

Furthermore, sand content is directly connected to processes like infiltration, as related soil properties (e.g. water conductivity) depend on the soil particle size distribution. The established relationship of sand content with the empirical factors is therefor sensible.

3. Results

3.1. *Calibration Results*

The empiric variables α and γ that regulate the initial speed of soil moisture loss and the decay of the decline of moisture are optimized on in situ station data.

The variables contributing to the third grade polynomial equations derived to establish a connection between the optimized variables α and γ on point and the respective sand content, which is extracted from the SoilGrids data set, are to be found in table 3. A graphical representation is shown in figure 3 where the colours follow the respective network affiliation. A summary of resulting α and γ values and associated RMSD values against the in situ measurements are provided as supplemental files to this article.

Table 3. Empirical variables of third grade polynomial function ($f(sand) = a*sand+b*sand^2+c*sand^3+d$) describing relationship of sand content and alpha and gamma respectively.

	a	b	c	d
α	-269.92098128	5.21569461	-0.03252417	7225.05427942
γ	0.6408379781	-0.0218790707	0.0001642598	12.2191527206

Aggregated RMSD values of the per point calculated API soil moisture values, the global calculated API soil moisture values and ESA CCI SM values against in situ measurements are shown in figure 4.

On station basis, the global GPM API, calculated with derived α and γ values, shows a mean (ub)RMSD of (4.68) 5.80 $Vol\%$ (ESA CCI SM: (5.03) 8.94 $Vol\%$).

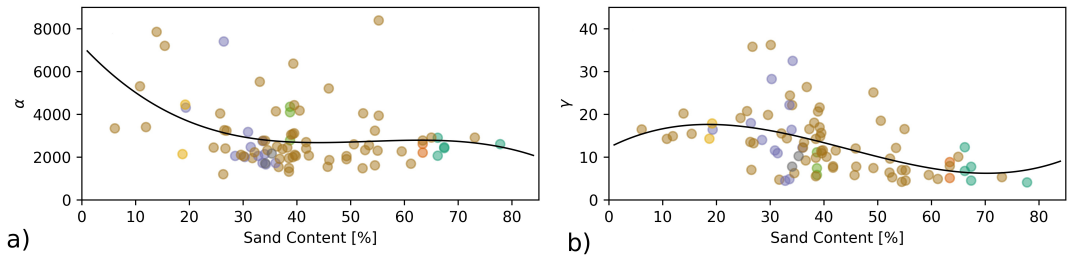

Figure 3. Optimized α (a) and γ (b) values for respective sand content at in situ stations and derived polynomial functions for global application. Colours indicate network affiliation (see figure 1)

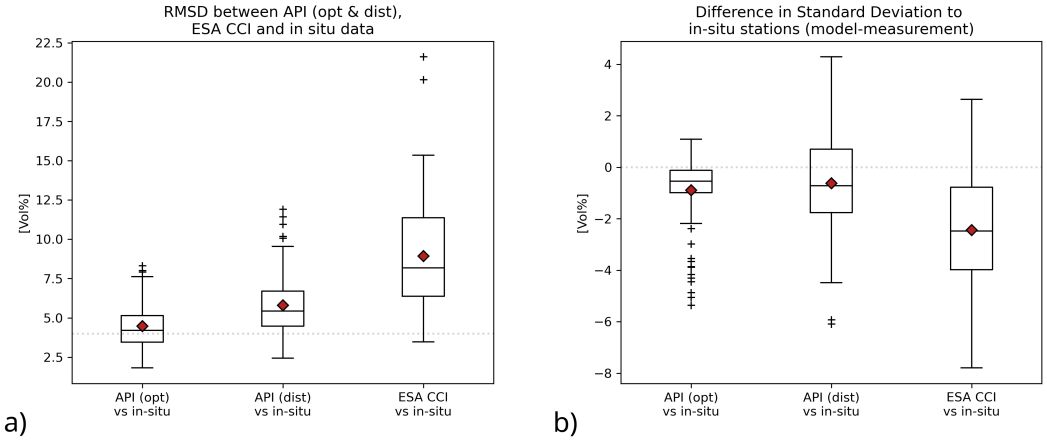

Figure 4. RMSD (a) and difference in standard deviation (b, modelled - measured) of API (optimized), API (distributed) and ESA CCI SM against in situ soil moisture measurements from the ISMN Network.

Figure 5 shows the ubRMSD between GPM API (local and global) and ESA CCI SM against measurements broken down according to the SREX regions.

On average, the retrieved soil moisture time series shows less variability than the measured in situ data (figure 4b). However, the global API centers close to around zero with positive and negative values of difference in standard deviation when compared to in situ measurements, whereas the ESA CCI SM data predominantly shows negative values, meaning less variability is present in the satellite retrieved soil moisture time series than the respective station data. Concerning bias, the global GPM API in turn is on average slightly biased with a mean deviance of 0.88 $Vol\%$ (figure 6).

Regarding comparisons in the SREX regions where measurements are available, the GPM API overall shows little bias with a region mean maximum value of 1.74 $Vol\%$ in Western North America (WNA). The moisture values of ESA CCI SM on average are also positively biased with a high mean bias of 5.83 $Vol\%$ and maximum deviation per region at stations in Western Africa (WAF) with 10.99 $Vol\%$ (table 4). Correlation of the derived soil moisture differs only slightly between GPM API and ESA CCI SM with mean of Pearson's R at the utilized in situ stations being 0.78 and 0.70 respectively.

A selection of soil moisture time series from GPM API (local and global), ESA CCI SM and in situ data is plotted in figure 7. For every SREX region that provided an in situ station for calibration, one example is shown. Plots for the remaining stations used in calibration and evaluation against ESA CCI SM are provided as supplemental material to the article.

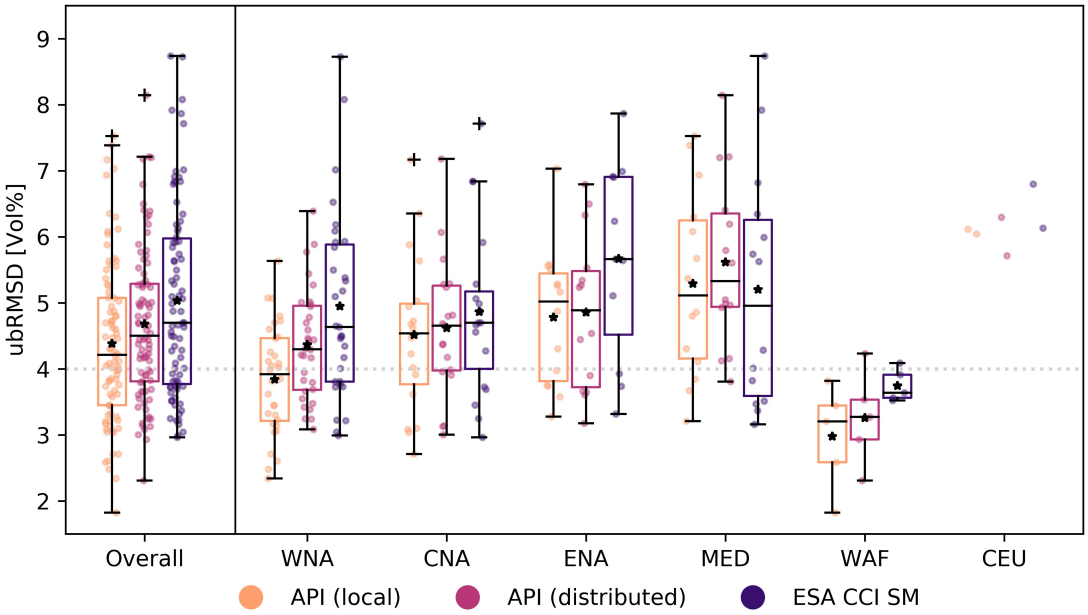

Figure 5. Overall ubRMSD between local optimized GPM API, distributed (global) GPM API and ESA CCI SM against in situ data from ISMN and grouped for SREX regions.

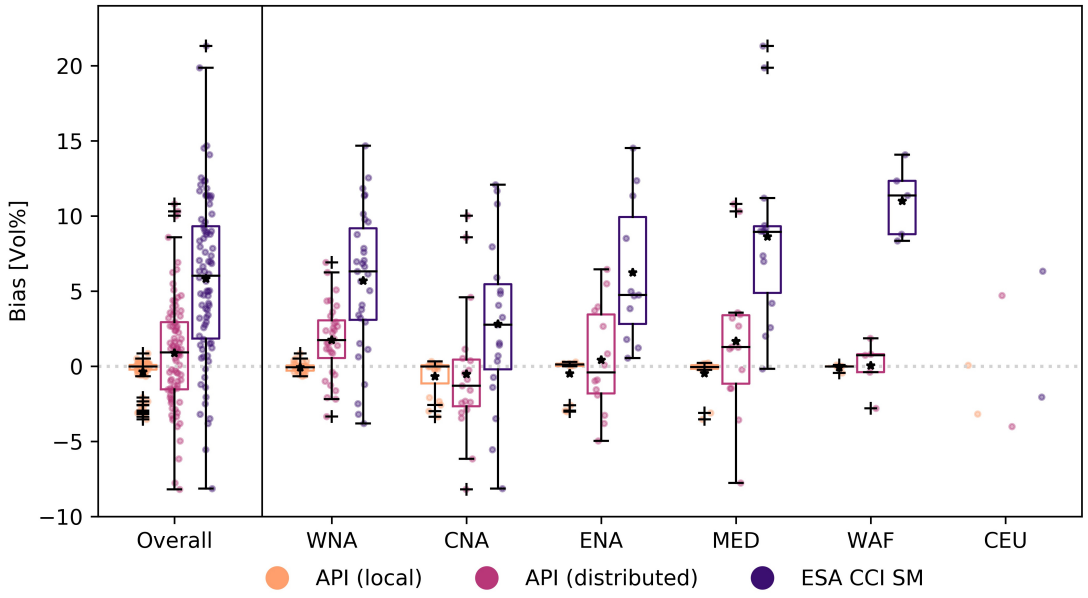

Figure 6. Overall bias between local optimized GPM API, distributed (global) GPM API and ESA CCI SM against in situ data from ISMN and grouped for SREX regions.

3.2. *Global Soil Moisture Data Set*

3.2.1. Properties

The global hourly soil moisture data set GPM API at spatial resolution of 0.1°×0.1° is resulting from this study. It is freely available online under the Creative Commons Attribution 4.0 International Public License (Ramsauer 2022a). Spatial representations of the minimum, maximum and mean SSM values across the data set's temporal

Table 4. List of error measures between local optimized GPM API (opt), distributed GPM API (dis), ESA CCI SM and in situ ISMN station data.

Measure		CEU	CNA	ENA	MED	WAF	WNA	Overall
RMSD	opt vs. stat	6.47	4.67	4.92	5.39	2.98	3.85	4.47
	dis vs. stat	7.42	6.05	5.95	7.24	3.58	5.21	5.80
	esa vs. stat	7.87	7.45	9.02	10.84	11.64	8.59	8.94
ubRMSD	opt vs. stat	6.08	4.51	4.78	5.29	2.97	3.84	4.38
	dis vs. stat	6.00	4.62	4.85	5.61	3.25	4.36	4.68
	esa vs. stat	6.46	4.86	5.66	5.20	3.74	4.95	5.03
MAE	opt vs. stat	5.11	3.68	3.84	4.10	2.06	2.90	3.43
	dis vs. stat	5.90	5.07	4.87	5.96	2.54	4.10	4.69
	esa vs. stat	6.52	6.37	7.65	9.70	11.00	7.55	7.84
BIAS	opt vs. stat	-1.55	-0.68	-0.50	-0.48	-0.08	-0.08	-0.38
	dis vs. stat	0.35	-0.53	0.42	1.66	0.04	1.74	0.88
	esa vs. stat	2.15	2.80	6.24	8.63	10.99	5.69	5.83
RVALUE	opt vs. stat	0.71	0.73	0.75	0.70	0.90	0.82	0.77
	dis vs. stat	0.71	0.73	0.75	0.72	0.90	0.83	0.78
	esa vs. stat	0.71	0.68	0.68	0.76	0.87	0.67	0.70

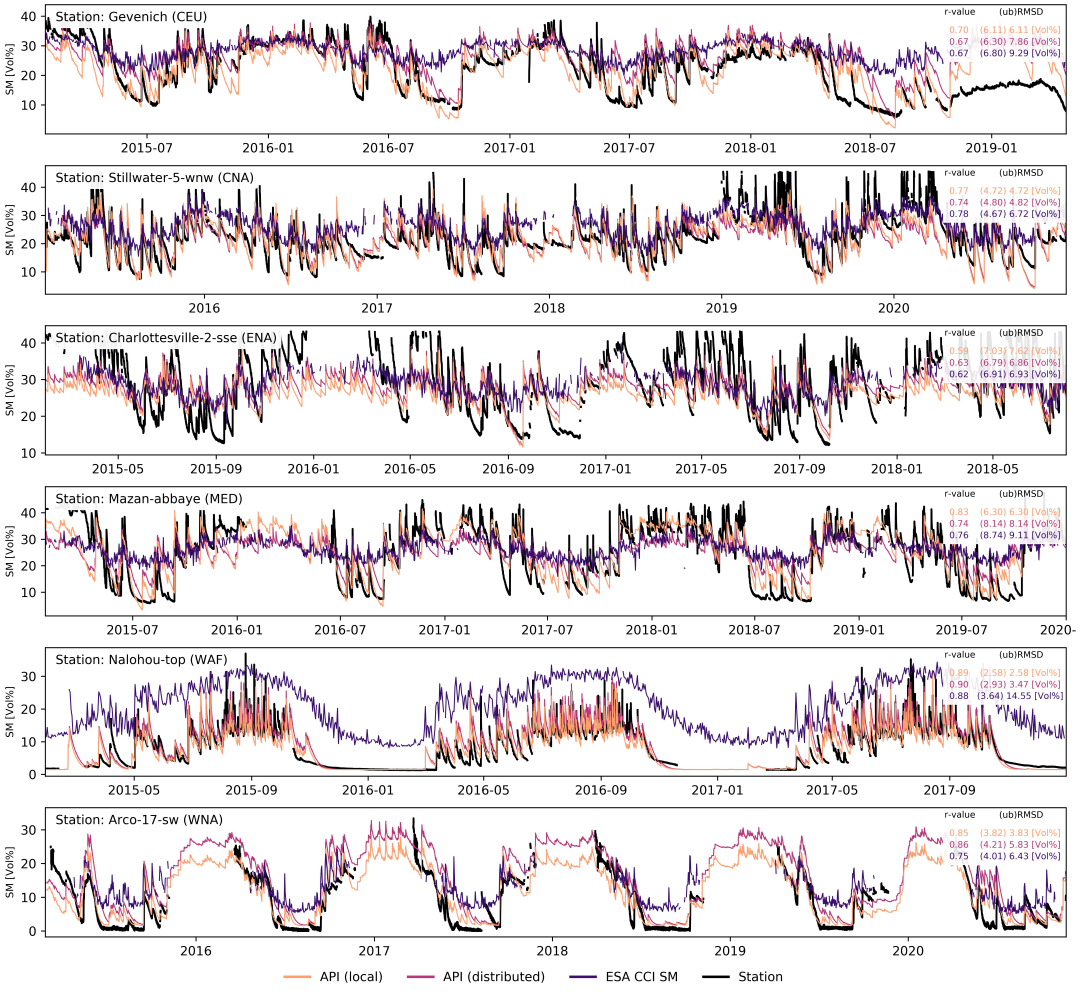

Figure 7. Soil moisture measurements from ISMN station data against locally adjusted GPM API, global distributed GPM API and ESA CCI SM data for randomly selected sites across 6 SREX regions (CEU, CNA, ENA, MED, WAF, WNA).

coverage is depicted in figure 8 a-c. Physically sound limits of soil moisture are given by the ISBA definitions and the implementation of the empirical API algorithm. Still, low minimum soil moisture values are prevalent for most regions. That is acceptable as explicitly SSM values that only represent the upper 5 cm are provided. The maximum moisture values reach feasible values around 40 $Vol\%$. Tropics and monsoon regions show expectable high values of soil moisture. Also, high standard deviation of moisture values is rightfully observed e.g. in Middle East, Southern Asia and Sahel. Overall, the

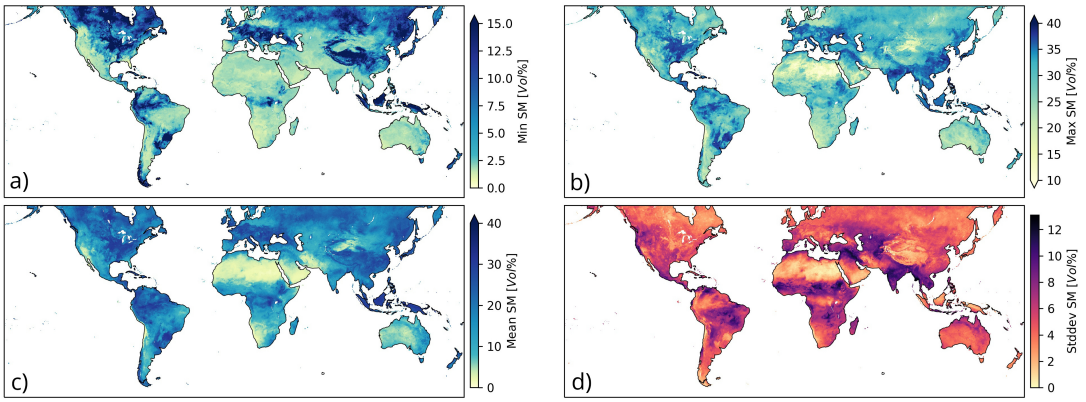

Figure 8. Minimum, maximum, mean and standard deviation of soil moisture values in the global GPM API data set.

global API data set reflects the global distribution of top soils that feature high sand contents. Sahara, southern Africa, Australia and parts of the Southern Americas show low maximum soil moisture values accordingly. Validity of the derived GPM API data set can however only be assumed for areas with similar soil characteristics and climate zones as have been used in the calibration process.

3.2.2. Spatial Evaluation and Comparison with ESA CCI SM

For spatial evaluation the GPM API data set is compared against ESA CCI SM data set. Differences in the derived soil moisture values has already been shown on a per station basis. Similarly, the data sets differ in the spatial patterns of soil moisture. Figure 9 shows the overall MAE and bias across the time period of investigation. Tropical border areas show spots of high divergence with the GPM API data set being negative biased compared to ESA CCI SM. South East China and North Eastern Europe are further regions, where negative bias is to be observed likewise. An overview of bias values between GPM API and ESA CCI SM per SREX region is provided in figure 10. African (14-17) and Australian (25, 26) regions show the least spread in bias values whereas a large spread in bias is to be observed for the regions of Central North America and Central Europe. Besides parts of Argentina and smaller patches in East Africa and Indonesia, the globally southern regions show the biggest bias between the two data sets. Central North America, Eastern Europe and parts of central Asia show positive bias for the GPM API with the highest values along the northern coastline of the Black Sea.

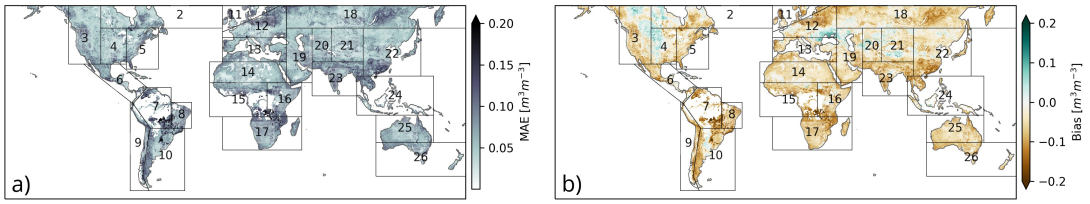

Figure 9. MAE (a) and Bias (b) between GPM API data and ESA CCI SM data with SREX regions overlayed.

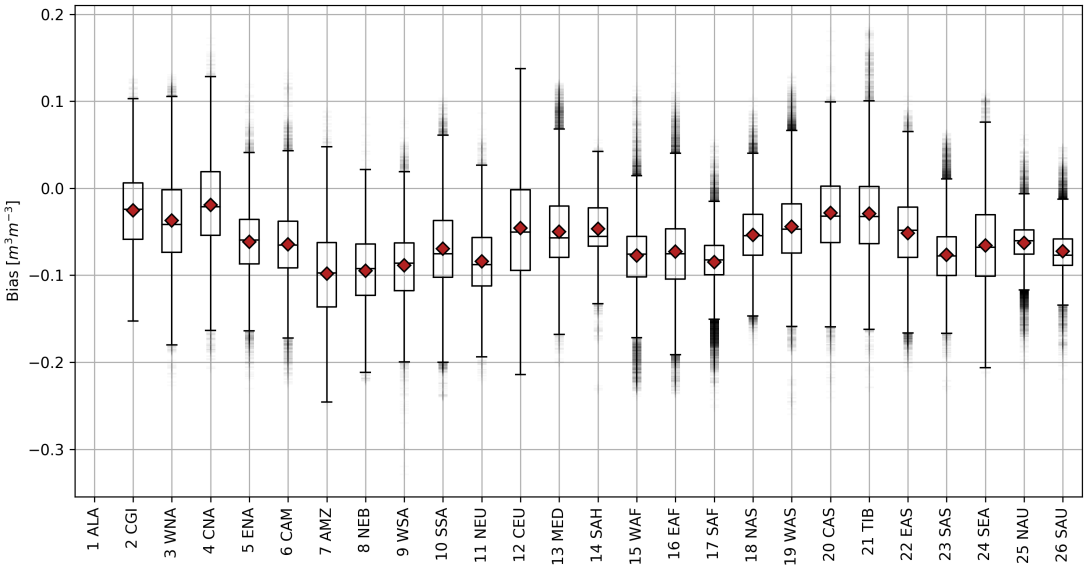

Figure 10. Bias for all respective pixel values of GPM API data against ESA CCI SM data, split up for all SREX regions.

4. Discussion

The presented GPM API data set shows high similarity when comparing with in situ soil moisture measurement data and follows the seasonal development of the moisture values very well. Spatial diversified soil water flow and storage characteristics are facilitated through globally available, spatial distinctive dampening factors. A global representation of contributing variables, α and γ, is derived from a polynomial relationship on point scale of optimized variants thereof with respective sand content at in situ measurement stations.

Good correlation between other co-variables than sand content and the optimized α and γ values for spatial computation of the GPM API was not found. However, within the bounds of validity of the API data set, very good representation of local soil moisture has been shown when comparing to in situ soil moisture measurement station data. Approaching relevant soil water processes, like percolation or evaporation, with the introduced empirical algorithms whilst supporting the calculation with high quality and tested input data, also does respect physical boundaries and conditions in modelling the soil water movement. And, influences of vegetation on soil moisture through rooting, transpiration, interception is indirectly captured in the empirical formulation. The empiricism of the GPM API seemingly addresses or mimics the underlying physics well enough for application in different climate and vegetation zones. Spatial patterns and amplitude of soil moisture are plausible (figure 8) and

meet the expectations towards a global data set. The fact that, on global scale, the GPM API data set is overall mostly negatively biased in comparison to the ESA CCI SM data set has to be taken with care. ESA CCI SM in turn itself is positively biased at 86% of the in situ stations and consequently also shows a positive mean bias of 5.83 $Vol\%$ (std: 5.49 $Vol\%$) across all utilized reference sites. Still, the ESA CCI SM product is used as evaluation basis because of its frequent use in the science community.

The study compares a satellite data derived product, which commits to physical principles in the form of exploitation of surface interaction of electromagnetic waves, with the empirically derived GPM API data set. The problem of representativeness and resulting errors due to subgrid processes are hence to be considered. ESA CCI SM already comes with a coarser spatial resolution which hinders a rightfully true comparison with exact true and false values (Gruber et al. 2020). This only allows for an evaluation of the two data sets, acknowledging impacts of altered spatial resolution on ESA CCI SM's side and bespoken issues of representativeness for both data sets when comparing to in situ (point) measurements. Finally, although totally different approaches lead to the GPM API and ESA CCI SM products, both data sets still must stand the comparison against such station measurements. There, the GPM API outperforms the ESA CCI SM data set in terms of correlation, bias, ubRMSD against in situ data. But validity of the GPM API product can only be given for non-irrigated regions, land cover like open shrubland and grassland and climate zones also covered by the in situ stations in the calibration phase.

5. Conclusion

This study introduces the GPM API data set as hourly SSM resource that is based off of the renown GPM IMERG precipitation product. The derivation of hourly global soil moisture in the top soil is demonstrated in preceding sections. Information on spatial distribution of soil composition and gridded temperature time series data allows the empirical algorithm to model local soil drainage and water holding capacities and hence to mimic the physical underlying processes in an empirical manner. Although these parts of the natural water flow are not present directly in the algorithm, the empirical implementation in the GPM API can replicate the implications and effects thereof very well. For example, a higher and long-enduring summerly depletion of soil water storage is mapped accordingly for drought years in certain regions. Similarly, seasonal rain and dry periods in the WAF region are modelled appropriately. The performance at in situ measurement stations across six SREX regions is very promising with a mean ubRMSD value of 4.68 $Vol\%$ and bias of 0.88 $Vol\%$. With that, the requirements of GCOS still cannot quite be fulfilled for all stations, but the accuracy is higher than ESA CCI SM at most in situ stations. Different moisture regimes across regions can be appropriately mapped with the GPM API as requested in this investigation. This study shows that the empirical soil moisture algorithm is capable to compete with established satellite soil moisture products without denying the usefulness and physical justification of these. The GPM API should provide additional input for data assimilation schemes aiming at high resolution soil moisture retrieval. In the effort to further increase the provided data set's merit, data spanning the whole IMERG era will be processed and published in the future.

Acknowledgements

The authors thank the responsible institutions for providing the utilized data sets: NASA (GPM), ECMWF (ERA5), International Soil Reference and Information Centre (SoilGrids), TU Wien (ISMN), ESA (ESA CCI SM).

Disclosure Statement

No potential conflict of interest was reported by the author(s).

Supplemetal Material

The GPM API data set is available at https://doi.org/10.5281/zenodo.6489998 (Ramsauer 2022a). Figures for all in situ stations as seen in figure 7 and a summary table depicting alpha, gamma and error values across stations are available at https://doi.org/10.5281/zenodo.6563944 (Ramsauer 2022b).

ORCID

- Thomas Ramsauer: 0000-0001-5322-4540
- Philip Marzahn: 0000-0002-2636-3438

References

Abolafia-Rosenzweig, R., B. Livneh, E.E. Small, and S.V. Kumar. 2019. "Soil Moisture Data Assimilation to Estimate Irrigation Water Use." *Journal of Advances in Modeling Earth Systems* 11 (11): 3670–3690.

Ahamed, Aakash, Rosemary Knight, Sarfaraz Alam, Rich Pauloo, and Forrest Melton. 2022. "Assessing the utility of remote sensing data to accurately estimate changes in groundwater storage." *Science of The Total Environment* 807: 150635.

Al-Yaari, A., S. Dayau, C. Chipeaux, C. Aluome, A. Kruszewski, D. Loustau, and J.-P. Wigneron. 2018. "The AQUI Soil Moisture Network for Satellite Microwave Remote Sensing Validation in South-Western France." *Remote Sensing* 10 (11): 1839.

Albergel, C., C. Rüdiger, T. Pellarin, J.-C. Calvet, N. Fritz, F. Froissard, D. Suquia, A. Petitpa, B. Piguet, and E. Martin. 2008. "From near-surface to root-zone soil moisture using an exponential filter: an assessment of the method based on in-situ observations and model simulations." *Hydrol. Earth Syst. Sci.* 12: 1323–1337.

Ali, Shakir, N.C. Ghosh, and Ranvir Singh. 2010. "Rainfall-runoff simulation using a normalized antecedent precipitation index." *Hydrological Sciences Journal* 55 (2): 266–274.

Alsumaiei, Abdullah A. 2020. "Monitoring Hydrometeorological Droughts Using a Simplified Precipitation Index." *Climate* 8 (2): 19.

Alvarez-Garreton, Camila, Dongryeol Ryu, Andrew W. Western, Wade T. Crow, Chun-Hsu Su, and David R. Robertson. 2016. "Dual assimilation of satellite soil moisture to improve streamflow prediction in data-scarce catchments." *Water Resources Research* 52 (7): 5357–5375.

Amazirh, Abdelhakim, Olivier Merlin, Salah Er-Raki, Qi Gao, Vincent Rivalland, Yoann Malbeteau, Said Khabba, and Maria José Escorihuela. 2018. "Retrieving surface soil moisture

at high spatio-temporal resolution from a synergy between Sentinel-1 radar and Landsat thermal data: A study case over bare soil." *Remote Sensing of Environment* 211: 321–337.

AMMA-CATCH. 1990. "AMMA-CATCH: a hydrological, meteorological and ecological observatory on West Africa." .

Babaeian, Ebrahim, Morteza Sadeghi, Scott B. Jones, Carsten Montzka, Harry Vereecken, and Markus Tuller. 2019. "Ground, Proximal, and Satellite Remote Sensing of Soil Moisture." *Reviews of Geophysics* 57 (2): 530–616.

Balsamo, Gianpaolo, Anna Agusti-Panareda, Clement Albergel, Gabriele Arduini, Anton Beljaars, Jean Bidlot, Eleanor Blyth, et al. 2018. "Satellite and In Situ Observations for Advancing Global Earth Surface Modelling: A Review." *Remote Sensing* 10 (12): 2038.

Bartalis, Zoltan, Wolfgang Wagner, Vahid Naeimi, Stefan Hasenauer, Klaus Scipal, Hans Bonekamp, Julia Figa, and Craig Anderson. 2007. "Initial soil moisture retrievals from the METOP-A Advanced Scatterometer (ASCAT)." *Geophysical Research Letters* 34 (20).

Bauer-Marschallinger, Bernhard, Christoph Paulik, Simon Hochstöger, Thomas Mistelbauer, Sara Modanesi, Luca Ciabatta, Christian Massari, Luca Brocca, and Wolfgang Wagner. 2018. "Soil Moisture from Fusion of Scatterometer and SAR: Closing the Scale Gap with Temporal Filtering." *Remote Sensing* 10 (7): 1030.

Bell, Bill, Hans Hersbach, Adrian Simmons, Paul Berrisford, Per Dahlgren, András Horányi, Joaquín Muñoz-Sabater, et al. 2021. "The ERA5 global reanalysis: Preliminary extension to 1950." *Quarterly Journal of the Royal Meteorological Society* 147 (741): 4186–4227.

Bell, Jesse E., Michael A. Palecki, C. Bruce Baker, William G. Collins, Jay H. Lawrimore, Ronald D. Leeper, Mark E. Hall, et al. 2013. "U.S. Climate Reference Network Soil Moisture and Temperature Observations." *Journal of Hydrometeorology* 14 (3): 977–988.

Bezdan, Jovana, Atila Bezdan, Boško Blagojević, Minučer Mesaroš, Borivoj Pejić, Milica Vranešević, Dragoslav Pavić, and Emilija Nikolić-orić. 2019. "SPEI-Based Approach to Agricultural Drought Monitoring in Vojvodina Region." *Water* 11 (7): 1481.

Blyverket, Jostein, Paul Hamer, Laurent Bertino, Clément Albergel, David Fairbairn, and William Lahoz. 2019a. "An Evaluation of the EnKF vs. EnOI and the Assimilation of SMAP, SMOS and ESA CCI Soil Moisture Data over the Contiguous US." *Remote Sensing* 11 (5): 478.

Blyverket, Jostein, Paul D. Hamer, Philipp Schneider, Clément Albergel, and William A. Lahoz. 2019b. "Monitoring Soil Moisture Drought over Northern High Latitudes from Space." *Remote Sensing* 11 (10): 1200.

Bogena, H., R. Kunkel, T. Pütz, H. Vereecken, E. Kruger, S. Zacharias, P. Dietrich, et al. 2012. "Tereno - long-term monitoring network for terrestrial environmental research." *Hydrologie und Wasserbewirtschaftung* 56: 138–143.

Bogena, Heye Reemt. 2016. "TERENO: German network of terrestrial environmental observatories." *Journal of large-scale research facilities JLSRF* 2.

Brocca, L., F. Melone, and T. Moramarco. 2008. "On the estimation of antecedent wetness conditions in rainfall–runoff modelling." *Hydrological Processes* 22 (5): 629–642.

Calvet, Jean-Christophe, Noureddine Fritz, Christine Berne, Bruno Piguet, William Maurel, and Catherine Meurey. 2016. "Deriving pedotransfer functions for soil quartz fraction in southern France from reverse modeling." *SOIL* 2 (4): 615–629.

Calvet, Jean-Christophe, Noureddine Fritz, Francis Froissard, David Suquia, Alain Petitpa, and Bruno Piguet. 2007. "In situ soil moisture observations for the CAL/VAL of SMOS: the SMOSMANIA network." In *2007 IEEE International Geoscience and Remote Sensing Symposium*, IEEE.

Chifflard, Peter, Julius Kranl, Georg zur Strassen, and Harald Zepp. 2017. "The significance of soil moisture in forecasting characteristics of flood events. A statistical analysis in two nested catchments." *Journal of Hydrology and Hydromechanics* 66 (1): 1–11.

Copernicus Climate Change Service (C3S). 2017. "ERA5: Fifth generation of ECMWF atmospheric reanalyses of the global climate." Copernicus Climate Change Service Climate Data Store (CDS). https://cds.climate.copernicus.eu/cdsapp#!/home.

Crow, Wade T., George J. Huffman, Rajat Bindlish, and Thomas J. Jackson. 2009. "Improving

Satellite-Based Rainfall Accumulation Estimates Using Spaceborne Surface Soil Moisture Retrievals." *Journal of Hydrometeorology* 10 (1): 199–212.

Das, Kousik, and Prabir Kumar Paul. 2015. "Present status of soil moisture estimation by microwave remote sensing." *Cogent Geoscience* 1 (1).

Das, Narendra N., Dara Entekhabi, R. Scott Dunbar, Mario J. Chaubell, Andreas Colliander, Simon Yueh, Thomas Jagdhuber, et al. 2019. "The SMAP and Copernicus Sentinel 1A/B microwave active-passive high resolution surface soil moisture product." *Remote Sensing of Environment* 233: 111380.

de Rosnay, P., C. Gruhier, F. Timouk, F. Baup, E. Mougin, P. Hiernaux, L. Kergoat, and V. LeDantec. 2009. "Multi-scale soil moisture measurements at the Gourma meso-scale site in Mali." *Journal of Hydrology* 375 (1-2): 241–252.

Dirmeyer, Paul A. 2011. "A History and Review of the Global Soil Wetness Project (GSWP)." *Journal of Hydrometeorology* 12 (5): 729–749.

Dorigo, W. A., W. Wagner, R. Hohensinn, S. Hahn, C. Paulik, A. Xaver, A. Gruber, et al. 2011. "The International Soil Moisture Network: a data hosting facility for global in situ soil moisture measurements." *Hydrology and Earth System Sciences* 15 (5): 1675–1698.

Dorigo, W.A., A. Xaver, M. Vreugdenhil, A. Gruber, A. Hegyiová, A.D. Sanchis-Dufau, D. Zamojski, C. Cordes, W. Wagner, and M. Drusch. 2013. "Global Automated Quality Control of In Situ Soil Moisture Data from the International Soil Moisture Network." *Vadose Zone Journal* 12 (3).

Dorigo, Wouter, Irene Himmelbauer, Daniel Aberer, Lukas Schremmer, Ivana Petrakovic, Luca Zappa, Wolfgang Preimesberger, et al. 2021. "The International Soil Moisture Network: serving Earth system science for over a decade." *Hydrology and Earth System Sciences* 25 (11): 5749–5804.

Dorigo, Wouter, Wolfgang Wagner, Clement Albergel, Franziska Albrecht, Gianpaolo Balsamo, Luca Brocca, Daniel Chung, et al. 2017. "ESA CCI Soil Moisture for improved Earth system understanding: State-of-the art and future directions." *Remote Sensing of Environment* 203: 185–215.

Ebrahimi, Mohsen, Seyed Kazem Alavipanah, Saeid Hamzeh, Farshad Amiraslani, Najmeh Neysani Samany, and Jean-Pierre Wigneron. 2018. "Exploiting the synergy between SMAP and SMOS to improve brightness temperature simulations and soil moisture retrievals in arid regions." *Journal of Hydrology* 557: 740–752.

Emil, Mustafa Kemal, Mohamed Sultan, Khaled Alakhras, Guzalay Sataer, Sabreen Gozi, Mohammed Al-Marri, and Esayas Gebremichael. 2021. "Countrywide Monitoring of Ground Deformation Using InSAR Time Series: A Case Study from Qatar." *Remote Sensing* 13 (4): 702.

Ezzahar, Jamal, Nadia Ouaadi, Mehrez Zribi, Jamal Elfarkh, Ghizlane Aouade, Said Khabba, Salah Er-Raki, Abdelghani Chehbouni, and Lionel Jarlan. 2019. "Evaluation of Backscattering Models and Support Vector Machine for the Retrieval of Bare Soil Moisture from Sentinel-1 Data." *Remote Sensing* 12 (1): 72.

Galle, S., M. Grippa, C. Peugeot, I. Bouzou Moussa, B. Cappelaere, J. Demarty, E. Mougin, et al. 2018. "AMMA-CATCH, a Critical Zone Observatory in West Africa Monitoring a Region in Transition." *Vadose Zone Journal* 17 (1): 180062.

GCOS. 2016. "The global observing system for climate: implementation needs." *WMO Pub GCOS - 200* .

Green, Julia K., Sonia I. Seneviratne, Alexis M. Berg, Kirsten L. Findell, Stefan Hagemann, David M. Lawrence, and Pierre Gentine. 2019. "Large influence of soil moisture on long-term terrestrial carbon uptake." *Nature* 565 (7740): 476–479.

Gruber, A., G. De Lannoy, C. Albergel, A. Al-Yaari, L. Brocca, J.-C. Calvet, A. Colliander, et al. 2020. "Validation practices for satellite soil moisture retrievals: What are (the) errors?" *Remote Sensing of Environment* 244: 111806.

Gruber, Alexander, Wouter Arnoud Dorigo, Wade Crow, and Wolfgang Wagner. 2017. "Triple Collocation-Based Merging of Satellite Soil Moisture Retrievals." *IEEE Transactions on Geoscience and Remote Sensing* 55 (12): 6780–6792.

Gruber, Alexander, Tracy Scanlon, Robin van der Schalie, Wolfgang Wagner, and Wouter Dorigo. 2019. "Evolution of the ESA CCI Soil Moisture climate data records and their underlying merging methodology." *Earth System Science Data* 11 (2): 717–739.

Guerschman, Juan P., Michael J. Hill, John Leys, and Stephan Heidenreich. 2020. "Vegetation cover dependence on accumulated antecedent precipitation in Australia: Relationships with photosynthetic and non-photosynthetic vegetation fractions." *Remote Sensing of Environment* 240: 111670.

Guswa, Andrew J., M. A. Celia, and I. Rodriguez-Iturbe. 2002. "Models of soil moisture dynamics in ecohydrology: A comparative study." *Water Resources Research* 38 (9): 5–1–5–15.

Hajj, Mohammad El, Nicolas Baghdadi, Mehrez Zribi, and Hassan Bazzi. 2017. "Synergic Use of Sentinel-1 and Sentinel-2 Images for Operational Soil Moisture Mapping at High Spatial Resolution over Agricultural Areas." *Remote Sensing* 9 (12): 1292.

Hao, Yonghong, Qi Liu, Chongwei Li, Gehendra Kharel, Lixing An, Elaine Stebler, Yu Zhong, and Chris B. Zou. 2019. "Interactive Effect of Meteorological Drought and Vegetation Types on Root Zone Soil Moisture and Runoff in Rangeland Watersheds." *Water* 11 (11): 2357.

Hengl, Tomislav, Jorge Mendes de Jesus, Gerard B. M. Heuvelink, Maria Ruiperez Gonzalez, Milan Kilibarda, Aleksandar Blagotić, Wei Shangguan, et al. 2017a. "SoilGrids250m: Global gridded soil information based on machine learning." *PLOS ONE* 12 (2): e0169748.

Hengl, Tomislav, Johan G. B. Leenaars, Keith D. Shepherd, Markus G. Walsh, Gerard B. M. Heuvelink, Tekalign Mamo, Helina Tilahun, et al. 2017b. "Soil nutrient maps of Sub-Saharan Africa: assessment of soil nutrient content at 250 m spatial resolution using machine learning." *Nutrient Cycling in Agroecosystems* 109 (1): 77–102.

Hersbach, Hans, Patricia de Rosnay, Bill Bell, Dinand Schepers, Adrian Simmons, Cornel Soci, Saleh Abdalla, et al. 2018. "Operational global reanalysis: progress, future directions and synergies with NWP." *ERA Report Series* .

Hirschi, M., B. Mueller, W. Dorigo, and S.I. Seneviratne. 2014. "Using remotely sensed soil moisture for land–atmosphere coupling diagnostics: The role of surface vs. root-zone soil moisture variability." *Remote Sensing of Environment* 154: 246–252.

Hirschi, Martin, Sonia I. Seneviratne, Vesselin Alexandrov, Fredrik Boberg, Constanta Boroneant, Ole B. Christensen, Herbert Formayer, Boris Orlowsky, and Petr Stepanek. 2010. "Observational evidence for soil-moisture impact on hot extremes in southeastern Europe." *Nature Geoscience* 4 (1): 17–21.

Hou, Arthur Y., Ramesh K. Kakar, Steven Neeck, Ardeshir A. Azarbarzin, Christian D. Kummerow, Masahiro Kojima, Riko Oki, Kenji Nakamura, and Toshio Iguchi. 2014. "The Global Precipitation Measurement Mission." *Bulletin of the American Meteorological Society* 95 (5): 701–722.

Hsu, Hsin, Min-Hui Lo, Benoit P. Guillod, Diego G. Miralles, and Sanjiv Kumar. 2017. "Relation between precipitation location and antecedent/subsequent soil moisture spatial patterns." *Journal of Geophysical Research: Atmospheres* 122 (12): 6319–6328.

Huffman, George, David T. Bolvin, Dan Braithwaite, Kuolin Hsu, Robert Joyce, Christopher Kidd, Eric J. Nelkin, Soroosh Sorooshian, Jackson Tan, and Pingping Xie. 2020. *Algorithm Theoretical Basis Document (ATBD)Version 06, NASA Global Precipitation Measurement (GPM) Integrated Multi-satellitE Retrievals for GPM (IMERG).* techreport. National Aeronautics and Space Administration.

Huffman, G.J., E.F. Stocker, D.T. Bolvin, E.J. Nelkin, and J. Tan. 2019. "GPM IMERG Final Precipitation L3 Half Hourly 0.1 degree x 0.1 degree V06." Greenbelt, MD, Goddard Earth Sciences Data and Information Services Center (GES DISC). Accessed: 2021-05-14.

Humphrey, Vincent, Alexis Berg, Philippe Ciais, Pierre Gentine, Martin Jung, Markus Reichstein, Sonia I. Seneviratne, and Christian Frankenberg. 2021. "Soil moisture–atmosphere feedback dominates land carbon uptake variability." *Nature* 592 (7852): 65–69.

Javelle, Pierre, Catherine Fouchier, Patrick Arnaud, and Jacques Lavabre. 2010. "Flash flood warning at ungauged locations using radar rainfall and antecedent soil moisture estimations." *Journal of Hydrology* 394 (1-2): 267–274.

Kala, Jatin, Jason P. Evans, and Andy J. Pitman. 2015. "Influence of antecedent soil moisture conditions on the synoptic meteorology of the Black Saturday bushfire event in southeast Australia." *Quarterly Journal of the Royal Meteorological Society* 141 (693): 3118–3129.

Kerr, Yann H., Philippe Waldteufel, Philippe Richaume, Jean Pierre Wigneron, Paolo Ferrazzoli, Ali Mahmoodi, Ahmad Al Bitar, et al. 2012. "The SMOS Soil Moisture Retrieval Algorithm." *IEEE Transactions on Geoscience and Remote Sensing* 50 (5): 1384–1403.

Kerr, Y.H., P. Waldteufel, J.-P. Wigneron, J. Martinuzzi, J. Font, and M. Berger. 2001. "Soil moisture retrieval from space: the Soil Moisture and Ocean Salinity (SMOS) mission." *IEEE Transactions on Geoscience and Remote Sensing* 39 (8): 1729–1735.

Kidd, C., and V. Levizzani. 2011. "Status of satellite precipitation retrievals." *Hydrology and Earth System Sciences* 15 (4): 1109–1116.

Kohler, Max Adam, and Ray K. Linsley. 1951. *Predicting the Runoff from Storm Rainfall.* Washington, DC: U.S. Department of Commerce, Weather Bureau.

Krakauer, N. Y., B. I. Cook, and M. J. Puma. 2010. "Contribution of soil moisture feedback to hydroclimatic variability." *Hydrol. Earth Syst. Sci.* 14: 505–520.

Kucera, Paul A., Elizabeth E. Ebert, F. Joseph Turk, Vincenzo Levizzani, Dalia Kirschbaum, Francisco J. Tapiador, Alexander Loew, and M. Borsche. 2013. "Precipitation from Space: Advancing Earth System Science." *Bulletin of the American Meteorological Society* 94 (3): 365–375.

Lawrence, David M., Rosie A. Fisher, Charles D. Koven, Keith W. Oleson, Sean C. Swenson, Gordon Bonan, Nathan Collier, et al. 2019. "The Community Land Model Version 5: Description of New Features, Benchmarking, and Impact of Forcing Uncertainty." *Journal of Advances in Modeling Earth Systems* 11: 4245–4287.

Lebel, Thierry, Bernard Cappelaere, Sylvie Galle, Niall Hanan, Laurent Kergoat, Samuel Levis, Baxter Vieux, et al. 2009. "AMMA-CATCH studies in the Sahelian region of West-Africa: An overview." *Journal of Hydrology* 375 (1-2): 3–13.

Lei, Fangni, Wade T. Crow, William P. Kustas, Jianzhi Dong, Yun Yang, Kyle R. Knipper, Martha C. Anderson, et al. 2020. "Data assimilation of high-resolution thermal and radar remote sensing retrievals for soil moisture monitoring in a drip-irrigated vineyard." *Remote Sensing of Environment* 239: 111622.

Levizzani, Vincenzo, and Elsa Cattani. 2019. "Satellite Remote Sensing of Precipitation and the Terrestrial Water Cycle in a Changing Climate." *Remote Sensing* 11 (19): 2301.

Long, Di, Liangliang Bai, La Yan, Caijin Zhang, Wenting Yang, Huimin Lei, Jinling Quan, Xianyong Meng, and Chunxiang Shi. 2019. "Generation of spatially complete and daily continuous surface soil moisture of high spatial resolution." *Remote Sensing of Environment* 233: 111364.

Manning, Colin, Martin Widmann, Emanuele Bevacqua, Anne F. Van Loon, Douglas Maraun, and Mathieu Vrac. 2018. "Soil Moisture Drought in Europe: A Compound Event of Precipitation and Potential Evapotranspiration on Multiple Time Scales." *Journal of Hydrometeorology* 19 (8): 1255–1271.

Miralles, D. G., M. J. van den Berg, A. J. Teuling, and R. A. M. de Jeu. 2012. "Soil moisture-temperature coupling: A multiscale observational analysis." *Geophysical Research Letters* 39 (21): n/a–n/a.

Moghaddam, M., A. Silva, D. Clewley, R. Akbar, S.A. Hussaini, J. Whitcomb, R. Devarakonda, et al. 2016. "Soil Moisture Profiles and Temperature Data from SoilSCAPE Sites, USA." http://daac.ornl.gov/cgi-bin/dsviewer.pl?ds_id=1339.

Moghaddam, Mahta, Dara Entekhabi, Yuriy Goykhman, Ke Li, Mingyan Liu, Aditya Mahajan, Ashutosh Nayyar, David Shuman, and Demosthenis Teneketzis. 2010. "A Wireless Soil Moisture Smart Sensor Web Using Physics-Based Optimal Control: Concept and Initial Demonstrations." *IEEE Journal of Selected Topics in Applied Earth Observations and Remote Sensing* 3 (4): 522–535.

Mohanty, Binayak P., Michael H. Cosh, Venkat Lakshmi, and Carsten Montzka. 2017. "Soil Moisture Remote Sensing: State-of-the-Science." *Vadose Zone Journal* 16 (1): 0.

Mougin, E., P. Hiernaux, L. Kergoat, M. Grippa, P. de Rosnay, F. Timouk, V. Le Dantec, et al.

2009. "The AMMA-CATCH Gourma observatory site in Mali: Relating climatic variations to changes in vegetation, surface hydrology, fluxes and natural resources." *Journal of Hydrology* 375 (1-2): 14–33.

Nguyen, Hoang Hai, Seongkeun Cho, and Minha Choi. 2022. "Spatial soil moisture estimation in agro-pastoral transitional zone based on synergistic use of SAR and optical-thermal satellite images." *Agricultural and Forest Meteorology* 312: 108719.

Njoku, Eni G., and Dara Entekhabi. 1996. "Passive microwave remote sensing of soil moisture." *Journal of Hydrology* .

Noilhan, J., and J.-F. Mahfouf. 1996. "The ISBA land surface parameterisation scheme." *Global and Planetary Change* 13 (1-4): 145–159.

Ochsner, Tyson E., Michael H. Cosh, Richard H. Cuenca, Wouter A. Dorigo, Clara S. Draper, Yutaka Hagimoto, Yann H. Kerr, et al. 2013. "State of the Art in Large-Scale Soil Moisture Monitoring." *Soil Science Society of America Journal* 77 (6): 1888–1919.

Ojha, Nitu, Olivier Merlin, Beatriz Molero, Christophe Suere, Luis Olivera-Guerra, Bouchra Ait Hssaine, Abdelhakim Amazirh, Ahmad Al Bitar, Maria Escorihuela, and Salah Er-Raki. 2019. "Stepwise Disaggregation of SMAP Soil Moisture at 100 m Resolution Using Landsat-7/8 Data and a Varying Intermediate Resolution." *Remote Sensing* 11 (16): 1863.

Or, D., and P. Lehmann. 2019. "Surface Evaporative Capacitance: How Soil Type and Rainfall Characteristics Affect Global-Scale Surface Evaporation." *Water Resources Research* 55 (1): 519–539.

Osenga, E. C., James C. Arnott, K. Arthur Endsley, and J. W. Katzenberger. 2019. "Bioclimatic and Soil Moisture Monitoring Across Elevation in a Mountain Watershed: Opportunities for Research and Resource Management." *Water Resources Research* 55 (3): 2493–2503.

Osenga, Elise C., Julie A. Vano, and James C. Arnott. 2021. "A community-supported weather and soil moisture monitoring database of the Roaring Fork catchment of the Colorado River Headwaters." *Hydrological Processes* 35 (3).

Pellarin, T., J.P. Laurent, B. Cappelaere, B. Decharme, L. Descroix, and D. Ramier. 2009. "Hydrological modelling and associated microwave emission of a semi-arid region in Southwestern Niger." *Journal of Hydrology* 375 (1-2): 262–272.

Pellarin, Thierry, Samuel Louvet, Claire Gruhier, Guillaume Quantin, and Cedric Legout. 2013. "A simple and effective method for correcting soil moisture and precipitation estimates using AMSR-E measurements." *Remote Sensing of Environment* 136: 28–36.

Peng, Jian, Clement Albergel, Anna Balenzano, Luca Brocca, Oliver Cartus, Michael H. Cosh, Wade T. Crow, et al. 2021. "A roadmap for high-resolution satellite soil moisture applications – confronting product characteristics with user requirements." *Remote Sensing of Environment* 252: 112162.

Peng, Jian, Simon Dadson, Feyera Hirpa, Ellen Dyer, Thomas Lees, Diego G. Miralles, Sergio M. Vicente-Serrano, and Chris Funk. 2020. "A pan-African high-resolution drought index dataset." *Earth System Science Data* 12 (1): 753–769.

Petropoulos, George P., Gareth Ireland, and Brian Barrett. 2015. "Surface soil moisture retrievals from remote sensing: Current status, products & future trends." *Physics and Chemistry of the Earth, Parts A/B/C* 83-84: 36–56.

Piles, María, Adriano Camps, Mercè Vall-llossera, Ignasi Corbella, Rocco Panciera, Christoph Rudiger, Yann H. Kerr, and Jeffrey Walker. 2011. "Downscaling SMOS-Derived Soil Moisture Using MODIS Visible/Infrared Data." *IEEE Transactions on Geoscience and Remote Sensing* 49 (9): 3156–3166.

Piles, María, George P. Petropoulos, Nilda Sánchez, Ángel González-Zamora, and Gareth Ireland. 2016. "Towards improved spatio-temporal resolution soil moisture retrievals from the synergy of SMOS and MSG SEVIRI spaceborne observations." *Remote Sensing of Environment* 180: 403–417.

Poggio, Laura, Luis M. de Sousa, Niels H. Batjes, Gerard B. M. Heuvelink, Bas Kempen, Eloi Ribeiro, and David Rossiter. 2021. "SoilGrids 2.0: producing soil information for the globe with quantified spatial uncertainty." *SOIL* 7 (1): 217–240.

Powell, M. J. D. 1964. "An efficient method for finding the minimum of a function of several

variables without calculating derivatives." *The Computer Journal* 7 (2): 155–162.
Preimesberger, Wolfgang, Tracy Scanlon, Chun-Hsu Su, Alexander Gruber, and Wouter Dorigo. 2021. "Homogenization of Structural Breaks in the Global ESA CCI Soil Moisture Multisatellite Climate Data Record." *IEEE Transactions on Geoscience and Remote Sensing* 59 (4): 2845–2862.
Ramsauer, Thomas. 2022a. "GPM_API - Global Hourly Soil Moisture from GPM IMERG Data." https://doi.org/10.5281/zenodo.6489998.
Ramsauer, Thomas. 2022b. "Supplemental Material for 'Global Soil Moisture Estimation based on GPM IMERG Data using a Site Specific Adjusted Antecedent Precipitation Index'." https://doi.org/10.5281/zenodo.6563944.
Ramsauer, Thomas, Thomas Weiß, Alexander Löw, and Philip Marzahn. 2021. "RADOLAN_API: An Hourly Soil Moisture Data Set Based on Weather Radar, Soil Properties and Reanalysis Temperature Data." *Remote Sensing* 13 (9): 1712.
Reichle, Rolf H., Randal D. Koster, Gabriëlle J. M. De Lannoy, Barton A. Forman, Qing Liu, Sarith P. P. Mahanama, and Ally Touré. 2011. "Assessment and Enhancement of MERRA Land Surface Hydrology Estimates." *Journal of Climate* 24 (24): 6322–6338.
Robinson, D. A., C. S. Campbell, J. W. Hopmans, B. K. Hornbuckle, S. B. Jones, R. Knight, F. Ogden, J. Selker, and O. Wendroth. 2008. "Soil Moisture Measurement for Ecological and Hydrological Watershed-Scale Observatories: A Review." *Vadose Zone Journal* 7 (1): 358–389.
Robock, Alan, Konstantin Y. Vinnikov, Govindarajalu Srinivasan, Jared K. Entin, Steven E. Hollinger, Nina A. Speranskaya, Suxia Liu, and A. Namkhai. 2000. "The Global Soil Moisture Data Bank." *Bulletin of the American Meteorological Society* 81 (6): 1281–1299.
Ross, C. Wade, Lara Prihodko, Julius Anchang, Sanath Kumar, Wenjie Ji, and Niall P. Hanan. 2018. "HYSOGs250m, global gridded hydrologic soil groups for curve-number-based runoff modeling." *Scientific Data* 5 (1).
Sadeghi, Morteza, Ebrahim Babaeian, Markus Tuller, and Scott B. Jones. 2017. "The optical trapezoid model: A novel approach to remote sensing of soil moisture applied to Sentinel-2 and Landsat-8 observations." *Remote Sensing of Environment* 198: 52–68.
Sadeghi, Morteza, Scott B. Jones, and William D. Philpot. 2015. "A linear physically-based model for remote sensing of soil moisture using short wave infrared bands." *Remote Sensing of Environment* 164: 66–76.
Sadri, Sara, Eric F. Wood, and Ming Pan. 2018. "Developing a drought-monitoring index for the contiguous US using SMAP." *Hydrology and Earth System Sciences* 22 (12): 6611–6626.
Santi, E., S. Paloscia, S. Pettinato, L. Brocca, L. Ciabatta, and D. Entekhabi. 2018. "Integration of microwave data from SMAP and AMSR2 for soil moisture monitoring in Italy." *Remote Sensing of Environment* 212: 21–30.
Santi, Emanuele, Mohammed Dabboor, Simone Pettinato, and Simonetta Paloscia. 2019. "Combining Machine Learning and Compact Polarimetry for Estimating Soil Moisture from C-Band SAR Data." *Remote Sensing* 11 (20): 2451.
Schamm, K., M. Ziese, A. Becker, P. Finger, A. Meyer-Christoffer, U. Schneider, M. Schröder, and P. Stender. 2014. "Global gridded precipitation over land: a description of the new GPCC First Guess Daily product." *Earth System Science Data* 6 (1): 49–60.
Schoener, Gerhard, and Mark C. Stone. 2019. "Impact of antecedent soil moisture on runoff from a semiarid catchment." *Journal of Hydrology* 569: 627–636.
Schoener, Gerhard, and Mark C. Stone. 2020. "Monitoring soil moisture at the catchment scale – A novel approach combining antecedent precipitation index and radar-derived rainfall data." *Journal of Hydrology* 589: 125155.
Seneviratne, Sonia I., Thierry Corti, Edouard L. Davin, Martin Hirschi, Eric B. Jaeger, Irene Lehner, Boris Orlowsky, and Adriaan J. Teuling. 2010. "Investigating soil moisture–climate interactions in a changing climate: A review." *Earth-Science Reviews* 99 (3-4): 125–161.
Seneviratne, Sonia I., Neville Nicholls, David Easterling, Clare M. Goodess, Shinjiro Kanae, James Kossin, Yali Luo, et al. 2012. "Changes in Climate Extremes and their Impacts on the Natural Physical Environment." In *Managing the Risks of Extreme Events and Disasters*

to Advance Climate Change Adaptation, edited by Christopher B. Field, Vicente Barros, Thomas F. Stocker, Qin Dahe, D.J. Dokken, K.L. Ebi, M.D. Mastrandrea, K.J. Mach, G.-K. Plattner, S.K. Allen, M. Tignor, and P.M. Midgley, Special Report of Working Groups I and II of the Intergovernmental Panel on Climate Change (IPCC), 109–230. Cambridge, UK, and New York, NY, USA: Cambridge University Press.

Shuman, David I, Ashutosh Nayyar, Aditya Mahajan, Yuriy Goykhman, Ke Li, Mingyan Liu, Demosthenis Teneketzis, Mahta Moghaddam, and Dara Entekhabi. 2010. "Measurement Scheduling for Soil Moisture Sensing: From Physical Models to Optimal Control." *Proceedings of the IEEE* 98 (11): 1918–1933.

Skofronick-Jackson, Gail, Walter A. Petersen, Wesley Berg, Chris Kidd, Erich F. Stocker, Dalia B. Kirschbaum, Ramesh Kakar, et al. 2017. "The Global Precipitation Measurement (GPM) Mission for Science and Society." *Bulletin of the American Meteorological Society* 98 (8): 1679–1695.

Small, Eric, Andrew Badger, Ronnie Abolafia-Rosenzweig, and Ben Livneh. 2018. "Estimating Soil Evaporation Using Drying Rates Determined from Satellite-Based Soil Moisture Records." *Remote Sensing* 10 (12): 1945.

Souza, Alzira Gabrielle Soares Saraiva, Alfredo Ribeiro Neto, and Laio Lucas de Souza. 2021. "Soil moisture-based index for agricultural drought assessment: SMADI application in Pernambuco State-Brazil." *Remote Sensing of Environment* 252: 112124.

Tavakol, Ameneh, Kelsey R. McDonough, Vahid Rahmani, Stacy L. Hutchinson, and J.M. Shawn Hutchinson. 2021. "The soil moisture data bank: The ground-based, model-based, and satellite-based soil moisture data." *Remote Sensing Applications: Society and Environment* 24: 100649.

Teng, W., J. Wang, and P Doraiswamy. 1993. "Relationship between satellite microwave radiometric data, antecedent precipitation index, and regional soil moisture." *International Journal of Remote Sensing* 14 (13): 2483–2500.

Toride, Sawada, Aida, and Koike. 2019. "Toward High-Resolution Soil Moisture Monitoring by Combining Active-Passive Microwave and Optical Vegetation Remote Sensing Products with Land Surface Model." *Sensors* 19 (18): 3924.

Tóth, Brigitta, Melanie Weynants, László Pásztor, and Tomislav Hengl. 2017. "3D soil hydraulic database of Europe at 250 m resolution." *Hydrological Processes* 31 (14): 2662–2666.

Tramblay, Y., R. Bouaicha, L. Brocca, W. Dorigo, C. Bouvier, S. Camici, and E. Servat. 2012. "Estimation of antecedent wetness conditions for flood modelling in northern Morocco." *Hydrology and Earth System Sciences* 16 (11): 4375–4386.

van Hateren, Theresa C., Marco Chini, Patrick Matgen, and Adriaan J. Teuling. 2021. "Ambiguous Agricultural Drought: Characterising Soil Moisture and Vegetation Droughts in Europe from Earth Observation." *Remote Sensing* 13 (10): 1990.

Vereecken, Harry, Lutz Weihermüller, Shmuel Assouline, Jirka Šimůnek, Anne Verhoef, Michael Herbst, Nicole Archer, et al. 2019. "Infiltration from the Pedon to Global Grid Scales: An Overview and Outlook for Land Surface Modeling." *Vadose Zone Journal* 18 (1): 1–53.

Vergopolan, Noemi, Nathaniel W. Chaney, Hylke E. Beck, Ming Pan, Justin Sheffield, Steven Chan, and Eric F. Wood. 2020. "Combining hyper-resolution land surface modeling with SMAP brightness temperatures to obtain 30-m soil moisture estimates." *Remote Sensing of Environment* 242: 111740.

Wagner, Wolfgang. 2003. "Evaluation of the agreement between the first global remotely sensed soil moisture data with model and precipitation data." *Journal of Geophysical Research* 108 (D19).

Wagner, Wolfgang, Sebastian Hahn, Richard Kidd, Thomas Melzer, Zoltan Bartalis, Stefan Hasenauer, Julia Figa-Saldaña, et al. 2013. "The ASCAT Soil Moisture Product: A Review of its Specifications, Validation Results, and Emerging Applications." *Meteorologische Zeitschrift* 22 (1): 5–33.

Wigneron, J.-P., T.J. Jackson, P. O'Neill, G. De Lannoy, P. de Rosnay, J.P. Walker, P. Ferrazzoli, et al. 2017. "Modelling the passive microwave signature from land surfaces: A review

of recent results and application to the L-band SMOS SMAP soil moisture retrieval algorithms." *Remote Sensing of Environment* 192: 238–262.

Wigneron, Jean-Pierre, Sylvia Dayan, Alain Kruszewski, Christelle Aluome, Marie Guillot-Ehret Amen AI-Yaari, Lei Fan, Serhat Guven, et al. 2018. "The Aqui Network: Soil Moisture Sites in the "Les Landes" Forest and Graves Vineyards (Bordeaux Aquitaine Region, France)." .

Wigneron, Jean-Pierre, Thomas Schmugge, Andre Chanzy, Jean-Claude Calvet, and Yann H. Kerr. 1998. "Use of passive microwave remote sensing to monitor soil moisture." *Agronomie* 18 (1): 27–43. https://hal.archives-ouvertes.fr/hal-00885868.

Wilke, Gregory D., and Marshall J. McFarland. 1986. "Correlations between Nimbus-7 Scanning Multichannel Microwave Radiometer Data and an Antecedent Precipitation Index." *Journal of Climate and Applied Meteorology* 25: 227–238.

Wu, Xiaotao, Guihua Lu, Zhiyong Wu, Hai He, Jianhong Zhou, and Zhenchen Liu. 2018. "An Integration Approach for Mapping Field Capacity of China Based on Multi-Source Soil Datasets." *Water* 10 (6): 728.

Zacharias, Steffen, Heye Bogena, Luis Samaniego, Matthias Mauder, Roland Fuß, Thomas Pütz, Mark Frenzel, et al. 2011. "A Network of Terrestrial Environmental Observatories in Germany." *Vadose Zone Journal* 10 (3): 955–973.

Zeman, Christian, Nils P. Wedi, Peter D. Dueben, Nikolina Ban, and Christoph Schär. 2021. "Model intercomparison of COSMO 5.0 and IFS 45r1 at kilometer-scale grid spacing." *Geoscientific Model Development* 14 (7): 4617–4639.

Zeng, Linglin, Shun Hu, Daxiang Xiang, Xiang Zhang, Deren Li, Lin Li, and Tingqiang Zhang. 2019. "Multilayer Soil Moisture Mapping at a Regional Scale from Multisource Data via a Machine Learning Method." *Remote Sensing* 11 (3): 284.

Zhang, Lijie, Yijian Zeng, Ruodan Zhuang, Brigitta Szabó, Salvatore Manfreda, Qianqian Han, and Zhongbo Su. 2021. "In Situ Observation-Constrained Global Surface Soil Moisture Using Random Forest Model." *Remote Sensing* 13 (23): 4893.

Zhao, Binru, Qiang Dai, Dawei Han, Huichao Dai, Jingqiao Mao, and Lu Zhuo. 2019a. "Probabilistic thresholds for landslides warning by integrating soil moisture conditions with rainfall thresholds." *Journal of Hydrology* 574: 276–287.

Zhao, Binru, Qiang Dai, Dawei Han, Huichao Dai, Jingqiao Mao, Lu Zhuo, and Guiwen Rong. 2019b. "Estimation of soil moisture using modified antecedent precipitation index with application in landslide predictions." *Landslides* 16 (12): 2381–2393.

Zhao, Y., F. Wei, H. Yang, and Y. Jiang. 2011. "Discussion on Using Antecedent Precipitation Index to Supplement Relative Soil Moisture Data Series." *Procedia Environmental Sciences* 10: 1489–1495.

Zhu, Qian, Yulin Luo, Yue-Ping Xu, Ye Tian, and Tiantian Yang. 2019a. "Satellite Soil Moisture for Agricultural Drought Monitoring: Assessment of SMAP-Derived Soil Water Deficit Index in Xiang River Basin, China." *Remote Sensing* 11 (3): 362.

Zhu, Qian, Yulin Luo, Dongyang Zhou, Yue-Ping Xu, Guoqing Wang, and Haiying Gao. 2019b. "Drought Monitoring Utility using Satellite-Based Precipitation Products over the Xiang River Basin in China." *Remote Sensing* 11 (12): 1483.

3 Discussion

The three studies at the core of this thesis demonstrate and compare the monitoring qualities of two precipitation estimates (article I), that are subsequently - in investigation II and III - applied to retrieve a high temporal resolution SM data set respectively, covering different domains and scales from regional to global. The focus on high temporal resolution unites both data sets, RADOLAN_API and GPM_API. The following paragraphs collectively summarize and discuss the key findings of the three presented publications along the research questions posed in Chapter 1.5.

RQ1.1: Does the GPM IMERG satellite-based precipitation data set show similar performance of detection of precipiation as the RADOLAN weather radar data?
The data sets were analyzed with a categorical statistics, that allowed for differences in detection accuracy to become apparent. Highest disagreement between the data sets is revealed for the winter season, with GPM showing low probability of detection of precipitation events in comparison with RADOLAN. These findings are in line with reports in literature, indicating difficulties of GPM to detect solid precipitation. Conversely, the sum of winter precipitation recorded by GPM is positively biased in comparison to the weather radar. Undercatch due to wind effects in the RADOLAN-incorporated gauge measurements might be the reason. Soil moisture state in winter is often close to saturation in Germany, which could allow for the conclusion to be drawn, that the observed differences in QPE would be less critical for a SM modeling task, than in the summer season.

RQ1.2: Do GPM and RADOLAN show the same spatial and seasonal trends in precipitation patterns?
Due to different spatial resolutions of the data sets in review, a fair comparison is difficult. However, it must nonetheless be noted, that, expectedly, the spatial variability of precipitation is better captured with the weather radar. Special focus must furthermore be placed on GPM's difficulties in binary detection of events and also quantitative difference in the estimates in the alpine region of the study area. As noted at RQ1.1, the estimations of winter precipitation were revealing big discrepancies. Due to increased uncertainty of in situ measurements, a decision for better or worse performance of the weather radar or satellite based data set is difficult.

RQ2.1: Can the empirical soil moisture index (RADOLAN_API) based off the antecedent precipitation index resemble the course of local soil moisture measurements throughout Germany?
A very good distinction between the different validation sites could be achieved, accounting mostly for the different soil characteristics. Seasonal variations are captured well, and dry spells are clearly discernible in the data set.

RQ2.2: Are rapid upsurges in soil moisture and seasonal variations captured in the data set?
Utilizing the weather radar data set inherently sets up the modeling for the upsurges to be captured well. The hourly resolution of the precipitation input data set therefore is highly beneficial. Furthermore, the applied RADOLAN RW data set integrates measurements of a five minute sampling rate, which in addition ensures, that respective precipitation events are recorded.

RQ2.3: Does the RADOLAN_API perform equally well as the renowned ESA CCI SM data set and adhere to GCOS defined error margins?
The RADOLAN_API data set was calculated with locally and globally optimized empirical parameters. In both cases at the vast majority of validation sites, the weather radar based SM data set outperformed ESA CCI SM concerning correlation and error metrics. The coarser original resolution of ESA CCI SM data in comparison to RADOLAN_API must be stated here. Despite ESA CCI SM algorithm's objective is to provide a spatially distributed, harmonized climate data record for soil moisture (Gruber et al. 2019), the comprised SM estimates must still be valid on point.

RQ3.1 Is a quality SSM product deducible from GPM data that adheres to the accuracy requirements for soil moisture products provided by the GCOS?
The quality requirements for operationally generated soil moisture data sets defined by GCOS is the error to be no greater than 4 $Vol\%$ (GCOS 2016). Across the validation sites, GPM_API did not reach this threshold with an unbiased $RMSE$ of 4.68 $Vol\%$. However, at the majority of validation stations the accordance is higher than with ESA CCI SM data set.

RQ3.2 Can GPM_API represent different soil moisture regimes on a global scale?
The addition of spatially adjusted loss coefficients allows for very appropriate soil moisture curse modeling throughout different soil moisture regimes. Further adjustments, concerning the boundary conditions of the enhanced antecedent precipitation index, moreover allow for

example to match the course of soil water in highly seasonal characterized regions of West Africa.

RQ3.3 Does the quality of GPM_API vary across regions and top soil compositions?
GPM_API did perform best in sandy regions of West Africa. However, drawing the conclusion, that soil composition is the main driver therefor, might also be misguided. Low soil moisture variability in dry season facilitates modeling, potentially resulting in overall smaller errors.

RQ3.4 How does the GPM_API data set compare with ESA CCI soil moisture data set?
As discussed for RQ3.1, the GPM_API does outperform ESA CCI SM data at most validation stations. Similar remark as to RQ2.3 must be added, that although the objective of ESA CCI SM might be a different one, still the pixel value must be applicable on point scale.

The RADOLAN_API and GPM_API, albeit on different scales, excel when timely information on soil moisture state change is needed and require little knowledge on the detailed physical properties of the soil column besides soil particle size distribution, i.e. sand and clay content, for the top soil layer. A shortcoming of the products is their reliance on natural moisture input only - false guidance is to be expected in irrigated areas. However, the detection and assessment of irrigation water use might be a future case of application. In the field of agricultural investigations, the importance of RZSM has been highlighted in Section 1.2 and 1.4, whereas the produced data sets solely provide SSM. Qiu et al. (2014) note, that for many instances SSM and RZSM are well correlated, meaning that focusing exclusively on SSM does not imperatively, significantly compromise information content.

Machine learning practices are on the rise in soil moisture modeling (Xia et al. 2022; Ezzahar et al. 2019; Zhang et al. 2021b; Qu et al. 2019; Kolassa et al. 2018). These are data driven technologies, that, according to Kasim et al. (2025), suffer from issues with respect to transferability and interpretability, and should not be recognized as estimation methods.

For the usage in a data fusion through e.g. a data assimilation scheme, uncertainty of a variable is an essential criteria. As a physical error propagation is hardly practicable, providing information on uncertainty was not part of the modeling, but can be integrated in such case through e.g. running window analysis of variability for example.

4 Conclusion

4.1 Summary and Outlook

Soil moisture is a connecting element in the Earth's water and energy cycles. Different ways lead to a robust and sensible monitoring scheme of this critical component. For spatial information on SM gridded data sets provide the most meaningful resource. Modeling the variable or monitoring via satellite acquisitions are both appropriate and promising approaches. This thesis discusses the very timely provision of soil moisture data derived from gridded precipitation data sets to fill the gap of a very high temporal resolution soil moisture data set. This characteristic is beneficial to either i) directly provide physically sound SM data that is at least comparable with existing satellite monitoring products or ii) for the utilization of the data set by specific exploitation of the high temporal resolution in a data fusion approach. Future satellites like the upcoming SAR missions NISAR (NASA ISRO Synthetic Aperture Radar), and ROSE-L (Radar Observing System for Europe at L-band) represent candidates therefor. These operate at longer wavelengths, suffer less from vegetation disturbance, and hence will show superior soil moisture monitoring capabilities. A timely auxiliary soil moisture data set like GPM_API or RADOLAN_API can make a valuable contribution in the future retrieval algorithms.

4.2 Scientific Outreach

Finally, the effort to make not only the publications available to the public but also to publish the produced data sets and supporting software packages online, is highlighted here. This is to foster continued usage and exploitation of the produced data sets and also to allow for further development of these. The following repositories contain the respective files:

- RADOLAN_API Data:
  Ramsauer, T., Weiß, T. & Marzahn, P. (2021). RADOLAN_API - A Soil Moisture Data Set derived from Weather Radar Data, *Zenodo*. DOI: 10.5281/zenodo.4588904

- GPM_API Data:
  Ramsauer, T. (2022). GPM_API - Global Hourly Soil Moisture from GPM IMERG Data, *Zenodo*. DOI: 10.5281/zenodo.6489998

- *raddo* Code:
  Ramsauer, T. (2021). raddo - A Python Package for RADOLAN Weather Radar Data Provision. *Zenodo*. https://doi.org/10.5281/zenodo.5642649

References

Abolafia-Rosenzweig, R., Livneh, B., Small, E., and Kumar, S. (2019). Soil moisture data assimilation to estimate irrigation water use. *Journal of Advances in Modeling Earth Systems*, 11(11):3670–3690.

Adler, R. F., Huffman, G. J., Chang, A., Ferraro, R., Xie, P.-P., Janowiak, J., Rudolf, B., Schneider, U., Curtis, S., Bolvin, D., Gruber, A., Susskind, J., Arkin, P., and Nelkin, E. (2003). The version-2 global precipitation climatology project (gpcp) monthly precipitation analysis (1979–present). *Journal of Hydrometeorology*, 4:1147–1167.

Ajaz, A., Taghvaeian, S., Khand, K., Gowda, P. H., and Moorhead, J. E. (2019). Development and evaluation of an agricultural drought index by harnessing soil moisture and weather data. *Water*, 11(7):1375.

Alvarez-Garreton, C., Ryu, D., Western, A. W., Crow, W. T., Su, C.-H., and Robertson, D. R. (2016). Dual assimilation of satellite soil moisture to improve streamflow prediction in data-scarce catchments. *Water Resources Research*, 52(7):5357–5375.

Ashouri, H., Hsu, K.-L., Sorooshian, S., Braithwaite, D. K., Knapp, K. R., Cecil, L. D., Nelson, B. R., and Prat, O. P. (2015). PERSIANN-CDR: Daily precipitation climate data record from multisatellite observations for hydrological and climate studies. *Bulletin of the American Meteorological Society*, 96(1):69–83.

Babaeian, E., Sadeghi, M., Franz, T. E., Jones, S., and Tuller, M. (2018). Mapping soil moisture with the OPtical TRApezoid model (OPTRAM) based on long-term MODIS observations. *Remote Sensing of Environment*, 211:425–440.

Babaeian, E., Sadeghi, M., Jones, S. B., Montzka, C., Vereecken, H., and Tuller, M. (2019). Ground, proximal, and satellite remote sensing of soil moisture. *Reviews of Geophysics*, 57(2):530–616.

Balsamo, G., Agusti-Panareda, A., Albergel, C., Arduini, G., Beljaars, A., Bidlot, J., Blyth, E., Bousserez, N., Boussetta, S., Brown, A., Buizza, R., Buontempo, C., Chevallier, F., Choulga, M., Cloke, H., Cronin, M. F., Dahoui, M., Rosnay, P. D., Dirmeyer, P. A., Drusch, M., Dutra,

E., Ek, M. B., Gentine, P., Hewitt, H., Keeley, S. P., Kerr, Y., Kumar, S., Lupu, C., Mahfouf, J.-F., McNorton, J., Mecklenburg, S., Mogensen, K., Muñoz-Sabater, J., Orth, R., Rabier, F., Reichle, R., Ruston, B., Pappenberger, F., Sandu, I., Seneviratne, S. I., Tietsche, S., Trigo, I. F., Uijlenhoet, R., Wedi, N., Woolway, R. I., and Zeng, X. (2018). Satellite and in situ observations for advancing global earth surface modelling: A review. *Remote Sensing*, 10(12):2038.

Bartalis, Z., Wagner, W., Naeimi, V., Hasenauer, S., Scipal, K., Bonekamp, H., Figa, J., and Anderson, C. (2007). Initial soil moisture retrievals from the METOP-a advanced scatterometer (ASCAT). *Geophysical Research Letters*, 34(20).

Beck, H. E., van Dijk, A. I. J. M., Levizzani, V., Schellekens, J., Miralles, D. G., Martens, B., and de Roo, A. (2017). MSWEP: 3-hourly 0.25° global gridded precipitation (1979–2015) by merging gauge, satellite, and reanalysis data. *Hydrology and Earth System Sciences*, 21(1):589–615.

Becker, A., Finger, P., Meyer-Christoffer, A., Rudolf, B., Schamm, K., Schneider, U., and Ziese, M. (2013). A description of the global land-surface precipitation data products of the global precipitation climatology centre with sample applications including centennial (trend) analysis from 1901–present. *Earth System Science Data*, 5(1):71–99.

Berg, A. and Sheffield, J. (2018). Climate change and drought: the soil moisture perspective. *Current Climate Change Reports*, 4(2):180–191.

Blöschl, G. and Sivapalan, M. (1995). Scale issues in hydrological modelling: A review. *Hydrological Processes*, 9(3–4):251–290.

Bolten, J. D., Crow, W. T., Zhan, X., Jackson, T. J., and Reynolds, C. A. (2010). Evaluating the utility of remotely sensed soil moisture retrievals for operational agricultural drought monitoring. *IEEE Journal of Selected Topics in Applied Earth Observations and Remote Sensing*, 3(1):57–66.

Bronstert, A., Agarwal, A., Boessenkool, B., Crisologo, I., Fischer, M., Heistermann, M., Köhn-Reich, L., López-Tarazón, J. A., Moran, T., Ozturk, U., Reinhardt-Imjela, C., and Wendi, D. (2018). Forensic hydro-meteorological analysis of an extreme flash flood: The 2016-05-29 event in braunsbach, SW germany. *Science of The Total Environment*, 630:977–991.

Busschaert, L., de Roos, S., Thiery, W., Raes, D., and De Lannoy, G. J. M. (2022). Net irrigation requirement under different climate scenarios using aquacrop over europe. *Hydrology and Earth System Sciences*, 26(14):3731–3752.

Böhnisch, A., Felsche, E., Mittermeier, M., Poschlod, B., and Ludwig, R. (2025). Future patterns of compound dry and hot summers and their link to soil moisture droughts in europe. *Earth's Future*, 13(2).

Cambardella, C. A., Moorman, T. B., Novak, J. M., Parkin, T. B., Karlen, D. L., Turco, R. F., and Konopka, A. E. (1994). Field-scale variability of soil properties in central iowa soils. *Soil Science Society of America Journal*, 58(5):1501–1511.

Carrão, H., Russo, S., Sepulcre-Canto, G., and Barbosa, P. (2016). An empirical standardized soil moisture index for agricultural drought assessment from remotely sensed data. *International Journal of Applied Earth Observation and Geoinformation*, 48:74–84.

Chifflard, P., Kranl, J., zur Strassen, G., and Zepp, H. (2017). The significance of soil moisture in forecasting characteristics of flood events. a statistical analysis in two nested catchments. *Journal of Hydrology and Hydromechanics*, 66(1):1–11.

Corson-Dosch, H., Nell, C., Volentine, R., Archer, A., Bechtel, E., Bruce, J., Felts, N., Gross, T. A., Lopez-Trujillo, D., Riggs, C. E., and Read, E. K. (2022). The water cycle. https://www.usgs.gov/media/images/water-cycle-png. [Online; accessed May 22, 2025].

Cosby, B., Hornberger, G. M., Clapp, R. B., and Ginn, T. R. (1984). A statistical exploration of the relationships of soil moisture characteristics to the physical properties of soils. *Water Resources Research*, 20:682–690.

Crow, W. T. and van den Berg, M. J. (2010). An improved approach for estimating observation and model error parameters in soil moisture data assimilation. *Water Resources Research*, 46(12).

Dai, A., Zhao, T., and Chen, J. (2018). Climate change and drought: a precipitation and evaporation perspective. *Current Climate Change Reports*, 4(3):301–312.

Das, K. and Paul, P. K. (2015). Present status of soil moisture estimation by microwave remote sensing. *Cogent Geoscience*, 1(1).

de Jeu, R. A. M., Wagner, W., Holmes, T. R. H., Dolman, A. J., van de Giesen, N. C., and Friesen, J. (2008). Global soil moisture patterns observed by space borne microwave radiometers and scatterometers. *Surveys in Geophysics*, 29(4-5):399–420.

de Rosnay, P., Polcher, J., Bruen, M., and Laval, K. (2002). Impact of a physically based soil water flow and soil-plant interaction representation for modeling large-scale land surface processes. *Journal of Geophysical Research: Atmospheres*, 107(D11).

Decharme, B., Boone, A., Delire, C., and Noilhan, J. (2011). Local evaluation of the interaction between soil biosphere atmosphere soil multilayer diffusion scheme using four pedotransfer functions. *Journal of Geophysical Research*, 116(D20).

Dorigo, W., Gruber, A., Jeu, R. D., Wagner, W., Stacke, T., Loew, A., Albergel, C., Brocca, L., Chung, D., Parinussa, R., and Kidd, R. (2015). Evaluation of the ESA CCI soil moisture product using ground-based observations. *Remote Sensing of Environment*, 162:380–395.

Dorigo, W., Himmelbauer, I., Aberer, D., Schremmer, L., Petrakovic, I., Zappa, L., Preimesberger, W., Xaver, A., Annor, F., Ardö, J., Baldocchi, D., Bitelli, M., Blöschl, G., Bogena, H., Brocca, L., Calvet, J.-C., Camarero, J. J., Capello, G., Choi, M., Cosh, M. C., van de Giesen, N., Hajdu, I., Ikonen, J., Jensen, K. H., Kanniah, K. D., de Kat, I., Kirchengast, G., Rai, P. K., Kyrouac, J., Larson, K., Liu, S., Loew, A., Moghaddam, M., Fernández, J. M., Bader, C. M., Morbidelli, R., Musial, J. P., Osenga, E., Palecki, M. A., Pellarin, T., Petropoulos, G. P., Pfeil, I., Powers, J., Robock, A., Rüdiger, C., Rummel, U., Strobel, M., Su, Z., Sullivan, R., Tagesson, T., Varlagin, A., Vreugdenhil, M., Walker, J., Wen, J., Wenger, F., Wigneron, J. P., Woods, M., Yang, K., Zeng, Y., Zhang, X., Zreda, M., Dietrich, S., Gruber, A., van Oevelen, P., Wagner, W., Scipal, K., Drusch, M., and Sabia, R. (2021). The international soil moisture network: serving earth system science for over a decade. *Hydrology and Earth System Sciences*, 25(11):5749–5804.

Dorigo, W., Wagner, W., Albergel, C., Albrecht, F., Balsamo, G., Brocca, L., Chung, D., Ertl, M., Forkel, M., Gruber, A., Haas, E., Hamer, P. D., Hirschi, M., Ikonen, J., de Jeu, R., Kidd, R., Lahoz, W., Liu, Y. Y., Miralles, D., Mistelbauer, T., Nicolai-Shaw, N., Parinussa, R., Pratola, C., Reimer, C., van der Schalie, R., Seneviratne, S. I., Smolander, T., and Lecomte, P.

(2017). ESA CCI soil moisture for improved earth system understanding: State-of-the art and future directions. *Remote Sensing of Environment*, 203:185–215.

Du, J., Kimball, J. S., Jones, L. A., Kim, Y., Glassy, J., and Watts, J. D. (2017). A global satellite environmental data record derived from amsr-e and amsr2 microwave earth observations. *Earth System Science Data*, 9(2):791–808.

Dumedah, G., Walker, J. P., and Merlin, O. (2015). Root-zone soil moisture estimation from assimilation of downscaled soil moisture and ocean salinity data. *Advances in Water Resources*, 84:14–22.

Duygu, M. B. and Akyürek, Z. (2019). Using cosmic-ray neutron probes in validating satellite soil moisture products and land surface models. *Water*, 11(7):1362.

Entekhabi, D., Njoku, E. G., O'Neill, P. E., Kellogg, K. H., Crow, W. T., Edelstein, W. N., Entin, J. K., Goodman, S. D., Jackson, T. J., Johnson, J., Kimball, J., Piepmeier, J. R., Koster, R. D., Martin, N., McDonald, K. C., Moghaddam, M., Moran, S., Reichle, R., Shi, J. C., Spencer, M. W., Thurman, S. W., Tsang, L., and Zyl, J. V. (2010). The soil moisture active passive (SMAP) mission. *Proceedings of the IEEE*, 98(5):704–716.

Entin, J. K., Robock, A., Vinnikov, K. Y., Hollinger, S. E., Liu, S., and Namkhai, A. (2000). Temporal and spatial scales of observed soil moisture variations in the extratropics. *Journal of Geophysical Research: Atmospheres*, 105(D9):11865–11877.

Ezzahar, J., Ouaadi, N., Zribi, M., Elfarkh, J., Aouade, G., Khabba, S., Er-Raki, S., Chehbouni, A., and Jarlan, L. (2019). Evaluation of backscattering models and support vector machine for the retrieval of bare soil moisture from sentinel-1 data. *Remote Sensing*, 12(1):72.

Fang, B., Lakshmi, V., Bindlish, R., and Jackson, T. (2018). AMSR2 soil moisture downscaling using temperature and vegetation data. *Remote Sensing*, 10(10):1575.

Foehn, A., Hernández, J. G., Schaefli, B., and Cesare, G. D. (2018). Spatial interpolation of precipitation from multiple rain gauge networks and weather radar data for operational applications in alpine catchments. *Journal of Hydrology*, 563:1092–1110.

Fredlund, M. D., Fredlund, D., and Wilson, G. (1994). Prediction of the soil-water characteristic curve from grain-size distribution and volume-mass properties.

Fécan, F., Marticorena, B., and Bergametti, G. (1999). Parametrization of the increase of the aeolian erosion threshold wind friction velocity due to soil moisture for arid and semi-arid areas. *Annales Geophysicae*, 17(1):149–157.

GCOS (2016). The global observing system for climate: implementation needs. *WMO Pub GCOS - 200*.

Green, J. K., Seneviratne, S. I., Berg, A. M., Findell, K. L., Hagemann, S., Lawrence, D. M., and Gentine, P. (2019). Large influence of soil moisture on long-term terrestrial carbon uptake. *Nature*, 565(7740):476–479.

Gruber, A., Scanlon, T., van der Schalie, R., Wagner, W., and Dorigo, W. (2019). Evolution of the ESA CCI soil moisture climate data records and their underlying merging methodology. *Earth System Science Data*, 11(2):717–739.

Guillod, B. P., Orlowsky, B., Miralles, D. G., Teuling, A. J., and Seneviratne, S. I. (2015). Reconciling spatial and temporal soil moisture effects on afternoon rainfall. *Nature Communications*, 6(1).

Guswa, A. J., Celia, M. A., and Rodriguez-Iturbe, I. (2002). Models of soil moisture dynamics in ecohydrology: A comparative study. *Water Resources Research*, 38(9):5–1–5–15.

Hari, V., Rakovec, O., Markonis, Y., Hanel, M., and Kumar, R. (2020). Increased future occurrences of the exceptional 2018–2019 central european drought under global warming. *Scientific Reports*, 10(1).

Hersbach, H., de Rosnay, P., Bell, B., Schepers, D., Simmons, A., Soci, C., Abdalla, S., Alonso-Balmaseda, M., Balsamo, G., Bechtold, P., Berrisford, P., Bidlot, J.-R., de Boisséson, E., Bonavita, M., Browne, P., Buizza, R., Dahlgren, P., Dee, D., Dragani, R., Diamantakis, M., Flemming, J., Forbes, R., Geer, A., Haiden, T., Hólm, E., Haimberger, L., Hogan, R., Horányi, A., Janiskova, M., Laloyaux, P., Lopez, P., Munoz-Sabater, J., Peubey, C., Radu, R., Richardson, D., Thépaut, J.-N., Vitart, F., Yang, X., Zsótér, E., and Zuo, H. (2018). Operational global reanalysis: progress, future directions and synergies with nwp. *ERA Report Series*.

Hirschi, M., Mueller, B., Dorigo, W., and Seneviratne, S. (2014). Using remotely sensed soil moisture for land–atmosphere coupling diagnostics: The role of surface vs. root-zone soil moisture variability. *Remote Sensing of Environment*, 154:246–252.

Hirschi, M., Seneviratne, S. I., Alexandrov, V., Boberg, F., Boroneant, C., Christensen, O. B., Formayer, H., Orlowsky, B., and Stepanek, P. (2010). Observational evidence for soil-moisture impact on hot extremes in southeastern europe. *Nature Geoscience*, 4(1):17–21.

Hohenegger, C., Brockhaus, P., Bretherton, C. S., and Schär, C. (2009). The soil moisture–precipitation feedback in simulations with explicit and parameterized convection. *Journal of Climate*, 22(19):5003–5020.

Humphrey, V., Berg, A., Ciais, P., Gentine, P., Jung, M., Reichstein, M., Seneviratne, S. I., and Frankenberg, C. (2021). Soil moisture–atmosphere feedback dominates land carbon uptake variability. *Nature*, 592(7852):65–69.

IPCC (2023). *Climate Change 2023: Synthesis Report. Contribution of Working Groups I, II and III to the Sixth Assessment Report of the Intergovernmental Panel on Climate Change* [*Core Writing Team, H. Lee and J. Romero (eds.)*]. IPCC, Geneva, Switzerland.

Javelle, P., Fouchier, C., Arnaud, P., and Lavabre, J. (2010). Flash flood warning at ungauged locations using radar rainfall and antecedent soil moisture estimations. *Journal of Hydrology*, 394(1-2):267–274.

Kasim, A. A., Leng, P., Li, Y.-X., Liao, Q.-Y., Geng, Y.-J., Ma, J., Sun, Y., Song, X., Duan, S.-B., and Li, Z.-L. (2025). Remote sensing of root zone soil moisture: A review of methods and products. *Journal of Hydrology*, 656:133002.

Katul, G. G., Oren, R., Manzoni, S., Higgins, C., and Parlange, M. B. (2012). Evapotranspiration: A process driving mass transport and energy exchange in the soil-plant-atmosphere-climate system. *Reviews of Geophysics*, 50(3).

Katul, G. G., Porporato, A., Daly, E., Oishi, A. C., Kim, H.-S., Stoy, P. C., Juang, J.-Y., and Siqueira, M. B. (2007). On the spectrum of soil moisture from hourly to interannual scales. *Water Resources Research*, 43(5).

Kerr, Y., Waldteufel, P., Wigneron, J.-P., Martinuzzi, J., Font, J., and Berger, M. (2001). Soil moisture retrieval from space: the soil moisture and ocean salinity (SMOS) mission. *IEEE Transactions on Geoscience and Remote Sensing*, 39(8):1729–1735.

Kerr, Y. H., Waldteufel, P., Wigneron, J.-P., Delwart, S., Cabot, F., Boutin, J., Escorihuela, M.-J., Font, J., Reul, N., Gruhier, C., Juglea, S. E., Drinkwater, M. R., Hahne, A., Martín-Neira, M., and Mecklenburg, S. (2010). The SMOS mission: New tool for monitoring key elements ofthe global water cycle. *Proceedings of the IEEE*, 98(5):666–687.

Kidd, C., Becker, A., Huffman, G. J., Muller, C. L., Joe, P., Skofronick-Jackson, G., and Kirschbaum, D. B. (2017). So, how much of the earth's surface is covered by rain gauges? *Bulletin of the American Meteorological Society*, 98(1):69–78.

Kidd, C. and Levizzani, V. (2011). Status of satellite precipitation retrievals. *Hydrology and Earth System Sciences*, 15(4):1109–1116.

Kim, H., Lakshmi, V., Kwon, Y., and Kumar, S. V. (2021). First attempt of global-scale assimilation of subdaily scale soil moisture estimates from CYGNSS and SMAP into a land surface model. *Environmental Research Letters*, 16(7):074041.

Kim, H., Parinussa, R., Konings, A. G., Wagner, W., Cosh, M. H., Lakshmi, V., Zohaib, M., and Choi, M. (2018). Global-scale assessment and combination of SMAP with ASCAT (active) and AMSR2 (passive) soil moisture products. *Remote Sensing of Environment*, 204:260–275.

Kochendorfer, J., Rasmussen, R., Wolff, M., Baker, B., Hall, M. E., Meyers, T., Landolt, S., Jachcik, A., Isaksen, K., Brækkan, R., and Leeper, R. (2017). The quantification and correction of wind-induced precipitation measurement errors. *Hydrology and Earth System Sciences*, 21(4):1973–1989.

Kolassa, J., Reichle, R., and Draper, C. (2017). Merging active and passive microwave observations in soil moisture data assimilation. *Remote Sensing of Environment*, 191:117–130.

Kolassa, J., Reichle, R., Liu, Q., Alemohammad, S., Gentine, P., Aida, K., Asanuma, J., Bircher, S., Caldwell, T., Colliander, A., Cosh, M., Collins, C. H., Jackson, T., Martínez-Fernández, J., McNairn, H., Pacheco, A., Thibeault, M., and Walker, J. (2018). Estimating surface soil

moisture from SMAP observations using a neural network technique. *Remote Sensing of Environment*, 204:43–59.

Koster, R. D., Dirmeyer, P. A., Guo, Z., Bonan, G., Chan, E., Cox, P., Gordon, C. T., Kanae, S., Kowalczyk, E., Lawrence, D., Liu, P., Lu, C.-H., Malyshev, S., McAvaney, B., Mitchell, K., Mocko, D., Oki, T., Oleson, K., Pitman, A., Sud, Y. C., Taylor, C. M., Verseghy, D., Vasic, R., Xue, Y., and Yamada, T. (2004). Regions of strong coupling between soil moisture and precipitation. *Science*, 305(5687):1138–1140.

Krakauer, N. Y., Cook, B. I., and Puma, M. J. (2010). Contribution of soil moisture feedback to hydroclimatic variability. *Hydrol. Earth Syst. Sci.*, 14:505–520.

Legates, D. R., Mahmood, R., Levia, D. F., DeLiberty, T. L., Quiring, S. M., Houser, C., and Nelson, F. E. (2010). Soil moisture: A central and unifying theme in physical geography. *Progress in Physical Geography: Earth and Environment*, 35(1):65–86.

Lehmann, P., Merlin, O., Gentine, P., and Or, D. (2018). Soil texture effects on surface resistance to bare-soil evaporation. *Geophysical Research Letters*, 45(19):nil.

Li, J., Wang, S., Gunn, G., Joosse, P., and Russell, H. A. (2018). A model for downscaling SMOS soil moisture using sentinel-1 SAR data. *International Journal of Applied Earth Observation and Geoinformation*, 72:109–121.

Lievens, H., Reichle, R. H., Liu, Q., Lannoy, G. J. M. D., Dunbar, R. S., Kim, S. B., Das, N. N., Cosh, M., Walker, J. P., and Wagner, W. (2017). Joint sentinel-1 and SMAP data assimilation to improve soil moisture estimates. *Geophysical Research Letters*, 44(12):6145–6153.

Liu, Y., Shi, Z., Zhang, G., Chen, Y., Li, S., Hong, Y., Shi, T., Wang, J., and Liu, Y. (2018). Application of spectrally derived soil type as ancillary data to improve the estimation of soil organic carbon by using the chinese soil vis-nir spectral library. *Remote Sensing*, 10(11):1747.

Liu, Y. and Yang, Y. (2022). Advances in the quality of global soil moisture products: A review. *Remote Sensing*, 14(15):3741.

Manning, C., Widmann, M., Bevacqua, E., Loon, A. F. V., Maraun, D., and Vrac, M. (2018). Soil moisture drought in europe: A compound event of precipitation and potential evapotranspiration on multiple time scales. *Journal of Hydrometeorology*, 19(8):1255–1271.

Mattia, F., Satalino, G., Balenzano, A., Rinaldi, M., Steduto, P., and Moreno, J. (2015). Sentinel-1 for wheat mapping and soil moisture retrieval. In *2015 IEEE International Geoscience and Remote Sensing Symposium (IGARSS)*, pages 2832–2835. IEEE.

McColl, K. A., Alemohammad, S. H., Akbar, R., Konings, A. G., Yueh, S., and Entekhabi, D. (2017a). The global distribution and dynamics of surface soil moisture. *Nature Geoscience*, 10(2):100–104.

McColl, K. A., Wang, W., Peng, B., Akbar, R., Gianotti, D. J. S., Lu, H., Pan, M., and Entekhabi, D. (2017b). Global characterization of surface soil moisture drydowns. *Geophysical Research Letters*, 44(8):3682–3690.

Merlin, O., Walker, J., Chehbouni, A., and Kerr, Y. (2008). Towards deterministic downscaling of SMOS soil moisture using MODIS derived soil evaporative efficiency. *Remote Sensing of Environment*, 112(10):3935–3946.

Miralles, D. G., Crow, W. T., and Cosh, M. H. (2010). Estimating spatial sampling errors in coarse-scale soil moisture estimates derived from point-scale observations. *Journal of Hydrometeorology*, 11(6):1423–1429.

Miralles, D. G., van den Berg, M. J., Teuling, A. J., and de Jeu, R. A. M. (2012). Soil moisture-temperature coupling: A multiscale observational analysis. *Geophysical Research Letters*, 39(21):n/a–n/a.

Montzka, C., Bogena, H., Zreda, M., Monerris, A., Morrison, R., Muddu, S., and Vereecken, H. (2017). Validation of spaceborne and modelled surface soil moisture products with cosmic-ray neutron probes. *Remote Sensing*, 9(2):103.

Naeimi, V., Scipal, K., Bartalis, Z., Hasenauer, S., and Wagner, W. (2009). An improved soil moisture retrieval algorithm for ERS and METOP scatterometer observations. *IEEE Transactions on Geoscience and Remote Sensing*, 47(7):1999–2013.

Naumann, G., Cammalleri, C., Mentaschi, L., and Feyen, L. (2021). Increased economic drought impacts in europe with anthropogenic warming. *Nature Climate Change*, 11(6):485–491.

New, M., Todd, M., Hulme, M., and Jones, P. (2001). Precipitation measurements and trends in the twentieth century. *International Journal of Climatology*, 21(15):1889–1922.

Nicolai-Shaw, N., Gudmundsson, L., Hirschi, M., and Seneviratne, S. I. (2016). Long-term predictability of soil moisture dynamics at the global scale: Persistence versus large-scale drivers. *Geophysical Research Letters*, 43(16):8554–8562.

Njoku, E., Jackson, T., Lakshmi, V., Chan, T., and Nghiem, S. (2003). Soil moisture retrieval from amsr-e. *IEEE Transactions on Geoscience and Remote Sensing*, 41(2):215–229.

Njoku, E. G. and Entekhabi, D. (1996). Passive microwave remote sensing of soil moisture. *Journal of Hydrology*.

O, S. and Orth, R. (2021). Global soil moisture data derived through machine learning trained with in-situ measurements. *Scientific Data*, 8(1).

Ochsner, T. E., Cosh, M. H., Cuenca, R. H., Dorigo, W. A., Draper, C. S., Hagimoto, Y., Kerr, Y. H., Larson, K. M., Njoku, E. G., Small, E. E., and Zreda, M. (2013). State of the art in large-scale soil moisture monitoring. *Soil Science Society of America Journal*, 77(6):1888–1919.

Or, D. and Lehmann, P. (2019). Surface evaporative capacitance: How soil type and rainfall characteristics affect global-scale surface evaporation. *Water Resources Research*, 55(1):519–539.

Owe, M., de Jeu, R., and Walker, J. (2001). A methodology for surface soil moisture and vegetation optical depth retrieval using the microwave polarization difference index. *IEEE Transactions on Geoscience and Remote Sensing*, 39(8):1643–1654.

Padrón, R. S., Gudmundsson, L., Decharme, B., Ducharne, A., Lawrence, D. M., Mao, J., Peano, D., Krinner, G., Kim, H., and Seneviratne, S. I. (2020). Observed changes in dry-season water availability attributed to human-induced climate change. *Nature Geoscience*, 13(7):477–481.

Peng, J., Albergel, C., Balenzano, A., Brocca, L., Cartus, O., Cosh, M. H., Crow, W. T., Dabrowska-Zielinska, K., Dadson, S., Davidson, M. W., de Rosnay, P., Dorigo, W., Gruber, A., Hagemann, S., Hirschi, M., Kerr, Y. H., Lovergine, F., Mahecha, M. D., Marzahn,

P., Mattia, F., Musial, J. P., Preuschmann, S., Reichle, R. H., Satalino, G., Silgram, M., van Bodegom, P. M., Verhoest, N. E., Wagner, W., Walker, J. P., Wegmüller, U., and Loew, A. (2021). A roadmap for high-resolution satellite soil moisture applications – confronting product characteristics with user requirements. *Remote Sensing of Environment*, 252:112162.

Peng, J., Loew, A., Merlin, O., and Verhoest, N. E. C. (2017). A review of spatial downscaling of satellite remotely sensed soil moisture. *Reviews of Geophysics*, 55(2):341–366.

Piles, M., Petropoulos, G. P., Sánchez, N., González-Zamora, Á., and Ireland, G. (2016). Towards improved spatio-temporal resolution soil moisture retrievals from the synergy of SMOS and MSG SEVIRI spaceborne observations. *Remote Sensing of Environment*, 180:403–417.

Qiu, J., Crow, W. T., Nearing, G. S., Mo, X., and Liu, S. (2014). The impact of vertical measurement depth on the information content of soil moisture times series data. *Geophysical Research Letters*, 41(14):4997–5004.

Qu, Y., Zhu, Z., Chai, L., Liu, S., Montzka, C., Liu, J., Yang, X., Lu, Z., Jin, R., Li, X., Guo, Z., and Zheng, J. (2019). Rebuilding a microwave soil moisture product using random forest adopting AMSR-e/AMSR2 brightness temperature and SMAP over the qinghai–tibet plateau, china. *Remote Sensing*, 11(6):683.

Rahmati, M., Amelung, W., Brogi, C., Dari, J., Flammini, A., Bogena, H., Brocca, L., Chen, H., Groh, J., Koster, R. D., McColl, K. A., Montzka, C., Moradi, S., Rahi, A., Sharghi S., F., and Vereecken, H. (2024). Soil moisture memory: State-of-the-art and the way forward. *Reviews of Geophysics*, 62(2).

Reich, P. B., Sendall, K. M., Stefanski, A., Rich, R. L., Hobbie, S. E., and Montgomery, R. A. (2018). Effects of climate warming on photosynthesis in boreal tree species depend on soil moisture. *Nature*, 562(7726):263–267.

Reichle, R. H., Koster, R. D., Dong, J., and Berg, A. A. (2004). Global soil moisture from satellite observations and land surface models and ground and data: Implications and for data and assimilation. *Journal of Hydrometeorology*, 5:430.

Reinermann, S., Gessner, U., Asam, S., Kuenzer, C., and Dech, S. (2019). The effect of droughts on vegetation condition in germany: An analysis based on two decades of satellite earth observation time series and crop yield statistics. *Remote Sensing*, 11(15):1783.

Rigden, A. J., Mueller, N. D., Holbrook, N. M., Pillai, N., and Huybers, P. (2020). Combined influence of soil moisture and atmospheric evaporative demand is important for accurately predicting us maize yields. *Nature Food*, 1(2):127–133.

Robinson, D. A., Campbell, C. S., Hopmans, J. W., Hornbuckle, B. K., Jones, S. B., Knight, R., Ogden, F., Selker, J., and Wendroth, O. (2008). Soil moisture measurement for ecological and hydrological watershed-scale observatories: A review. *Vadose Zone Journal*, 7(1):358–389.

Robock, A., Vinnikov, K. Y., Srinivasan, G., Entin, J. K., Hollinger, S. E., Speranskaya, N. A., Liu, S., and Namkhai, A. (2000). The global soil moisture data bank. *Bulletin of the American Meteorological Society*, 81(6):1281–1299.

Sadeghi, M., Jones, S. B., and Philpot, W. D. (2015). A linear physically-based model for remote sensing of soil moisture using short wave infrared bands. *Remote Sensing of Environment*, 164:66–76.

Sadeghi, M., Tabatabaeenejad, A., Tuller, M., Moghaddam, M., and Jones, S. (2016). Advancing nasa's airmoss p-band radar root zone soil moisture retrieval algorithm via incorporation of richards' equation. *Remote Sensing*, 9(1):17.

Samaniego, L., Thober, S., Kumar, R., Wanders, N., Rakovec, O., Pan, M., Zink, M., Sheffield, J., Wood, E. F., and Marx, A. (2018). Anthropogenic warming exacerbates european soil moisture droughts. *Nature Climate Change*, 8(5):421–426.

Santi, E., Dabboor, M., Pettinato, S., and Paloscia, S. (2019). Combining machine learning and compact polarimetry for estimating soil moisture from c-band SAR data. *Remote Sensing*, 11(20):2451.

Santi, E., Paloscia, S., Pettinato, S., Brocca, L., Ciabatta, L., and Entekhabi, D. (2018). Integration of microwave data from SMAP and AMSR2 for soil moisture monitoring in italy. *Remote Sensing of Environment*, 212:21–30.

Schamm, K., Ziese, M., Becker, A., Finger, P., Meyer-Christoffer, A., Schneider, U., Schröder, M., and Stender, P. (2014). Global gridded precipitation over land: a description of the new GPCC first guess daily product. *Earth System Science Data*, 6(1):49–60.

Scholten, T. (2004). Bodenwasser. https://www.spektrum.de/lexikon/geographie/bodenwasser/1174. [Online; accessed June 23, 2025].

Schwalm, C. R., Anderegg, W. R. L., Michalak, A. M., Fisher, J. B., Biondi, F., Koch, G., Litvak, M., Ogle, K., Shaw, J. D., Wolf, A., Huntzinger, D. N., Schaefer, K., Cook, R., Wei, Y., Fang, Y., Hayes, D., Huang, M., Jain, A., and Tian, H. (2017). Global patterns of drought recovery. *Nature*, 548(7666):202–205.

Sehler, R., Li, J., Reager, J. T., and Ye, H. (2019). Investigating relationship between soil moisture and precipitation globally using remote sensing observations. *Journal of Contemporary Water Research Education*, 168:106–118.

Seneviratne, S. I., Corti, T., Davin, E. L., Hirschi, M., Jaeger, E. B., Lehner, I., Orlowsky, B., and Teuling, A. J. (2010). Investigating soil moisture–climate interactions in a changing climate: A review. *Earth-Science Reviews*, 99(3-4):125–161.

Seo, E., Lee, M.-I., and Reichle, R. H. (2021). Assimilation of SMAP and ASCAT soil moisture retrievals into the JULES land surface model using the local ensemble transform kalman filter. *Remote Sensing of Environment*, 253.

Shiklomanov, I. A. (1993). *World Fresh Water Resources*. Oxford University Press, New York, NY [u.a.].

Singh, G. and Das, N. N. (2022). A data-driven approach using the remotely sensed soil moisture product to identify water-demand in agricultural regions. *Science of The Total Environment*, 837:155893.

Skofronick-Jackson, G., Petersen, W. A., Berg, W., Kidd, C., Stocker, E. F., Kirschbaum, D. B., Kakar, R., Braun, S. A., Huffman, G. J., Iguchi, T., Kirstetter, P. E., Kummerow, C., Meneghini, R., Oki, R., Olson, W. S., Takayabu, Y. N., Furukawa, K., and Wilheit, T. (2017). The global precipitation measurement (GPM) mission for science and society. *Bulletin of the American Meteorological Society*, 98(8):1679–1695.

Small, E., Badger, A., Abolafia-Rosenzweig, R., and Livneh, B. (2018). Estimating soil evaporation using drying rates determined from satellite-based soil moisture records. *Remote Sensing*, 10(12):1945.

Sobaga, A., Decharme, B., Habets, F., Delire, C., Enjelvin, N., Redon, P.-O., Faure-Catteloin, P., and Moigne, P. L. (2023). Assessment of the ISBA land surface model soil hydrology using four closed-form soilwater relationships and several lysimeters.

Souza, A. G. S. S., Neto, A. R., and de Souza, L. L. (2021). Soil moisture-based index for agricultural drought assessment: SMADI application in pernambuco state-brazil. *Remote Sensing of Environment*, 252:112124.

Sun, Q., Miao, C., Duan, Q., Ashouri, H., Sorooshian, S., and Hsu, K.-L. (2018). A review of global precipitation data sets: Data sources, estimation, and intercomparisons. *Reviews of Geophysics*, 56(1):79–107.

Torres, R., Snoeij, P., Geudtner, D., Bibby, D., Davidson, M., Attema, E., Potin, P., Rommen, B., Floury, N., Brown, M., Traver, I. N., Deghaye, P., Duesmann, B., Rosich, B., Miranda, N., Bruno, C., L'Abbate, M., Croci, R., Pietropaolo, A., Huchler, M., and Rostan, F. (2012). Gmes sentinel-1 mission. *Remote Sensing of Environment*, 120:9–24.

Vereecken, H., Amelung, W., Bauke, S. L., Bogena, H., Brüggemann, N., Montzka, C., Vanderborght, J., Bechtold, M., Blöschl, G., Carminati, A., Javaux, M., Konings, A. G., Kusche, J., Neuweiler, I., Or, D., Steele-Dunne, S., Verhoef, A., Young, M., and Zhang, Y. (2022). Soil hydrology in the earth system. *Nature Reviews Earth amp; Environment*, 3(9):573–587.

Vereecken, H., Huisman, J., Pachepsky, Y., Montzka, C., van der Kruk, J., Bogena, H., Weihermüller, L., Herbst, M., Martinez, G., and Vanderborght, J. (2014). On the spatio-temporal dynamics of soil moisture at the field scale. *Journal of Hydrology*, 516:76–96.

Vereecken, H., Huisman, J. A., Hendricks Franssen, H. J., Brüggemann, N., Bogena, H. R., Kollet, S., Javaux, M., van der Kruk, J., and Vanderborght, J. (2015). Soil hydrology: Recent methodological advances, challenges, and perspectives. *Water Resources Research*, 51(4):2616–2633.

Vereecken, H., Weihermüller, L., Assouline, S., Šimůnek, J., Verhoef, A., Herbst, M., Archer, N., Mohanty, B., Montzka, C., Vanderborght, J., Balsamo, G., Bechtold, M., Boone, A., Chadburn, S., Cuntz, M., Decharme, B., Ducharne, A., Ek, M., Garrigues, S., Goergen, K., Ingwersen, J., Kollet, S., Lawrence, D. M., Li, Q., Or, D., Swenson, S., Vrese, P., Walko, R., Wu, Y., and Xue, Y. (2019). Infiltration from the pedon to global grid scales: An overview and outlook for land surface modeling. *Vadose Zone Journal*, 18(1):1–53.

Vergopolan, N., Xiong, S., Estes, L., Wanders, N., Chaney, N. W., Wood, E. F., Konar, M., Caylor, K., Beck, H. E., Gatti, N., Evans, T., and Sheffield, J. (2021). Field-scale soil moisture bridges the spatial-scale gap between drought monitoring and agricultural yields. *Hydrology and Earth System Sciences*, 25(4):1827–1847.

Wagner, W., Hahn, S., Kidd, R., Melzer, T., Bartalis, Z., Hasenauer, S., Figa-Saldaña, J., de Rosnay, P., Jann, A., Schneider, S., Komma, J., Kubu, G., Brugger, K., Aubrecht, C., Züger, J., Gangkofner, U., Kienberger, S., Brocca, L., Wang, Y., Blöschl, G., Eitzinger, J., and Steinnocher, K. (2013). The ASCAT soil moisture product: A review of its specifications, validation results, and emerging applications. *Meteorologische Zeitschrift*, 22(1):5–33.

Wang, Y., Peng, J., Song, X., Leng, P., Ludwig, R., and Loew, A. (2018). Surface soil moisture retrieval using optical/thermal infrared remote sensing data. *IEEE Transactions on Geoscience and Remote Sensing*, 56(9):5433–5442.

Weil, R. R. and Brady, N. C. (2017). *The nature and properties of soils*. Pearson.

Weiß, T., Jagdhuber, T., Ramsauer, T., LÖw, A., and Marzahn, P. (2024). Rtm-based downscaling of medium resolution soil moisture using sentinel-1 data over agricultural fields. *IEEE Journal of Selected Topics in Applied Earth Observations and Remote Sensing*, pages 1–21.

Western, A. W., Grayson, R. B., and Blöschl, G. (2002). Scaling of soil moisture: A hydrologic perspective. *Annual Review of Earth and Planetary Sciences*, 30(1):149–180.

White, J., Berg, A. A., Champagne, C., Zhang, Y., Chipanshi, A., and Daneshfar, B. (2020). Improving crop yield forecasts with satellite-based soil moisture estimates: An example for township level canola yield forecasts over the canadian prairies. *International Journal of Applied Earth Observation and Geoinformation*, 89:102092.

Wigneron, J.-P., Schmugge, T., Chanzy, A., Calvet, J.-C., and Kerr, Y. H. (1998). Use of passive microwave remote sensing to monitor soil moisture. *Agronomie*, 18(1):27–43.

Winterrath, T., Brendel, T., Junghänel, T., Klameth, A., Lengfeld, K., Walawender, E., Weigl, E., Hafer, M., and Becker, A. (2019). An overview of the new radar-based precipitation climatology of the deutscher wetterdienst – data, methods, products.

Wu, K., Rodriguez, G. A., Zajc, M., Jacquemin, E., Clément, M., Coster, A. D., and Lambot, S. (2019). A new drone-borne GPR for soil moisture mapping. *Remote Sensing of Environment*, 235:111456.

Xia, Y., Watts, J. D., Machmuller, M. B., and Sanderman, J. (2022). Machine learning based estimation of field-scale daily, high resolution, multi-depth soil moisture for the western and midwestern united states. *PeerJ*, 10:e14275.

Zeng, L., Hu, S., Xiang, D., Zhang, X., Li, D., Li, L., and Zhang, T. (2019). Multilayer soil moisture mapping at a regional scale from multisource data via a machine learning method. *Remote Sensing*, 11(3):284.

Zhang, L., Zeng, Y., Zhuang, R., Szabó, B., Manfreda, S., Han, Q., and Su, Z. (2021a). In situ observation-constrained global surface soil moisture using random forest model. *Remote Sensing*, 13(23):4893.

Zhang, L., Zeng, Y., Zhuang, R., Szabó, B., Manfreda, S., Han, Q., and Su, Z. (2021b). In situ observation-constrained global surface soil moisture using random forest model. *Remote Sensing*, 13(23):4893.

Zhang, Y., Liang, S., Ma, H., He, T., Wang, Q., Li, B., Xu, J., Zhang, G., Liu, X., and Xiong, C. (2023). Generation of global 1 km daily soil moisture product from 2000 to 2020 using ensemble learning. *Earth System Science Data*, 15(5):2055–2079.

Zhao, G., Webber, H., Hoffmann, H., Wolf, J., Siebert, S., and Ewert, F. (2015). The implication of irrigation in climate change impact assessment: a european-wide study. *Global Change Biology*, 21(11):4031–4048.

Zhao, L. and Yang, Z.-L. (2018). Multi-sensor land data assimilation: Toward a robust global soil moisture and snow estimation. *Remote Sensing of Environment*, 216:13–27.

Zhao, M. and Running, S. W. (2010). Drought-induced reduction in global terrestrial net primary production from 2000 through 2009. *Science*, 329(5994):940–943.

Zhou, L., Yu, D., Wang, Z., and Wang, X. (2019). Soil water content estimation using high-frequency ground penetrating radar. *Water*, 11(5):1036.

Zhu, Q., Luo, Y., Xu, Y.-P., Tian, Y., and Yang, T. (2019). Satellite soil moisture for agricultural drought monitoring: Assessment of SMAP-derived soil water deficit index in xiang river basin, china. *Remote Sensing*, 11(3):362.

Zucco, G., Brocca, L., Moramarco, T., and Morbidelli, R. (2014). Influence of land use on soil moisture spatial–temporal variability and monitoring. *Journal of Hydrology*, 516:193–199.

Šimůnek, J. and van Genuchten, M. T. (2008). Modeling nonequilibrium flow and transport processes using hydrus. *Vadose Zone Journal*, 7(2):782–797.